Achieving Peak Flow and Sediment Loading Reductions through Increased Water Storage in the Le Sueur Watershed, Minnesota: A Modeling Approach

A Thesis
SUBMITTED TO THE FACULTY OF
UNIVERSITY OF MINNESOTA
BY

Nathaniel Mitchell

IN PARTIAL FULFILLMENT OF THE REQUIREMENTS
FOR THE DEGREE OF
MASTER OF SCIENCE

Dr. Karen Gran, Advisor

September 2015

Acknowledgements

This research was supported by funding provided by the National Science Foundation, Clear Water Legacy Fund, Minnesota Department of Agriculture, and the Department of Earth and Environmental Sciences at the University of Minnesota Duluth. I thank these supporters, as well as the scientists and researchers that guided this study along the way. Guidance was especially provided by Karen Gran, Peter Wilcock, Patrick Belmont, Ben Hobbs, Brent Dalzell, and Se Jong Cho. Many thanks to Karthik Kumarasamy for creating the SWAT models used in this study.

Abstract

Climate change, land clearing, and artificial drainage have increased the Minnesota River Basin's stream flows and the rates at which channel banks and bluffs are eroded. Increasing erosion rates have contributed to higher sediment-loading rates, excess turbidity levels, and increases in sedimentation rates in Lake Pepin further downstream. These issues have motivated the discussion of flood management through either wetland restoration or the implementation of simple detention basins. This study uses the Soil and Water Assessment Tool (SWAT) to assess a wide variety of water retention site (WRS) implementation scenarios in the Le Sueur watershed in south-central Minnesota, a subwatershed of the Minnesota River Basin. Projected flows were used in conjunction with an empirical relationship developed from gauging data to assess changes in sediment-loading rates from near-channel features in the lower watershed. The WRS term is used as a general term for depressional storage areas, and sites could be made into wetlands or detention basins. Sites were delineated as topographic depressions with specific land uses, minimum areas (3000 m^2), and relatively high compound topographic index (CTI) values. Contributing areas were manually measured for the WRS delineated. These contributing areas were used with existing depression depths, and different site characteristics to create 210 initial WRS scenarios. The contributing areas measured for the initial scenarios were used to create a generalized relationship between WRS area and contributing area. This relationship was used with different design depths, placement scenarios, and K values to create 225 generalized WRS scenarios. Reductions in peak flow volumes and sediment-loading rates are generally maximized by placing sites with high K values in the upper half of the watershed. High K values allow sites to lose more water through seepage, emptying their storages between precipitation events and preventing frequent overflowing. Reductions in peak flow volumes and sediment-loading rates also level off as WRS extent increases. This reduction in cost effectiveness with increasing site extent is due to the decreasing frequencies of high-magnitude events. The generalized WRS scenarios were used to create a simplified empirical model capable of generating peak flows and sediment-loading rates from near-channel features in the lower watershed. This simplified model is being incorporated into a decision-analysis model portraying a wide variety of management options in the Le Sueur watershed. This tool may better enable local stakeholders to evaluate, select, and promote management scenarios that best address the issues faced in the region.

Table of Contents

List of Tables

List of Figures

1: Introduction

The Minnesota River and many of its tributaries carry large suspended sediment loads, causing the Minnesota Pollution Control Agency (MPCA) to list multiple reaches within the Minnesota River Basin as impaired for turbidity under Section 303d of the Clean Water Act (MPCA, 2014). Within this basin (Figure 1), anthropogenic influences have exacerbated the basin's ongoing transient adjustment following the last glacial period. Steep clay-till bluffs created within the basin during its adjustment contribute large quantities of sediment to the channel network (Gran et al., 2013), but such contributions have increased again following agricultural alterations to the landscape (Schottler et al., 2013). While these ongoing problems contribute to the degradation of habitats and water quality, the causes are part natural and part anthropogenic in origin and have therefore sparked intense debates regarding how to best manage these landscapes while also minimizing sediment-loading rates.

Many of the sediment-related water quality issues faced are related to the draining of glacial Lake Agassiz about 13,400 years ago, an event that caused a drop in base-level that streams within the Minnesota River Basin are still adjusting to (Gran et al., 2009; 2011). The low-gradient uplands in the basin have not yet received the signal of base-level fall, but the lower reaches of Minnesota River Basin subwatersheds feature knickzones, areas that are responding to the signal by incising aggressively. This state of adjustment is reflected in the steep bluffs and pronounced slope discontinuities created

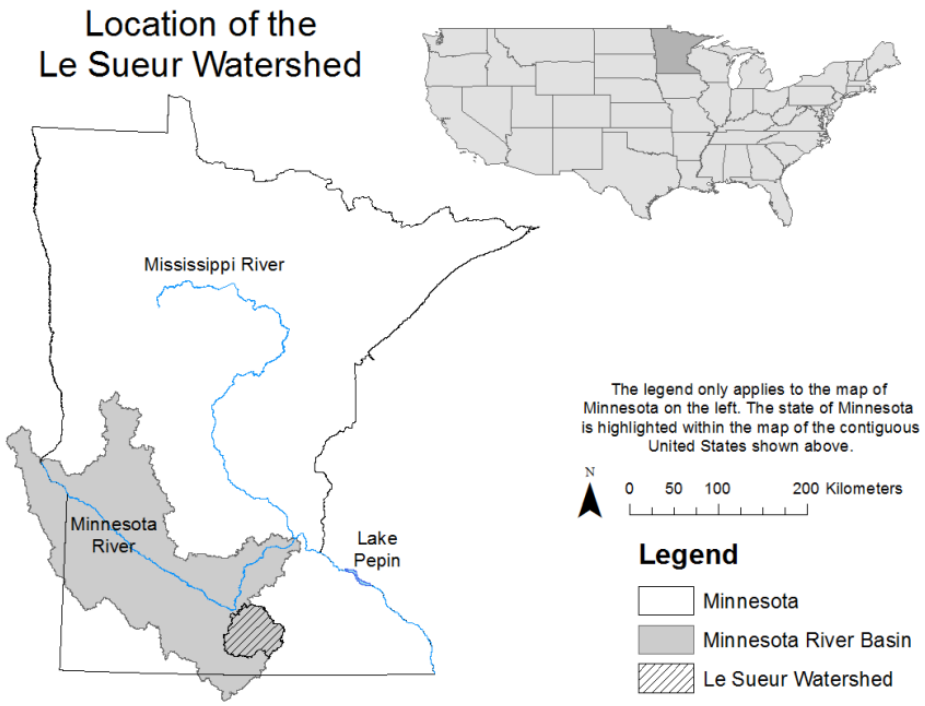

Figure 1. Map showing the positions of the Minnesota River Basin, Le Sueur Watershed, and Lake Pepin relative to the state of Minnesota and the contiguous United States.

as the wave of incision propagates through the basin (Gran et al., 2009; 2011). While this state of transient adjustment already created substantial erosion and high sediment-loading rates, these rates have increased yet again following the development of agriculture in the region (Engstrom et al., 2009). The sediment loads delivered to Lake Pepin, which are derived from the Upper Mississippi, Minnesota, and St. Croix watersheds further upstream, have increased by an order of magnitude since 1830 CE (Engstrom et al., 2009). Both Engstrom et al. (2009) and Kelly and Nater (2000) found that most of this increase originated in the Minnesota River Basin. Kelley and Nater (2000) further showed that the Minnesota River's contribution to Lake Pepin's sediment

loads has increased from 83.9% (± 1.1) to 90.0% (± 1.4) after European settlement began in about 1830 CE.

This apparent increase in the delivery of material from the Minnesota River Basin to Lake Pepin has been attributed to increases in stream flows and the resulting increases in the erosion of near-channel features like stream banks and bluffs (Belmont et al., 2011). Novotny and Stefan (2007) found the largest changes in stream flow from 1980 to 2002 within Minnesotan watersheds to have occurred within the Minnesota River Basin. Within this basin, five-year averages of mean annual stream flow, summer and winter low flow, summer peak flow, and flood duration all increased from 1980 to 2002, exhibiting considerably higher values in the 1990s than any of the previous time periods studied. These increased stream flows wield higher shear stresses along bluff toes, causing higher bluff erosion rates (Gran et al., 2013). The majority of eroded bluff material quickly becomes part of a stream's suspended or wash load, increasing turbidity levels (Day et al., 2013).

The erosion and sediment loading issues faced within the Minnesota River Basin are well demonstrated within the Le Sueur watershed in south-central Minnesota (Figure 1). This 2800 km^2 subwatershed of the Minnesota River basin provides the highest sediment yield of any Minnesota River tributary, delivering about 73.5 $Mg/km^2/yr$ and as much as 30% of the Minnesota River's annual sediment load (Belmont et al., 2011) despite draining only about 6% of the basin's area. Belmont et al. (2011) found that the dominant source of sediment in the Le Sueur watershed has

shifted from agricultural fields to near-channel sources following the implementation of more effective soil conservation practices on agricultural fields and increases in stream discharge (since at least about 1940; Schottler et al. 2013) that lead to increased rates of bank and bluff erosion. Although these near-channel sources comprise less than 1% of the watershed, they provided 70% of the Le Sueur River's sediment load from 2000 to 2010 (Belmont et al., 2011). The hydrologic changes highlighted by Novotny and Stefan (2007) are believed to be responsible for accelerating the erosion of such near-channel features, increasing valley excavation rates within the Le Sueur watershed by a factor of three since European settlement (Gran et al., 2013).

Although some of this hydrologic change has been attributed to climate change, Schottler et al. (2013) found a local land-use effect to be the main driver in most Minnesota River tributaries rather than a trend in regional rain-fall (Figs. 2 and 3). The watersheds found by these authors to have statistically significant trends ($p<0.1$) in May-June water yields and/or runoff ratios showed an increase of 45-200% in these values since the middle of the 20th century (Figure 2). The increased water yield of these two months accounted for 1/3rd of the total annual increase in water yield. While annual precipitation has increased by less than 15%, much of this increase occurs late in the year (Sept-Oct. in Fig. 2) and May-June precipitation has been largely constant or decreasing since about 1940. Schottler et al. (2013) observed that watersheds located near each other could experience significantly different hydrologic regimes (i.e., increasing stream flows vs. steady stream flows), with those watersheds experiencing

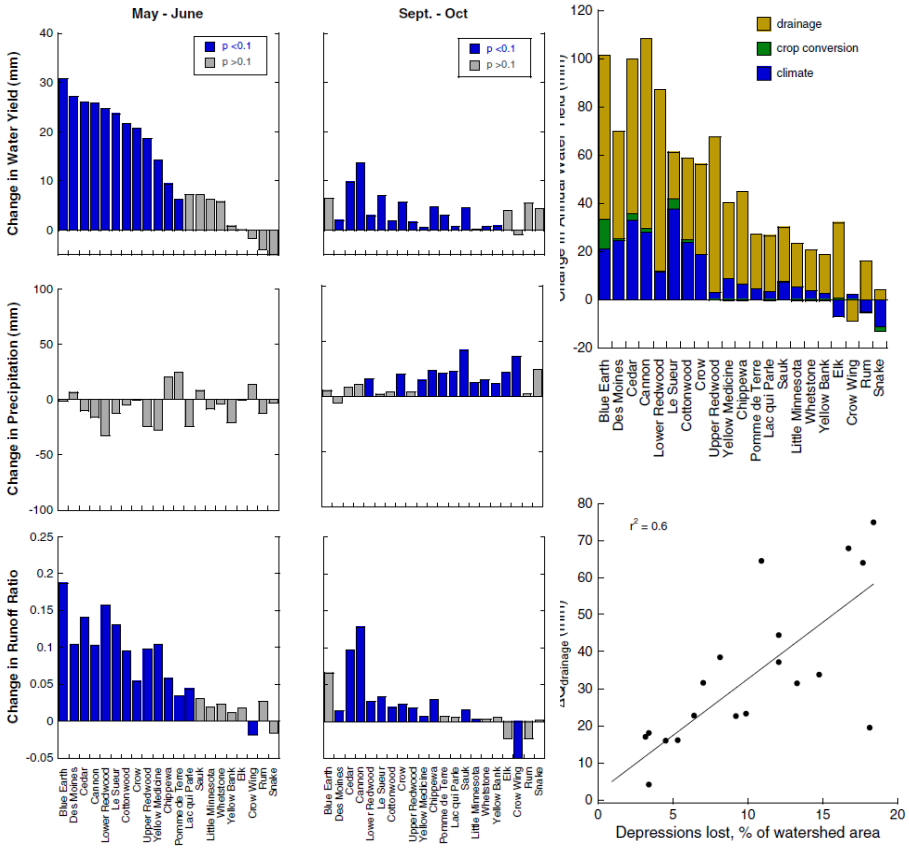

Left: Figure 2. Seasonal changes in water yield (stream flow volume/watershed area), precipitation, and runoff ratio (water yield/precipitation) for the 21 watersheds studied by Schottler et al. (2013). Changes reflect those between the median values of two 35-year periods: 1940-1974 and 1975-2009. Schottler et al. (2013) reported annual changes to follow similar patterns. From Schottler et al. (2013).

Right: Figure 3. (a) Graph showing the extents to which artificial drainage, crop conversion, and climate have contributed to changes in the annual water yields of the 21 watersheds studied by Schottler et al. (2013). Artificial drainage was often found to be the greater driver of changes in water yield. (b) Graph showing the relationship between watersheds' increases in water yield from artificial drainage and the loss of depressions in those watersheds. From Schottler et al. (2013).

increased stream flows being more agricultural. Crop yields within this region are enhanced by artificial drainage (i.e., ditches and tile drains), and farmers have been implementing increasing amounts of artificial drainage during the period over which Schottler et al. identified stream flow increases. These authors also found that, on average, changes in precipitation and crop evapotranspiration explained less than 50% of the stream flow increases observed, while the unexplained flow increases correlated

highly with artificial drainage and the loss of depressional areas (Figure 3). Such observations lead Schottler et al. to cite artificial drainage as the largest contributor to such streamflow increases, followed by climate change and crop conversions (e.g., increased cultivation of soybeans, which are planted later in the season and do not contribute to evapotranspiration in May-June; Figure 3). The expediting effect of artificial drainage was further demonstrated by Lenhart et al. (2011), who found ditches and subsurface tiling to have connected previously isolated basins to stream networks within two subwatersheds of the Minnesota River Basin. These subwatersheds, the Elm and Center Creek Watersheds, had their drainage areas effectively increase by 15 to 20%. Such alterations have caused the loss of depressional storage areas that are often occupied by wetlands. These storage features can increase water residence times and attenuate peak flows, and the features' loss has deprived the region of such services.

The restoration of depressional wetlands or the implementation of water retention sites (WRS) may aid in reducing peak flows, erosion rates, turbidity levels, and pollution by fertilizers. The WRS term used here is a more general reference for depressional storage areas that could be designed to act as either ecologically-functional wetlands or simple detention basins. While landowners and farmers may be more receptive to the implementation of simple detention basins, the biological functions of wetlands can improve water quality by intercepting and treating the agricultural fertilizers that would otherwise travel through tiles, drains, and streams (Mitsch and Day, 2006). Excess nutrients have caused much of the Gulf of Mexico, the

outlet for the $3 \cdot 10^6$ km^2, heavily agricultural Mississippi River Basin, to become hypoxic (Mitsch and Day, 2006; Goolsby et al., 2000; Rabalais et al., 2002). While wetlands have therefore been advanced as a solution to the Gulf hypoxia, they have also been proposed as one for flood mitigation (Mitsch and Day, 2006). Wetlands' storage capacities can allow them to reduce floods peaks and contribute to baseflows (Bullock and Acreman, 2003). The achievement of such peak flow reductions would likely be an important step in the reduction of both the Le Sueur River's turbidity levels and Lake Pepin's sedimentation rates. Wetlands that fill up and overflow may increase the magnitudes of floods (Bullock and Acreman, 2003), however, a capacity that could exacerbate the turbidity issues of the Le Sueur River. Determining the hydrologic effects of a wetland restoration or WRS implementation regime is therefore crucial to the implementation of a successful management strategy.

This study assesses the effects of a wide range of WRS implementation scenarios on peak flows and sediment-loading rates in the lower reaches of the Le Sueur watershed. A wide range of extent scenarios is used to test the rates at which peak flow and sediment loading reductions are gained with increasing site extent. Site placement within the watershed (e.g., close to or far from the watershed outlet), design depth, and the hydraulic conductivity of site beds are all varied to test the sensitivity of sites to such factors. Projections are made with a widely used watershed-scale hydrological model, the Soil and Water Assessment Tool (SWAT), but these projections are also used to create a simplified model for generating peak flows in the lower watershed.

All of the considerations discussed above are motivated by the need for peak flow and sediment-loading rate reductions in the Minnesota River Basin. The creation of a simplified model, however, is specifically needed for research purposes; hydrological models capable of portraying these landscapes are highly complex and often time-consuming. A simplified empirical model providing relatively accurate peak flow and sediment-loading rate projections can be used in conjunction with other models assessing the effectiveness of different management options. Models offering more information regarding the benefits of management options like water storage structures may better enable regional stakeholders to select and promote incentivized management scenarios that address the region's issues and benefit all parties involved.

2: Methods

This study used a calibrated 2012 SWAT model to estimate the stream flow alterations offered by WRS implementation scenarios in the Le Sueur watershed. SWAT is a theoretical, semi-distributed, and actively used and updated watershed-scale hydrological model. A 30-subbasin SWAT model was used in this study, but results from the 30-subbasin model were compared to both gauging records and a later generation of the model using 175 subbasins. Information regarding the setup of each model is presented in Appendix A. The 175-subbasin SWAT model offers a significantly higher performance, but this highly-resolved model was not built when this study began and

such a high resolution can hinder the convenient use of SWAT's subbasin-level wetlands. Each simulation with the 30-subbasin model began in 1980 and ended in 2009; output was not recorded for the first five years in order to allow the model to adjust from the initial conditions. Data from this 30-subbasin model were compared with those from gauging records and the 175-subbasin model for 2006-2009, as data from each source were only available for this period.

SWAT output was used to assess reductions in both peak flows and the amount of time spent above certain discharge thresholds. Such output was also combined with relationships developed from gauging data to determine the effects of peak flow reduction on sediment loading from the knickzone within the lower watershed. The 435 WRS implementation scenarios presented here were used to create a simplified model

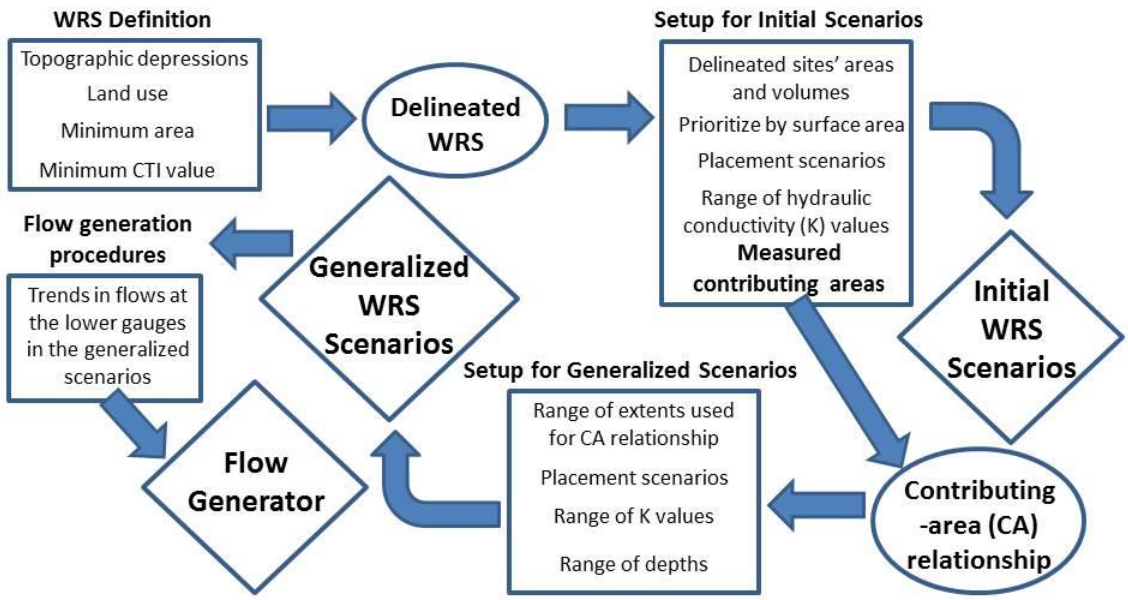

Figure 4. Flow chart showing the methodology employed in this study.

capable of generating peak flow and sediment-loading rates in the lower reaches of the Le Sueur watershed. The steps involved in producing this study's results and the simplified model are shown in Figure 4; the following sections detail each of these steps.

2.1: SWAT's wetlands

SWAT's subbasin-level wetlands are used in this study to simulate the WRS. The following description of SWAT's wetlands largely paraphrases the SWAT theoretical documentation created by Neitsch et al. (2009); a more general overview of SWAT's hydrological functions is presented in Appendix B. SWAT's reservoirs, ponds, and potholes are not used, as the reservoirs are located on the main channel network, receiving water from upstream reaches; ponds change their outflow to pursue a targeted storage volume; and potholes are identified as individual Hydrologic Response Units (HRU). The WRS in this study are not always meant to be located on the channel network itself, and must be able to freely alter their storages. The use of HRU-level potholes would require rebuilding the model for every scenario, rather than simply adjusting the subbasin-level inputs required for wetlands.

The water balance of wetlands in SWAT is simulated as:

$$V_f = V_i + V_{flowin} - V_{flowout} + V_{pcp} - V_{evap} - V_{seep} \quad (1)$$

where V_f is the volume of water at the end of the day (m^3 H_2O), V_i is the volume of water at the beginning of the day (m^3 H_2O), V_{flowin} is the volume of water flowing into the wetland (from surficial runoff, groundwater, and lateral flow) during the day (m^3 H_2O), V_{pcp} is the volume of direct precipitation during the day (m^3 H_2O), V_{evap} is the

volume of water evaporated during the day (m^3 H_2O), and V_{seep} is the volume of water lost through seepage during the day (m^3 H_2O). See Neitsch et al. (2009) for the equations used to solve each variable in Equation 1.

Outflow from wetlands through spilling and surface runoff occurs when the water volume exceeds the normal storage volume and is calculated as:

$$\text{If } V < V_{nor}, \quad V_{flowout} = 0 \tag{2}$$

$$\text{If } V_{nor} \leq V \leq V_{mx}, \quad V_{flowout} = \frac{V - V_{nor}}{10} \tag{3}$$

$$\text{If } V > V_{mx}, \quad V_{flowout} = V - V_{mx} \tag{4}$$

where V is the volume of water stored in the wetland (m^3 H_20), V_{nor} is the volume of water in the wetland when filled to the normal water level (m^3 H_2O), V_{mx} is the volume of water in the wetland when filled to the maximum water level (m^3 H_2O), and $V_{flowout}$ is the volume discharged from the wetland during the day (m^3 H_2O). Note that outflow begins when wetlands exceed their normal storage volumes, but this outflow occurs at one tenth of the difference between the current volume and the normal storage volume. When wetlands exceed their maximum storage volumes, all of the excess volume is released. Defining different spilling thresholds for numerous, hypothetical water bodies would involve a great deal of uncertainty. It is also doubtful that sites could always be constructed to guarantee the outflow relationship shown in Equation 3. This study therefore takes the normal and maximum water levels to be equal to each other, so that any excess water is simply spilled (i.e., only Equations 2 and 4 are used).

Certain scenarios using lower spilling thresholds (90% of the maximum capacity) are evaluated and compared with scenarios using the maximum capacity as the threshold; this comparison is discussed below in section 2.7. Using a lower spilling threshold and the relationship depicted in Equation 3 tends to provide greater peak flow reductions; sites can spill without exceeding their maximum storage, losing more water and having more storage to fill during the next precipitation event. The peak flow reductions presented in this study may therefore be conservative relative to similar SWAT scenarios employing a lower spilling threshold.

Wetland behavior in SWAT is considerably sensitive to the hydraulic conductivity (K) used to solve the V_{seep} term in Equation 2. The uplands of the Le Sueur watershed are dominated by glacial moraine and lacustrine sediments, as glacial Lake Minnesota covered the western two-thirds of the Le Sueur watershed and left up to 3 m of flat-lying glaciolacustrine silts and clays (Gran et al., 2013). These sediments offer quite low K values, providing water-logged soils that can inhibit crop growth without artificial drainage. Saturated K values obtained from Soil Survey Geographic database (SSURGO) layers are generally on the order of 1E-6 to 1E-5 m/s in the agricultural uplands of the Le Sueur watershed (Figures 5 and 6). Due to the abundance of silts and clays, the highly variable nature of K over both space and time, the possible accumulation of fine sediment in the sites, and the fact that seepage calculations for SWAT's wetlands do not consider hydraulic gradients, the scenarios considered in this study use K values within a range of 1E-9 to 1E-6 m/s. Table 1 shows the values used for each scenario.

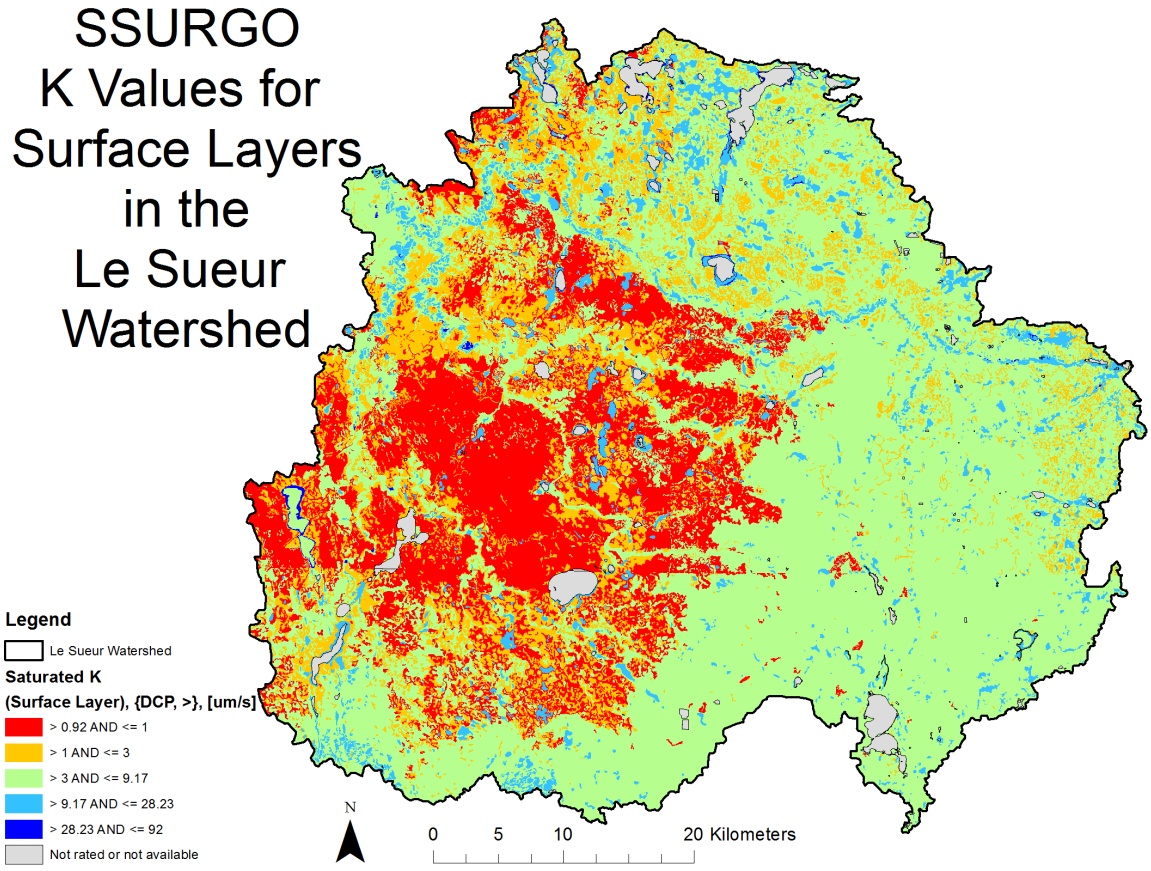

Figure 5. SSURGO saturated K values (10^{-6} m/s; um/s in legend) for surface soil layers in the Le Sueur watershed.

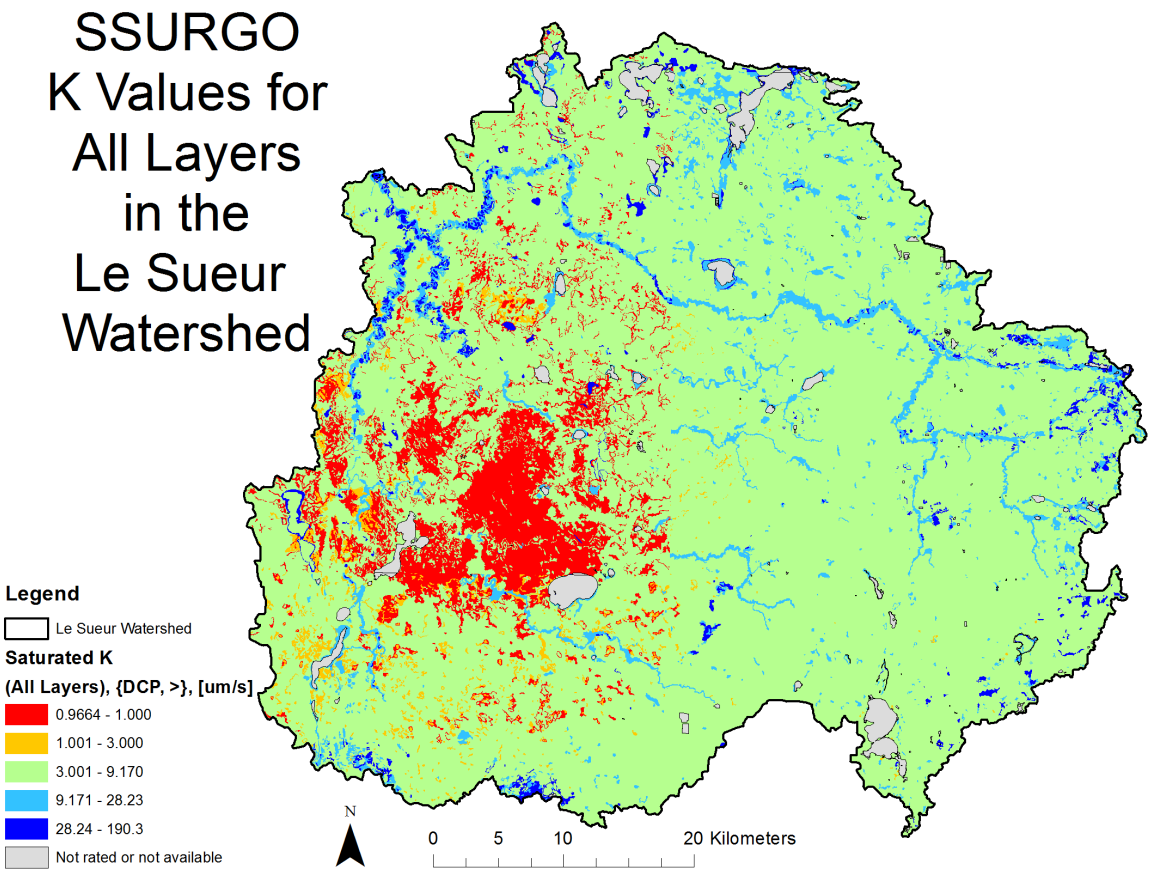

Figure 6. SSURGO saturated K values (10^{-6} m/s; um/s in legend) for all soil layers in the Le Sueur watershed. The labeling system used in Figure 5 is used here to allow for comparison.

Table 1. Parameter spaces considered and the bins used to assess peak flow volumes in both initial and generalized WRS implementation scenarios.

Variable	Initial Scenarios	Generalized Scenarios
Hydraulic Conductivity (m/s)	1E-9, 1E-8, 5E-8, 1E-7, 2.5E-7, 5E-7, and 1E-6	1E-8, 1E-7, and 1E-6
Depth (m)	Existing depression depths	0.5, 1, and 2
Extents	Top 5, 10, 20, 30, 33, 40, 46, 50, and 60% of sites by surface area (considering all sites in the watershed) as well as the full extent (100%)	0.5, 1, 2, 4, and 7.5% of the zone(s) used
Placement Scenarios	All Zones, Zone 1, and Zones 2 and 3	All Zones, Zone 1, Zone 2, Zone 3, and Zones 2 and 3
Bins for peak flows	Bins defined by exceedance probability for the flows over 0.01 $m^3/s/km^2$: 0-25, 25-50, 50-75, 75-90, 90-95, 95-97.5, 97.5-99, 99.5-99.75, 99.75-100%	Bins begin at 0.01 $m^3/s/km^2$ and are spaced every 0.0025 $m^3/s/km^2$

Although K values are presented in this study in m/s (e.g., Table 1), SWAT takes inputs for wetlands' K values in mm/hr. Despite this study's focus on units of m/s, SWAT inputs for K values were used as mm/hr (e.g., 1E-7 m/s as 0.36 mm/hr).

The coefficient used to scale the actual evaporation relative to the potential evaporation was set to one here, rather than the default value of 0.6. This decision was motivated in part by the lack of simulated plants within SWAT's wetlands. The differences in wetland behavior caused by this adjustment are slight and only noticeable when K values are relatively low (i.e., 1E-9 to 1E-8 m/s).

The contributing areas of all wetlands within a subbasin are lumped together and treated with the "WET_FR" input parameter (contributing area to all wetlands in

the subbasin/subbasin area), which is used in the solving of the V_{flowin} parameter in Equation 2. Despite the parameter's significant influence on wetland behavior, many studies employing wetlands in SWAT do not provide clear explanations regarding how contributing areas were defined. For example, Martinez-Martinez et al. (2014) used the approach of Wang et al. (2010) by assuming that half of the area remaining in a subbasin after removing the maximum wetland extent drain into the wetlands. Even if Wang et al. (2010) had data supporting such a relationship, Martinez-Martinez (2014) did not present any such data for their study area. Wang et al. (2008) assumed that the contributing area of each subbasin's wetlands was the ratio of the wetland area to subbasin area times the subbasin area. This approach only considers the area of the wetlands themselves, possibly providing a severe underestimation. Here, contributing areas were defined by manually measuring the flow accumulation values occurring at the farthest downstream outlets of the WRS. These values were then used to solve for the WET_FR parameter as:

$$WET\_FR = \frac{(\sum FlwAcc_{downstream\ outlets}) - SA_{WRS}}{Subbasin\ Area} \quad (5)$$

where *WET_FR* is the lumped contributing area of all wetlands as a fraction of the subbasin area, $\Sigma FlwAcc_{downstream\ outlets}$ is the sum of all flow accumulation values (m^2) occurring at the furthest downstream outlets of all the WRS used in a single subbasin (i.e., all locations where flow accumulation paths exit the WRS and these paths do not lead to other WRS further downstream), SA_{WRS} is the total surface area (m^2) of the WRS

used in the subbasin, and *Subbasin Area* is the area (m^2) of the subbasin. Manually measuring the flow accumulation values can certainly be time-consuming, but it provides an objective portrayal of the sites' contributing areas. Measured contributing areas were also used to define generalized relationships between sites' surface and contributing areas; the creation of this relationship is described in section 2.5.

2.2: WRS Definition

The WRS used here are defined as (1) topographic depressions defined by the difference between filled and unfilled 9-meter digital elevation models (DEM) with (2) specific land use types defined by NLCD 2011 layers (only barren land, cultivated cropland, hay/pasture, and herbaceous from NLCD 2011), (3) relatively high compound topographic index (CTI) values, (4) areas over 3,000 m^2, and areas not featuring either (5) sites from the Fish and Wildlife Service's CONUS wetland inventory or (6) current conservation easements. Figure 7 shows the resulting population; sites are colored by flow length classes (FLC) representing proximity to the watershed outlet (i.e., FLC 1 is farthest, FLC 6 is closest). The minimum area was selected in order to limit the number of widely-distributed small sites, as farmers do not want such sites to act as obstacles for their equipment. CTI values are solved as (Babbar-Sebens et al., 2013):

$$CTI = \ln\left(\frac{(flwacc+1)*cell\ size}{slope * \frac{\pi}{180}}\right) \quad (6)$$

where *flwacc* is flow accumulation from ArcGIS in m^2, *cell size* is the raster resolution (81 m^2 raster, which was resampled from a 9 m^2 raster), and *slope* is the slope value in

degrees. All sites have average CTI values over 11.5, as other authors have employed this value as a threshold (e.g., Babbar-Sebens et al., 2013). Each site's volume is defined as the surface area multiplied by the average depression depth.

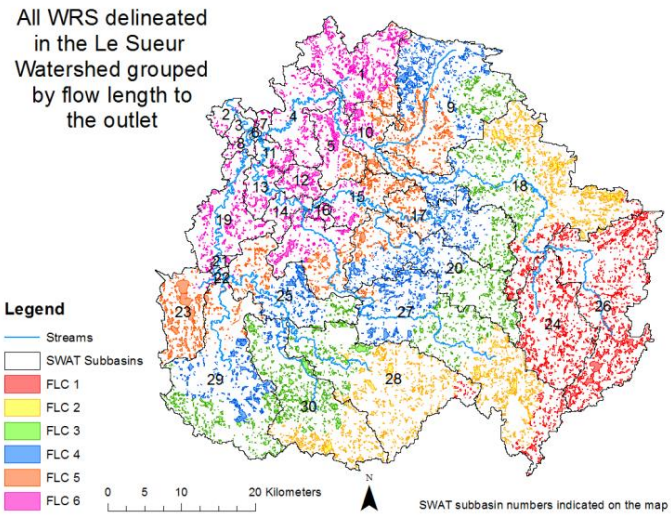

Figure 7. All water retention sites (WRS) delineated in the Le Sueur Watershed grouped into flow length classes (FLC) reflecting the sites' average flow lengths to the outlet. FLC 1 is furthest from the outlet while FLC 6 is closest to the outlet. FLC are shown to demonstrate the sites' general proximity to the watershed outlet, which was used to group the subbasins into zones.

2.3: WRS Implementation Scenarios

WRS implementation scenarios were created according to combinations of prioritization schemes and different placement and hydraulic conductivity scenarios. Prioritization schemes define the selections of WRS for different extents; low extents use only the sites defined as most desirable, while higher extents add sites that are defined as less desirable. While many prioritization schemes were considered (e.g., selection by soil class, proximity to existing wetlands, or land value), most of these schemes either did not allow for convenience in scenario creation (e.g., each scenario's contributing areas can be defined relative to those measured for another scenario) or

were burdened by too many social considerations (i.e., criteria pertinent to individual preferences or economics, rather than site performance). Prioritization by site surface area was chosen for its simplicity and offering of scenarios that build upon each other. Both small and large site prioritizations were considered here. WRS implementation on relatively small sites may be more realistic, as large sites may cover too many properties (i.e., adding complications related to property ownership and land acquisition); while implementation on large sites would offer greater storage volumes (large sites tend to have greater depression depths) and fewer obstacles for farmers.

Placement scenarios were defined by grouping subbasins based on their general proximity to the watershed outlet; Figure 8 shows the three groups used as placement zones. The upper half of the watershed is defined as zone 1, while the lower half is divided into zones 2 and 3, with zone 3 being the closest to the outlet. Zone 1, zone 2, and zone 3 have areas of 657.1, 223.2, and 284.4 km^2 in the Le Sueur subwatershed; 376.5, 273.2, and 133.2 km^2 in the Cobb subwatershed; and 397.7, 394.5, and 95.22 km^2 in the Maple subwatershed. Subbasin 27 is included in zone 1 even though it extends farther down in the watershed. Much of this subbasin is composed of the farthest upstream reaches of the Cobb subwatershed, however, and zone definition by flow length to the outlet is only relative here and limited by the model's existing subbasin delineation.

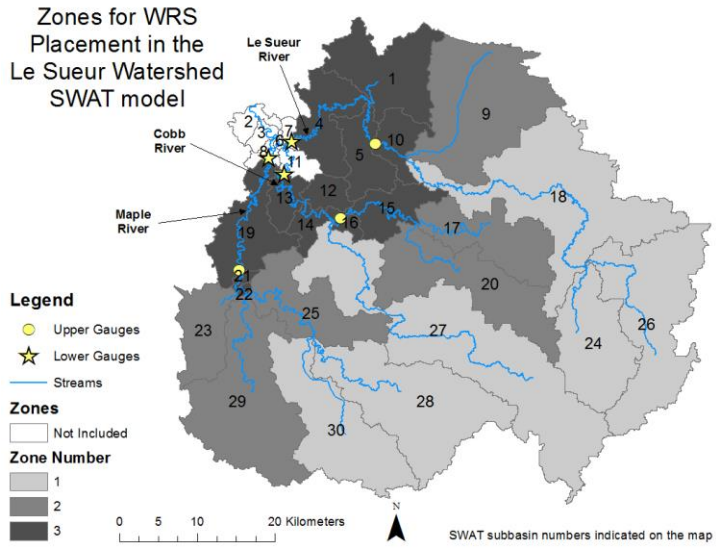

Figure 8. Map showing the zones used for the different WRS placement scenarios in the Le Sueur Watershed. The watershed is divided into the Le Sueur, Cobb, and Maple subwatersheds that are defined by the subbasins upstream of subbasins 4, 13, and 19, respectively.

WRS implementation scenarios were divided into two groups: initial and generalized. The initial WRS scenarios use the actual WRS sites delineated to define the surface areas, volumes, and contributing areas for the WRS used. Generalized scenarios do not use the sites delineated, instead using generalized relationships between WRS area and contributing area as well as a range of design depths. These generalized scenarios and the contributing-area relationship used to create them are discussed in section 2.5.

Table 1 shows the variables considered (K, design depth, WRS extent, and site placement) in both the initial and generalized WRS scenarios. Although small site prioritizations were also assessed, the results for such scenarios are not presented here due to issues with SWAT's portrayal of such sites; initial WRS scenarios only use large

site prioritizations, while generalized scenarios use contributing-area relationships identified in large site prioritizations.

2.4: Scenario Assessment

There are 8 gauges in the Le Sueur watershed, and discharges occurring at three of these gauges (the stars in Figure 8) were used in the assessment of peak flows. The Le Sueur, Cobb, and Maple Rivers each have two gauges, with one located just upstream of the watershed's knickzone and another just upstream of the mouth of each river. These pairs of gauges are referred to here as the upper and lower gauges. One gauge is located at the mouth of Beauford Ditch, a tributary to the Cobb River (outlet of subbasin 12 in Figure 8), while another gauge is located at the watershed's outlet. The yellow circles and stars shown in Figure 8 represent the upper and lower gauges, respectively, on each of the three major rivers in the watershed (Le Sueur, Cobb, and Maple). Discharges at the lower gauges are assessed for peak flows and used for sediment loading relationships described below. The small subbasins downstream of the lower gauges are not included in the zones shown in Figure 8, but peak flow reductions in the generalized WRS scenarios are evaluated at the watershed outlet in subbasin 2.

Rivers within the Minnesota River Basin experience a sharp increase in sediment loading from gauges located above the knickzone to gauges downstream of or within the knickzone, reflecting the erosion of near-channel features like bluffs within the knickzone. Se Jong Cho (John Hopkins University) developed an empirical relationship between discharge occurring at the lower gauges and sediment-loading rates for the

reaches between the upper and lower gauges on multiple rivers within the Minnesota River Basin (Le Sueur, Cobb, Maple, and Rush Rivers as well as Seven Mile and High Island Creeks). Such reaches within the Le Sueur watershed are referred to here as the gauged reaches. The upper gauges are located above each river's knickzone, while the lower gauges are within or below the knickzone and just upstream of a confluence.

The relationship developed by Cho was based on observations of differences in measurements of total suspended sediment (TSS) between the gauges. Such differences in TSS were used to calculate the sediment contribution from near-channel features as:

$$Q_{sNCS} = Q_{sLG} - Q_{sUG} - \left(Q_{sUG}\frac{A_{side}}{A_{UG}}\right) \quad (7)$$

where Q_{sNCS} is the sediment contributed from near-channel sources along the gauged reach (Mg/day), Q_{sLG} and Q_{sUG} are the sediment sampled at the lower and upper gauges (Mg/day), respectively, A_{side} is the area of uplands that drain into the channel between the two gauges (km^2), and A_{UG} is the watershed area above the upper gauge (km^2). Only pairs of TSS measurements taken within 60 minutes of each other at upper and lower gauges were used. The sediment-loading rate sampled at the upper gauge (Q_{sUG}) is dominated by the low relief, agricultural uplands, and scaling this rate down to the upland area represented by the A_{side} variable helps to account for the upland sediment that enters each river between its upper and lower gauges. The resulting differences in sediment are further reduced by a factor reflecting the proportion of sediment added by

bluffs within the corresponding subwatershed's knickzone (62, 65, and 69% in the Le Sueur, Cobb, and Maple; average proportion used for the gauged reaches on the Rush River, Seven Mile Creek, and High Island Creek), which was determined by Belmont et al. (2011). Values are then normalized by the length of active bluffs along the gauged reach (i.e., those in contact with the channel). Since active bluff lengths were not available for the gauged reaches on Seven Mile Creek, High Island Creek, and Rush River, the average percent length of bluffs along the Le Sueur, Cobb, and Maple Rivers' gauged reaches were applied to the reaches.

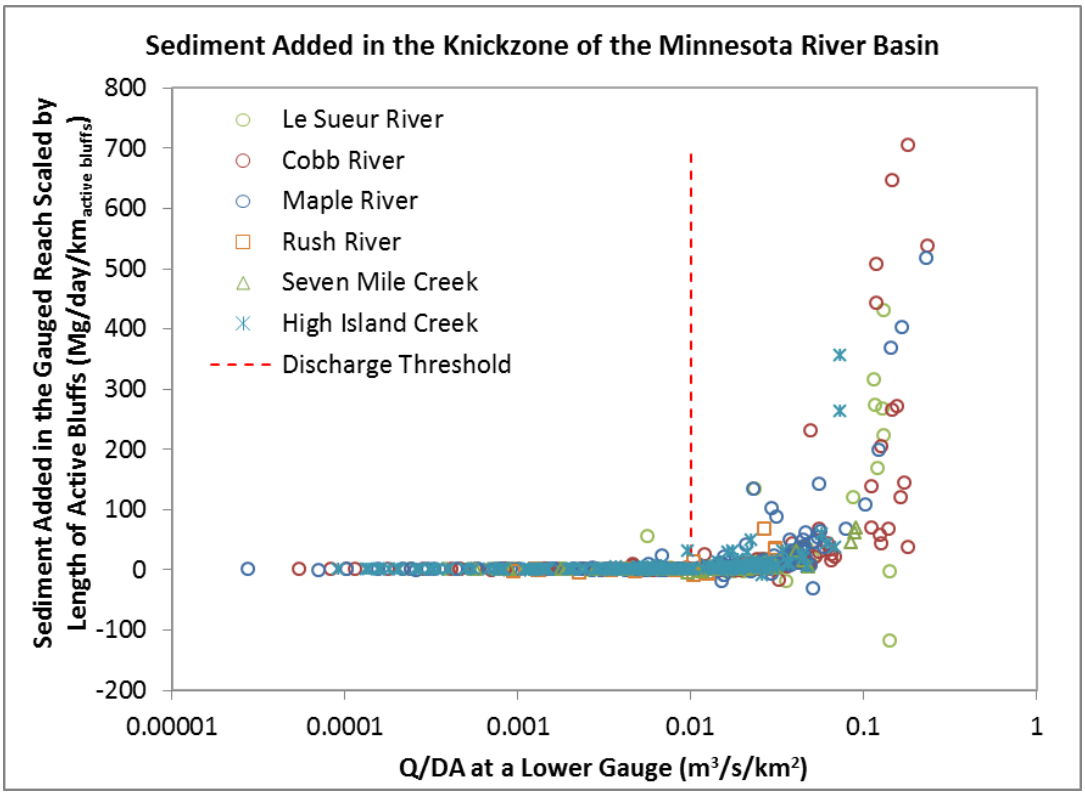

Figure 9. Differences per unit of active bluff length in the sediment sampled at a lower gauge within the knickzone and that sampled at an upper gauge above the knickzone for different discharge per unit area values. The sediment added within these gauged reaches tends to increase abruptly over a threshold of 0.01 $m^3/s/km^2$. The data above this threshold yield the relationship depicted by Equation 8.

Figure 9 shows the relationship developed by Cho; the x-axis represents discharge per unit area ("Q/DA") at a lower gauge, where discharge is derived from 15-minute data, while the y-axis represents the difference in sediment sampled Q_{sNCS} scaled by the length of active bluffs along the reach (Mg/day/$km_{active\ bluffs}$). This scaled difference is zero for lower discharge values; the gauged reaches do not act as net sources of sediment. At high discharge values, however, the difference increases abruptly, indicating that more sediment is leaving the gauged reaches than entering them in a manner inconsistent with the increase in drainage area between the gauges. During these peak flows, material deposited at bluff toes from previous failures is carried away and further failures are induced. Keeping the discharges entering the knickzones beneath the threshold at which the increase occurs may aid in reducing sediment-loading rates within the knickzones. A power function was fit to the data with Q/DA values above a threshold of 0.01 $m^3/s/km^2$ (0.864 mm/day), yielding:

$$S = \alpha\left(\frac{Q}{DA}\right)^{\beta} \quad (8)$$

where *S* is the sediment added in the incised zone scaled by active bluff length along the reach (Mg/day/$km_{active\ bluffs}$), *Q* is discharge ($m^3/s/km^2$) at a lower gauge, *D*A is drainage area (km^2) at a lower gauge, and both α and β are constants taken here as 19953 and 2.18, respectively. These constants are based on all available Q and TSS data available through 2011. To determine average annual sediment-loading rates for the gauged reaches, this relationship was applied to all flows over the threshold at the lower gauges, multiplying each resulting *S* value by the length of active bluffs along the reach (16.54, 10.52, and 14.75 km for the Le Sueur, Cobb, and Maple Rivers' gauged reaches,

respectively; Bevis, 2015), summing the resulting values, and dividing the sum by the number of years assessed (here, 25 years). This average annual sediment-loading rate is then normalized by the rate in the baseline scenario and hereafter referred to as *S'*, with a subscript denoting the location (i.e., S_T' for the total of all three lower gauges, S_L' for the Le Sueur, S_C' for the Cobb, and S_M' for the Maple). All Q/DA values exceeding the threshold of 0.01 $m^3/s/km^2$ at the lower gauges are referred to here as "peak flows," and the exceedance probabilities for this threshold at the lower gauges in the model and gauging records were evaluated.

Changes in peak flows for the initial WRS scenarios were assessed by dividing all discharge values exceeding 0.01 $m^3/s/km^2$ and occurring at the three lower gauges into groups defined by exceedance probabilities within the population of flows above the threshold. The ranges of exceedance probabilities used to define the discharge bins in these initial WRS scenarios are shown in Table 1. The highest flows were divided more finely in order to limit the standard deviations of each group. The volumes of each group (average discharge value multiplied by the number of days within the group) were then summed to provide a total volume of water occurring over the discharge threshold. These total volumes can then be evaluated as a fraction of the total volume in the baseline scenario (i.e., no WRS implemented) in order to express reductions in peak flows offered by WRS. This fraction is hereafter referred to as *V'*, with a subscript denoting the location (i.e., V_T' for the total of all three lower gauges, V_L' for Le Sueur, V_C' for Cobb, and V_M' for Maple).

2.5: Generalized Contributing-Area Relationships and Generalized Scenarios

The contributing areas measured for the initial WRS scenarios were used to define a generalized relationship between WRS area and contributing area. The generalized contributing-area relationship was then used to create WRS implementation scenarios that do not employ specific sites; contributing areas were defined as multiples of the WRS area. To create this relationship, the WRS extent of each subbasin in each initial WRS scenario was assessed against the corresponding "treated area," the sum of the WRS and contributing areas, as a fraction of the subbasin area. Treated areas were used rather than contributing areas because they provide much clearer trends; small sites can have the same treated area values as large sites if these sites share the same outlets. The data used only included values from large-site prioritization schemes due to observations of problematic trends in values for small-site prioritizations. Contributing-area relationships were examined for different types of subbasins: those without other subbasins further upstream (e.g., 1, 27, and 28 in Figure 8) and those with other subbasins further upstream (e.g., 4, 15, and 25 in Figure 8). These selections were used because WRS were often located on the main channels of subbasins without other subbasins further upstream, causing such sites to drain the entire subbasin. In contrast, sites never occurred on the main channels of subbasins with other subbasins further upstream. This distinction in site location relative to the channel network was not enforced, instead emerging from the subbasin delineation already constructed.

Extents for these generalized scenarios were taken as 0.5, 1, 2, 4, and 7.5% of each subbasin's area (Table 1), and within the specified zone(s) composed by selections of these subbasins. These extents were selected due to the range of values allowed by the contributing-area relationship used. While the initial WRS scenarios define volumes by existing depression depths, these generalized scenarios instead define volumes by different design depths (0.5, 1, and 2 m). Only hydraulic conductivity values of 1E-8, 1E-7, and 1E-6 m/s were used for these scenarios based on observations from initial WRS scenarios.

Although the analyses of these scenarios employ the same sediment-loading rates assessment methods described in Section 2.4, peak flows themselves are evaluated differently. Instead of defining groups by exceedance probability, Q/DA values were separated into bins by thresholds starting at 0.01 $m^3/s/km^2$ and spaced every 0.0025 $m^3/s/km^2$. This binned approach was selected because it offers symmetrical group structures, severely limits the standard deviations of each group, and was also used for the creation of an empirical method for generating peak flows for generalized WRS scenarios. The methods used for assessing peak flow reductions in the initial WRS scenarios yield almost exactly the same results, and were not used for flow generation procedures requiring binned flows.

2.6: Flow Generation

Relationships between frequencies of discharge values and WRS extent in generalized WRS scenarios were used to create a method for generating peak flows for

arbitrary WRS extents in any of the 225 generalized WRS scenarios assessed (Table 1). The methods described in section 2.4 for evaluating sediment-loading rates at a lower gauge could then be applied to the generated flows. Q/DA values for generalized WRS scenarios were separated into bins by thresholds starting at 0.01 $m^3/s/km^2$ and spaced every 0.0025 $m^3/s/km^2$, as described above. These binned flows were then divided into three ranges: 0.01 to 0.05 $m^3/s/km^2$, 0.04 to 0.1 $m^3/s/km^2$, and 0.06 $m^3/s/km^2$ to the maximum value achieved. Ranges overlap in order to increase the continuity between the different sections' regressions. Q/DA values were normalized by the corresponding lower gauge's maximum value in the baseline scenario and exponential regressions were fit to the data. Each regression takes the form:

$$F = \gamma e^{\delta} \tag{9}$$

where F is the average frequency (days per year) of a specific normalized Q/DA value at a lower gauge, and γ and δ are constants. The F values of each WRS implementation scenario (F_{WRS}) were then normalized by the F value for the corresponding normalized Q/DA value in the baseline scenario ($F_{baseline}$). The data yielded by this process show how the frequencies of specific Q/DA values change, relative to the baseline frequencies, at different WRS extents. Appendix C presents examples of different scenarios' F values, and how these values are used in the flow generation procedures discussed below.

Linear regressions of moving averages of $F_{WRS}/F_{baseline}$ values versus WRS extent as a fraction of the watershed area (for the Le Sueur, Cobb, and Maple subwatersheds individually) were then used to predict Q/DA values occurring at the lower gauges.

Averages of $F_{WRS}/F_{baseline}$ were taken for moving windows of 3 bins, only considering bins with values. Linear regressions of these average $F_{WRS}/F_{baseline}$ values versus WRS extent used fixed intercepts, so that the baseline value is always preserved as the starting point. The frequency of each discharge value for a WRS extent was then solved as:

$$F_{WRS} = \left(m_F \frac{A_{WRS}}{A_{Watershed}}\right) F_{baseline} \quad (10)$$

where F_{WRS} is the frequency (days per year) for a certain Q/DA bin average, m_F is the slope of the linear regression of $F_{WRS}/F_{baseline}$ values versus WRS extent, A_{WRS} and $A_{Watershed}$ are the areas (m^2) of the WRS employed and subwatershed considered, and $F_{baseline}$ is the frequency (days per year) of the discharge value in the baseline scenario. The maximum Q/DA achieved was also predicted as:

$$\left(\frac{Q}{DA}\right)_{max} = \left(m_Q \frac{A_{WRS}}{A_{Watershed}}\right)\left(\frac{Q}{DA}\right)_{baseline\ max} \quad (11)$$

where $(Q/DA)_{max}$ is the maximum discharge per unit area achieved for the input WRS extent, $(Q/DA)_{baseline\ max}$ is the maximum discharge per unit area achieved for the corresponding lower gauge in the baseline scenario, and m_Q is the slope of the linear regression of $(Q/DA_{max})/(Q/DA_{baseline\ max})$ versus WRS extent as a fraction of the watershed area. A fixed intercept is also maintained for this relationship, so that the baseline scenario is always the starting point. WRS scenarios can decrease the maximum discharges achieved, and Equation 11 was used to dictate the maximum Q/DA at which the prediction of frequency values would cease. Although some WRS implementation scenarios, such as those using K = 1E-8 m/s, produced discharges at the lower gauges

exceeding the maximum values in the baseline value, the data generation procedures used here cannot project frequencies for Q/DA values higher than the maximum Q/DA in the baseline scenario.

2.7: Assessment of Lower Spilling Thresholds

The lower spilling thresholds available for SWAT's wetlands are not used in this study; sites only overflow when their maximum capacity is exceeded (see section 2.1). The lower and maximum spilling thresholds available can be considered principal and emergency spillways, and the use of lower thresholds allows sites to spill through overland flow at a rate that decays as the volume approaches the lower threshold (see Equation 3). Although all initial and generalized WRS scenarios use only the maximum capacity as a spilling threshold, a selection of generalized scenarios were redone with a lower a spilling threshold to demonstrate the resulting effects. The scenarios considered use all zones, depths of 1 meter, K values of 1E-8, 1E-7, and 1E-6 m/s, and lower spilling thresholds of 90% of the maximum capacities. Details of the site design required to achieve the relationship portrayed by Equation 3 are beyond the scope of this study, and it is assumed that the hypothetical sites begin spilling at 90% of their maximum capacities. The 90% threshold was selected so that sites could not maintain too much water above a spilling threshold.

3: Results

The results presented below show that WRS implementation can decrease peak flow and sediment-loading rates in the lower reaches of the Le Sueur watershed. These reductions are provided at different rates for different scenarios, with WRS placement in certain zones being more effective at reducing peak flows. WRS characteristics like design depth and the K value of the site bottoms do influence peak flows in the lower watershed. Results from generalized WRS scenarios were used to create a simplified empirical model capable of instantly reproducing the generalized scenarios' results. Before the results of the initial WRS scenarios, generalized WRS scenarios, and flow generation procedures are presented, however, the performance of the 30-subbasin SWAT model is examined in relation to that of the 175-subbaisn SWAT model described in Appendix A and the gauge records themselves.

Figure 10 shows both the gauged and SWAT-predicted flows at the outlet of the Le Sueur watershed. The seasonal performance of the 30-subbasin model at the watershed outlet is presented in Appendix D. The 30-subbasin SWAT model under-predicts the lower 90% of flows at the outlet, with the bottom 30% of flows dropping to zero. The need for the model to capture peak flows seems to have made the watershed so "flashy" that the stream flow goes to zero with greater frequency, especially during the summer and fall (i.e., July-October). Despite these issues, this study only considers the peak flows occurring in the lower watershed. Table 2 shows the exceedance

probabilities for the threshold of 0.01 $m^3/s/km^2$ at the lower gauges and watershed outlet in the 30-subbasin model, 175-subbasin model, and gauging records. Exceedance probabilities for the threshold at the lower gauges and watershed outlet range from 16 to 26% (Table 2). Although this threshold is not used for the assessment of flows at the outlet, exceedance probabilities at the outlet are presented for greater context. While the 30-subbasin model over-predicts the upper 10% of flows at the outlet, the upper 30% of flows at the outlet are relatively similar to the gauged flows. The 175-subbasin SWAT model provided a better representation of base flows than the 30-subbasin model used here (Figure 11), but the peak flows in each model are more similar.

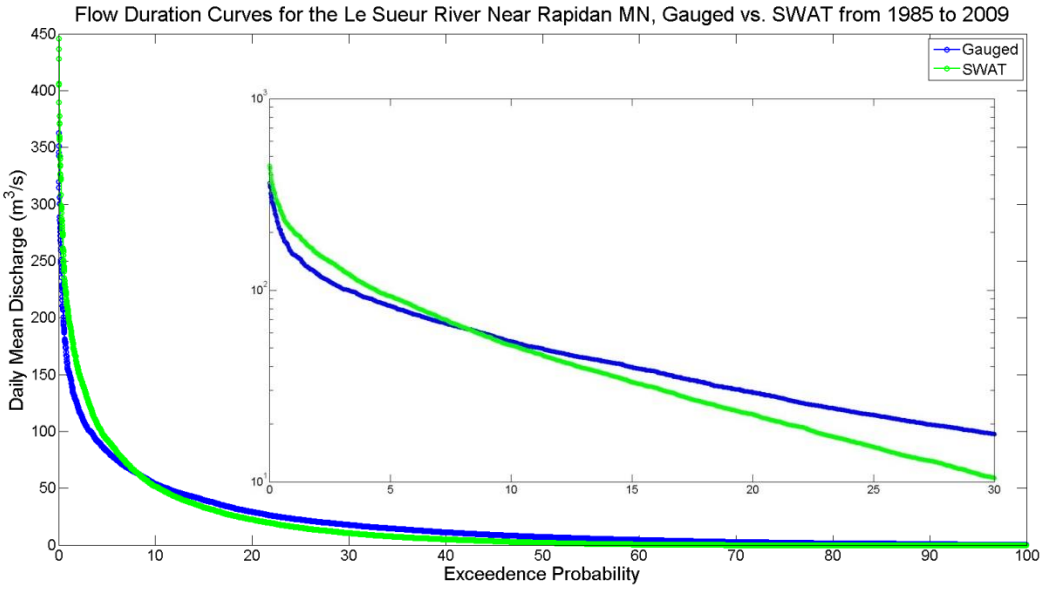

Figure 10. Flow duration curves for gauged and SWAT-predicted flows at the outlet of the Le Sueur Watershed. The 30 subbasin SWAT model used here under-predicts the bottom 90% of flows, but over-predicts the top 8%.

Table 2. Exceedance probabilities for the threshold of 0.01 $m^3/s/km^2$ in the gauging records and different baseline simulations employing the 30 and 175 subbasin ("S.") models.

Location	30 S. Model, 1985-2009	30 S. Model, 2006-2009	175 S. Model, 2006-2009	Gauging Records, 2006-2009
Le Sueur River Lower Gauge	19%	18%	16%	26%
Cobb River Lower Gauge	18%	19%	19%	23%
Maple River Lower Gauge	16%	16%	19%	20%
Watershed Outlet	17%	16%	17%	17%

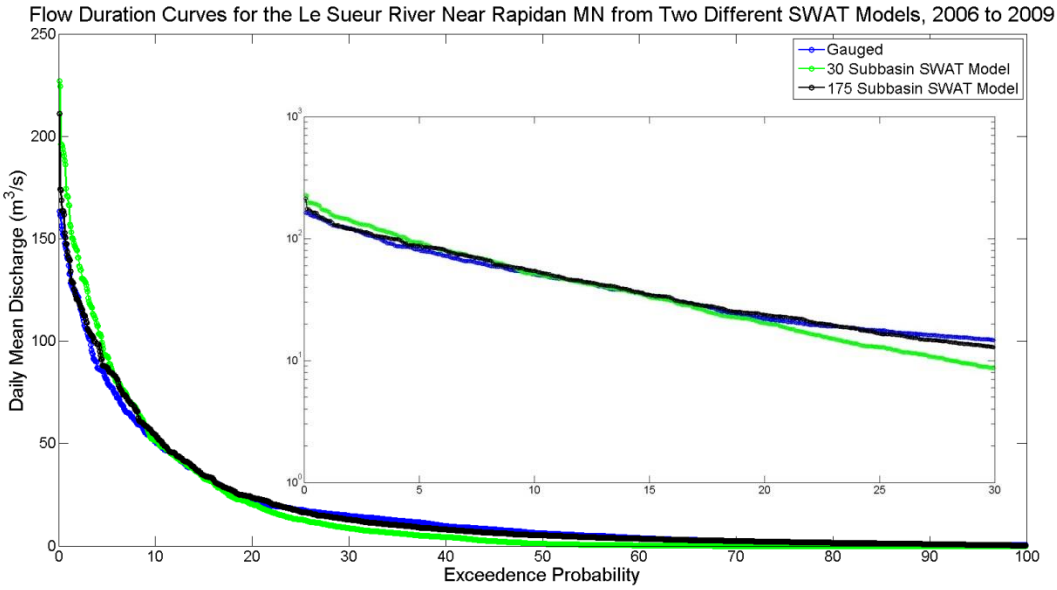

Figure 11. Flow duration curves for gauged flows and SWAT-predicted flows, from both the 30-subbasin model used here and a 175-subbasin model, at the outlet of the Le Sueur Watershed from 2006 to 2009. These three different sources of data were used to obtain the sediment-loading rates and peak flow volumes show in Table 2.

Sediment-loading rates for the gauged reaches of the Le Sueur, Cobb, and Maple Rivers in the baseline scenario, derived through the application of Equation 8 to SWAT output, are presented in Table 3. Each value's percent error relative to the corresponding sediment-loading rates derived from the sediment budget created by

Table 3. Sediment-loading rates obtained for each river's gauged reach (Figure 8) from the application of Equation 8 to all flows over the threshold of 0.01 $m^3/s/km^2$. "Actual" sediment-loading rates are the values provided by the sediment budget created by Bevis (2015).

River	Predicted Sediment-loading rate (Mg/yr)	Actual Sediment-loading rate (Mg/yr)	Percent Error
Le Sueur	1.71E+04	2.14E+04	20.1%
Cobb	1.17E+04	2.77E+04	57.7%
Maple	1.53E+04	1.92E+04	20.4%

Table 4. Sediment-loading rates for the gauged reaches and peak flow (i.e., Q/DA values exceeding the threshold of 0.01 $m^3/s/km^2$) volumes occurring at the lower gauges derived from discharges produced by the 30 subbasin SWAT model, 175 subbasin SWAT model, and gauging records for 2006-2009.

	River		
	Le Sueur	Cobb	Maple
30-subbasin model Sediment-loading rate (Mg/yr)	1.26E+04	9.28E+03	9.51E+03
30 Subbasin Rate/175 Subbasin Rate	2.16	1.04	0.90
30 Subbasin Rate/Rate from Gauging Records	2.15	1.64	1.22
30-subbasin model Peak Flow Volume (m^3)	1.83E+08	1.22E+08	1.18E+08
30 Subbasin Volume/175 Subbasin Volume	1.45	0.98	0.83
30 Subbasin Volume/Volume from Gauging Records	1.43	1.19	1.08

Bevis (2015) is also shown (21367, 27667, and 19233 Mg/yr for the gauged reaches of the Le Sueur, Cobb, and Maple, respectively).

Sediment-loading rates and peak flow volumes (i.e., volumes of flows exceeding the threshold of 0.01 $m^3/s/km^2$) were also assessed for 2006-2009 using three different sources of data: the 30-subbasin model used here, the 175-subbasin model, and the gauging records themselves (Figure 11). Table 4 presents these values. A period of 2006 to 2009 was considered, as data were available for all three sources during this period. While the gauging records are incomplete, they only lack data for winter months (i.e., varies but typically November through March) and always have data for the spring and early summer months that typically feature the highest peak flows (i.e., May and June).

The sediment-loading rates and peak flow volumes obtained for the Le Sueur River's lower gauge in the 30-subbasin model are considerably higher than the values derived from both the 175-subbasin model and the gauging records. The values for the Cobb River's lower gauge in the 30-subbasin model are also relatively high, while those for the Maple River's lower gauge are quite close to the values based on the other sources of data. Although the sediment-loading rates and peak flow volumes shown can differ by factors up to about 2 and 1.5, respectively, they do not differ by orders of magnitude. The changes in such values assessed here are mainly considered in relation to baseline values, however, and the model's performance from 2006 to 2009 may not be representative of its performance over the entire period considered in this study (1985-2009).

Figure 12 shows reductions in both the total volumes of water occurring over the threshold at all three lower gauges and associated reductions in near-channel sediment-loading rates of the gauged reaches achieved by initial WRS scenarios using all zones. Such surfaces are unique for each of the three rivers' lower gauges, and are shown in Appendix E. The Le Sueur River's surface achieves much lower values (e.g., minimum values of $V_L' = 0.36$ and $S_L' = 0.17$ instead of $V_T' = 0.46$ and $S_T' = 0.26$ in Figure 12) and has a stronger upwards concavity, while the Maple and Cobb River's surfaces do not achieve such low values (e.g., minimum values of $V_M' = 0.53$, $S_M = 0.31$, $V_C = 0.56$, and $S_C = 0.34$) and exhibit less upwards concavity.

Reductions for small-site prioritizations are not shown here due to complications regarding SWAT's treatment of wetlands. The maximum reduction achieved in Figure 12 was maintained in small-site prioritizations, for the highest K value, at much lower extents (i.e., 4% of the watershed area). The surface remained largely flat at lower extents because of problems with SWAT's portrayal of small sites, rather than small sites' greater effectiveness. Contributing areas did not decrease with decreasing WRS extent in small-site prioritizations as they do in large-site prioritizations because of SWAT's lumping of all sites within each subbasin. Small sites can achieve much higher contributing areas by being widely distributed throughout the subbasin, intercepting more of the subbasin's runoff. In contrast, large sites with the same total area are more concentrated within the subbasin, often receiving a lower fraction of the subbasin's runoff. Although individual small sites may be overwhelmed by disproportionately large contributing areas in reality, the sites in SWAT may not be overwhelmed easily because each can access the storages of other sites in the subbasin (i.e., only the total water volume for all sites is tracked, and a small site that would normally spill given large inputs will not if the total capacity is not exceeded). Even though SWAT does not portray such interactions explicitly, the implied redistribution of water amongst the sites is problematic. Large-site prioritizations were favored here because the use of fewer larger sites may aid in limiting the effects of the lumped wetlands in SWAT.

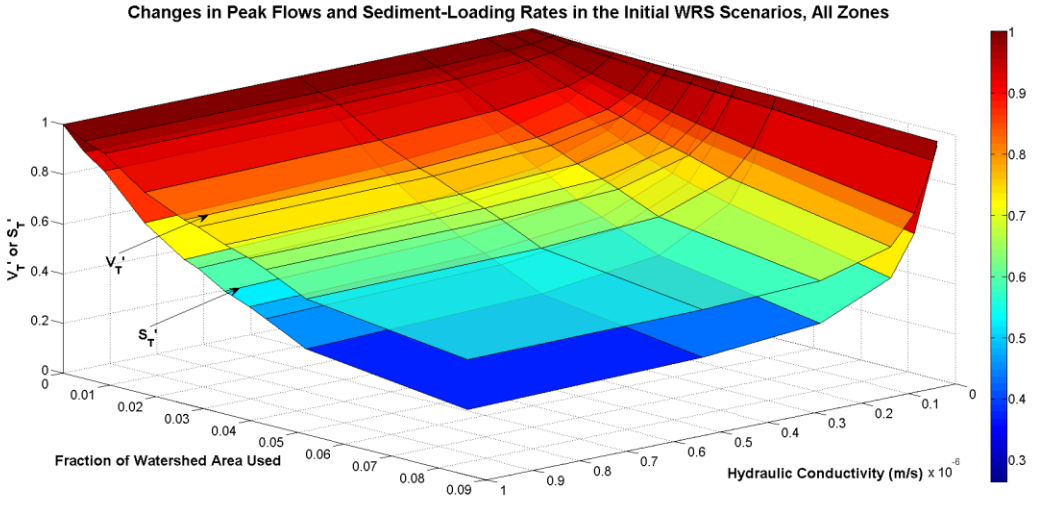

Figure 12. Changes in peak flow volumes at all three lower gauges normalized by the baseline total (V_T') and sediment-loading rates of all three gauged reaches normalized by the baseline rate (S_T') with both WRS extent and hydraulic conductivity. These initial WRS scenarios use all zones.

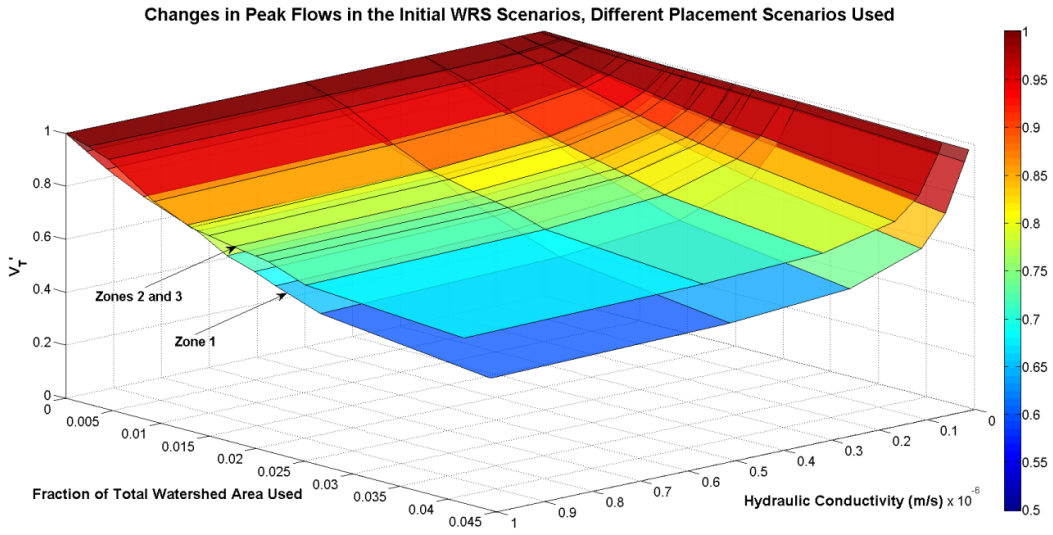

Figure 13. Changes in peak flow volumes at all three lower gauges normalized by the baseline total (V_T') with both WRS extent and hydraulic conductivity in scenarios using either zone 1 or zones 2 and 3.

Total volumes of water occurring over the discharge threshold at all three lower gauges differ when sites are placed in either the upper watershed (zone 1) or lower watershed (zones 2 and 3; Figure 13). The reductions offered by scenarios using zone 1 (farthest from the outlet) are almost always greater than those using zones 2 and 3 (closer to the outlet). Surfaces for each of the lower gauges are shown in Appendix E. The sediment-loading rate curves for these scenarios exhibit relationships with their corresponding total water curves that are similar to those shown in Figure 12. Each sediment curve features more upwards concavity, with total sediment-loading rates typically reaching lower values in scenarios using zone 1. Initial WRS scenarios using zone 1 tend to achieve higher reductions in part because sites can be placed directly onto the channel networks of subbasins in zone 1, unlike many of the subbasins in zone 2 or 3. Placement directly onto the channel network provides greater contributing areas for the subbasin's wetlands, and sites with higher K values can keep pace with the inputs offered by such disproportionately large contributing areas. This capacity for sites to be located on the channel network of subbasins in the upper watershed is important to the generalized contributing-area relationships discussed below. Although sites in zone 1 generally offer the highest performances, the Maple River achieves higher reductions with sites placed in zones 2 and 3 (see Appendix E). This distinction for the Maple in the initial WRS scenarios appears again in the generalized WRS scenarios below.

Relationships between "treated areas" (the sum of WRS area and contributing area in a subbasin) and WRS extent in different subbasins for a large-site prioritization are presented in Figure 14. Data are shown for all subbasins utilizing the extents in the initial WRS scenarios (Table 1). The x's represent all of the data, while the diamonds and squares offer different selections of the data. Both of these selections only include subbasins with other subbasins upstream and do not include small subbasins (11, 12, 16, 21, and 22; see Figure 8) that can have anomalously high WRS extents as fractions of the subbasin area. The relationships between WRS area and contributing area in these small

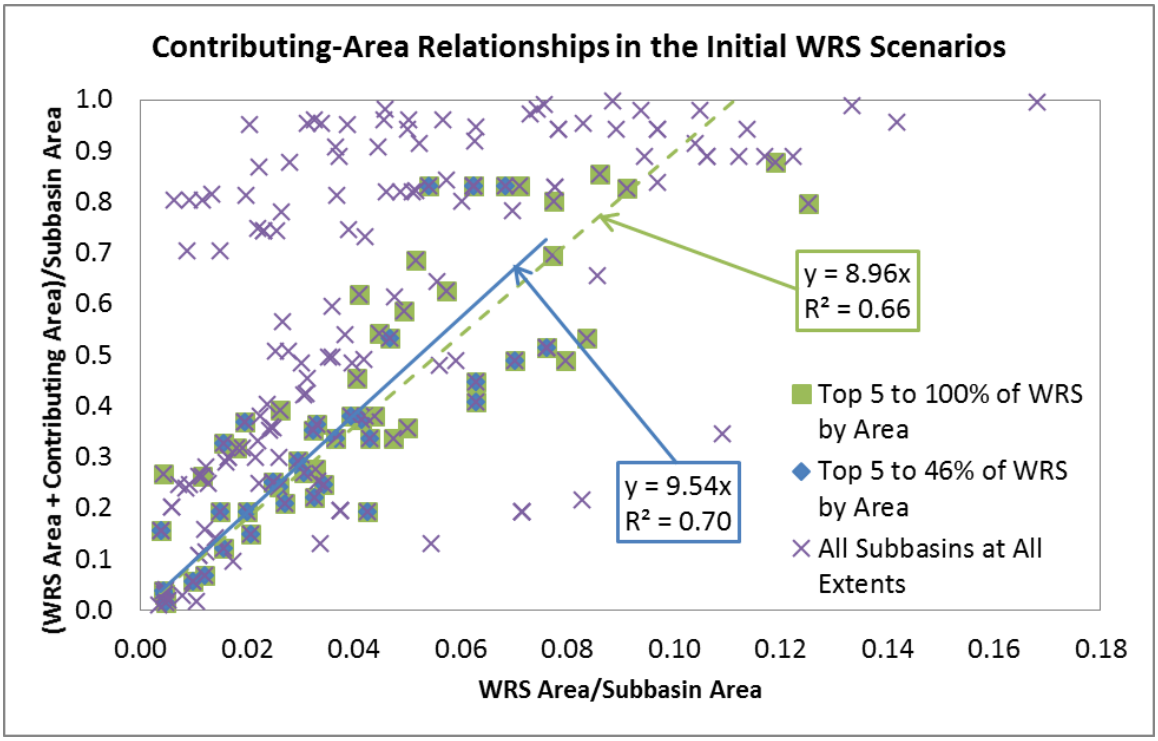

Figure 14. WRS extent versus "treated area" (WRS area + contributing area) for different selections from the initial WRS scenarios (see Table 1). No clear pattern emerges for all data, as sites with no other subbasins further upstream can experience abrupt changes in contributing areas when sites are placed on the subbasins' main channel networks. Subbasins that are not anomalously small (subbasins 11, 12, 16, 21 and 22; see Figure 8) and have other subbasins further upstream ("Downstream" subbasins) are used in the diamond and square scenarios, as these subbasins offer clearer trends.

subbasins are generally poorly defined and unrepresentative of those throughout the entire watershed. Subbasins with no other subbasins further upstream (e.g., those in zone 1 discussed above) can experience abrupt changes in contributing areas due to sites being placed on their main channel. For example, a subbasin can have a treated area beneath 10% of the subbasin area, only for this treated area to jump to over 80% of the subbasin area with only a slight increase in WRS extent. These subbasins are therefore not used in the identification of contributing-area relationships.

The blue diamond scenarios shown in Figure 14 use the top 5 to 46% of WRS by surface area, while the green square use all scenarios from the top 5% by area to the full extent. These selections yield relationships depicting contributing area in a subbasin as 8.5 (diamond scenarios, solid line) and 8 (square scenarios, dashed line) times the WRS area. While the slopes are about 9.5 and 9, these slopes relate treated areas to WRS extent; removing the WRS area from the treated area decreases the slopes by one. The relationship in which contributing area is 8.5 times the surface area was used in this study in order to avoid the leveling off that occurs as subbasins become saturated with sites. The slope of the relationship for the square scenarios is slightly lower due to this saturation, but the contributing-area relationship portrayed is still highly similar to the relationship used in this study.

Examples of WRS implementation scenarios created with the generalized relationship between WRS area and contributing area are shown in Figure 15. These scenarios place WRS in all zones, consider a range of K values (1E-8, 1E-7, and 1E-6 m/s),

and use a design depth of 1 meter. Scenarios with higher K values offer greater peak flow and sediment-loading rate reductions. For example, every 1% of watershed area utilized for WRS with K = 1E-6 m/s in this scenario offers about a 5.7% reduction in the total volume of water occurring at discharges exceeding the threshold, while every 1% of watershed area utilized for WRS with K = 1E-8 m/s offers only about a 1.6% reduction. The projected sediment-loading rate reductions for scenarios with K = 1E-8 m/s offer an almost linear relationship, while the relationships for K = 1E-7 or 1E-6 m/s feature more

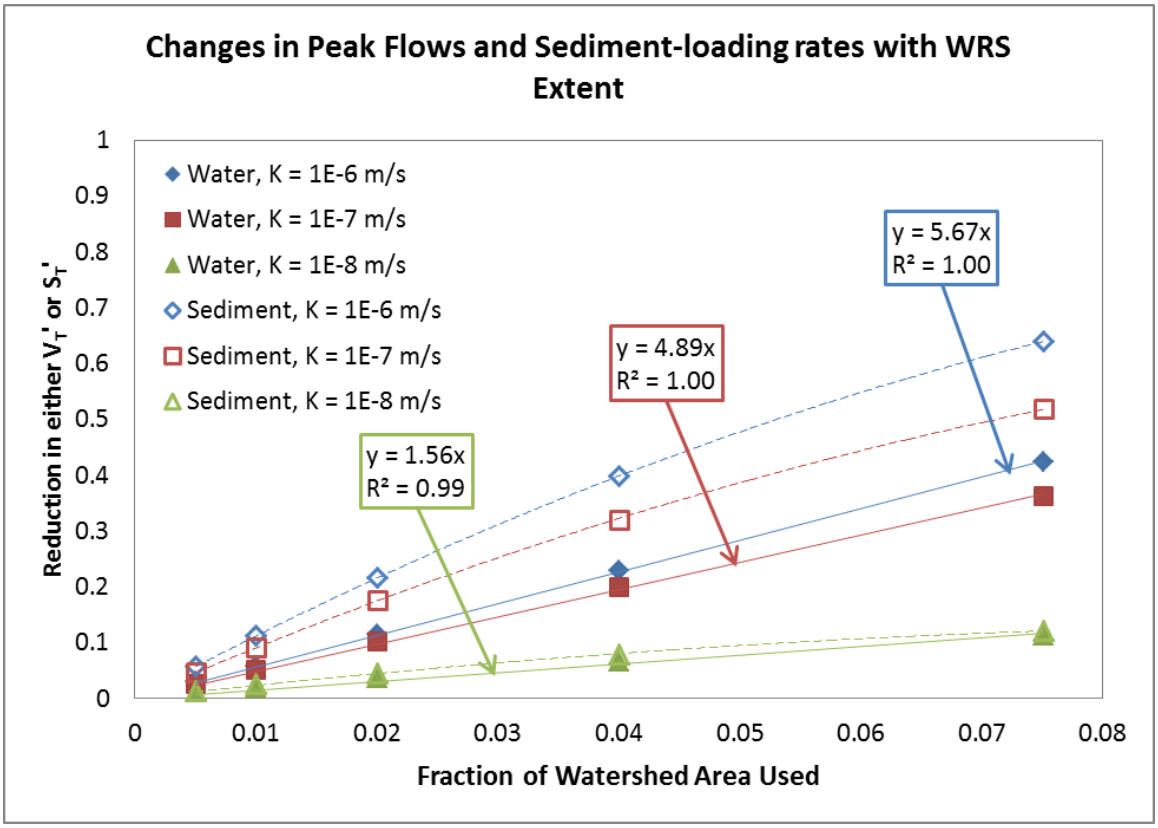

Figure 15. Reductions in both normalized total volumes of peak flows occurring at all three lower gauges (V_T') and normalized total sediment-loading rates for all three gauged reaches (S_T') offered by WRS implementation scenarios utilizing generalized contributing-area relationships (Figure 14), all zones, different hydraulic conductivity (K) values, and design depths of 1m. See section 2.4 for descriptions of V_T' and S_T'. While the linear regressions for the reduction of total peak flow volumes (solid lines, "Water") are shown, parameters for the polynomial regressions for total sediment-loading rate reductions (dashed lines, "Sediment") are shown in Tables 6-8.

downwards concavity.

The slopes of other linear regressions of reductions in V_T' vs. WRS extent as a fraction of the watershed area are shown in Figure 16. Higher slope values indicate a greater reduction of peak flows, and these reductions will likely be reflected in sediment-loading rate reductions. All of the relationships portrayed in Figure 16 have the same form of those shown in Figure 15 and similarly high R^2 values (i.e., all above 0.95). The scenarios shown in Figure 16 include all WRS placement scenarios, design depths, and K values, but only portray reductions in the total peak flow volume at all three gauges (V_T'); slopes for reductions at each of the gauges as well as their total are

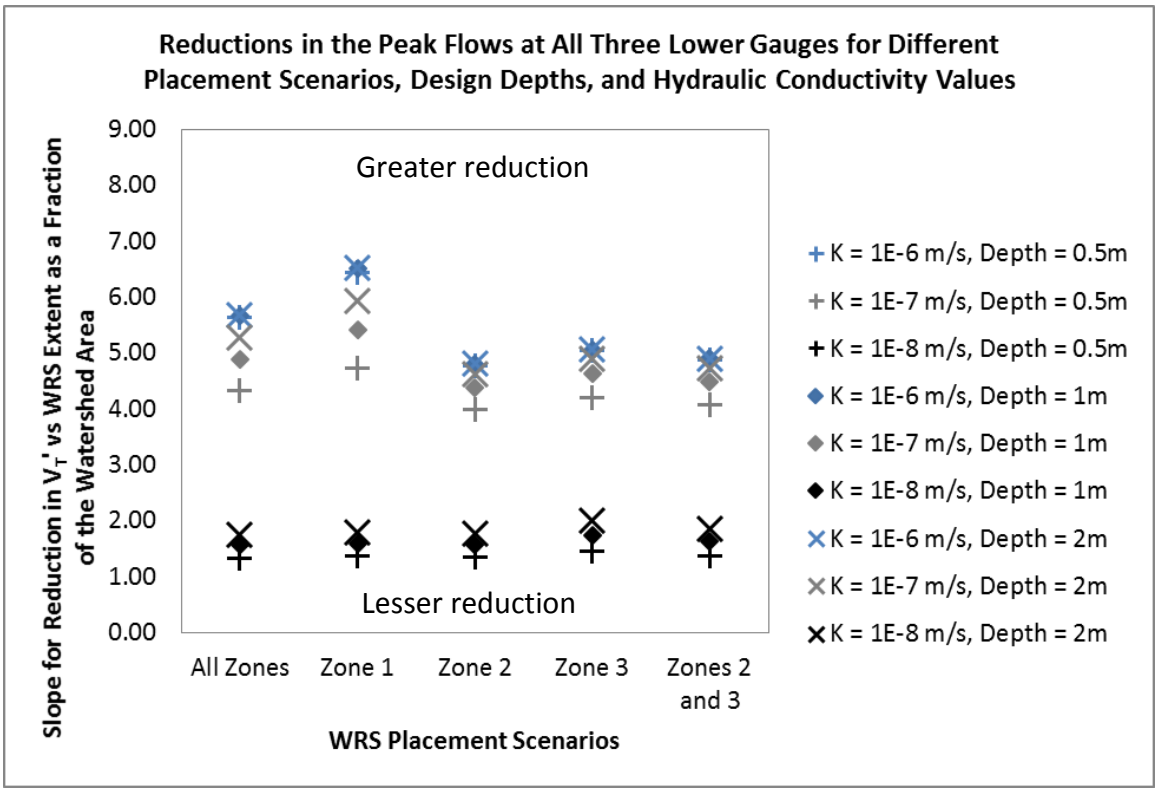

Figure 16. Slopes for the reduction of peak flows at all three lower gauges. See Figure 15 for examples of the relationships depicted here. All linear regressions had R^2 values over 0.98. The higher and lower ends of the range of values are labelled ("Greater reduction" and "Lesser reduction") for clarification.

shown in Table 5. Rates of reductions in peak flow volumes increase with higher K and design depth values, with the exception of scenarios using K = 1E-6 m/s; with hydraulic conductivity at this level, the range of design depth values considered here does not strongly influence results. Rates of reductions in peak flow volumes are maximized for the Le Sueur and Cobb in scenarios with K = 1E-7 or 1E-6 m/s by using zone 1, the upper watershed, but these rates are maximized for the Maple in all K scenarios by using zone 3 (i.e., close to the watershed outlet; see Figure 8). Low-K scenarios are less sensitive to placement, but almost all scenarios using K = 1E-8 m/s achieve the highest rates of peak flow reductions by utilizing zone 3. Only the Le Sueur subwatershed obtained a higher rate with K = 1E-8 m/s by using zones 2 and 3. It should also be noted that scenarios using K values of 1E-7 m/s can achieve almost the same reductions offered by scenarios using K = 1E-6 m/s by using design depths of 2 meters.

While peak flow volumes are somewhat insensitive to the distribution of flow magnitudes, sediment-loading rates are sensitive to flow magnitudes. Tables 6, 7, and 8 show components for sediment-loading rate reduction relationships for initial WRS scenarios using K = 1E-8, 1E-7, and 1E-6 m/s, respectively. In each scenario, two values are shown for all three lower gauges and their total: the concavity, shown in gray, and slope. All concavity values are negative, while all slope values are positive. Each regression takes the form:

Table 5. Slopes for linear regressions of total peak flow volume reductions vs WRS extent as a fraction of the watershed area. T, L, C, and M stand for the total (T) of all three gauges, the lower gauge of the Le Sueur (L), the lower gauge of the Cobb (C), and the lower gauge of the Maple (M). See Figure 14 for examples of the relationships depicted here. All linear regressions had R^2 values over 0.98.

Design Depth (m)	Scenario	K = 1E-8 m/s				K = 1E-7 m/s				K = 1E-6 m/s			
		T	L	C	M	T	L	C	M	T	L	C	M
0.5	All Zones	1.33	1.14	1.41	1.55	4.33	4.80	3.80	4.96	5.63	6.82	4.48	4.96
	Zone 1	1.37	1.09	1.54	1.67	4.73	5.25	4.22	5.05	6.45	7.79	5.23	5.05
	Zone 2	1.34	1.07	1.34	1.58	3.98	4.61	3.50	4.91	4.78	6.02	3.84	4.91
	Zone 3	1.46	1.18	1.58	2.06	4.21	4.20	3.61	5.50	5.04	5.21	4.04	5.50
	Zones 2 and 3	1.37	1.20	1.37	1.58	4.07	4.46	3.52	4.97	4.88	5.63	3.89	4.97
1	All Zones	1.56	1.32	1.65	1.84	4.89	5.53	4.19	5.01	5.67	6.86	4.52	5.01
	Zone 1	1.60	1.25	1.81	1.98	5.41	6.08	4.79	5.10	6.51	7.86	5.31	5.10
	Zone 2	1.57	1.25	1.56	1.84	4.39	5.22	3.71	4.97	4.81	6.02	3.86	4.97
	Zone 3	1.74	1.43	1.85	2.44	4.63	4.68	3.87	5.54	5.06	5.21	4.06	5.54
	Zones 2 and 3	1.62	1.43	1.61	1.88	4.48	4.99	3.74	5.03	4.90	5.64	3.91	5.03
2	All Zones	1.76	1.47	1.87	2.08	5.28	6.10	4.42	5.01	5.67	6.86	4.52	5.01
	Zone 1	1.78	1.39	2.02	2.22	5.93	6.82	5.13	5.10	6.51	7.86	5.31	5.10
	Zone 2	1.78	1.42	1.78	2.09	4.63	5.59	3.82	4.97	4.81	6.02	3.86	4.97
	Zone 3	1.99	1.67	2.08	2.75	4.88	4.97	4.01	5.55	5.06	5.21	4.06	5.55
	Zones 2 and 3	1.85	1.63	1.84	2.14	4.73	5.32	3.87	5.03	4.91	5.64	3.91	5.03

$$Reduction\ in\ S' = cx^2 + mx \quad (12)$$

where the *Reduction in S' is* a fraction, *c* is concavity, *m* is slope, and *x* is WRS extent as a fraction of the watershed area. *Reduction in S'* can be expressed as (Reduction in sediment loading rate [Mg/yr])/(Baseline sediment loading rate [Mg/yr]), and the baseline sediment-loading rates presented in Table 3 can be used to determine the sediment-loading rate reduction in Mg/yr. Values calculated with Equation 12 only reflect changes in sediment-loading from active bluffs (i.e., bluffs in contact with the channel) situated along the gauged reach of each river. These reductions in sediment loading would also only reflect the bluffs' contributions during periods with flows above the discharge threshold of 0.01 $m^3/s/km^2$. Table 9 shows the minimum and maximum WRS extents for each placement scenario used in the generalized WRS scenarios. The regression parameters shown in Tables 5-8 should not be applied to WRS extents outside of the ranges shown in Table 9.

Appendix F presents normalized (S') and non-normalized sediment-loading rate reductions in the generalized WRS scenarios. The reductions were created with Equation 12, the concavity and slope values in Tables 6-8, the range of WRS extents considered (Table 9), and the baseline sediment-loading rates (Table 3). Similar trends are exhibited by both the peak flow (Table 5) and sediment-loading rate reduction relationships. For example, larger reductions in sediment-loading rates are achieved with increasing K values. The highest reductions are achieved with zone 1 for scenarios using K = 1E-7 or 1E-6 m/s within the Le Sueur and Cobb subwatersheds. The highest

reductions within the Maple subwatershed, however, are provided by scenarios using zone 3, and all scenarios using K = 1E-8 m/s obtain the highest reductions by using zone 3.

Table 6. Concavity (gray) and slope values for regressions of sediment-loading rate reductions. Parameters are shown for all three lower gauges and their total (same designations as those in Table 5) in scenarios using K = 1E-8 m/s. All R^2 values for these regressions are above 0.98.

Design Depth (m)	Scenario	Concavity and slope values for Equation 12, K = 1E-8 m/s							
		T		L		C		M	
0.5	All Zones	-8.02	1.80	-5.84	1.45	-8.61	1.87	-10.02	2.13
	Zone 1	-13.07	1.83	-8.71	1.28	-17.36	2.21	-17.13	2.32
	Zone 2	-17.88	1.66	-22.10	1.40	-12.27	1.40	-15.41	1.88
	Zone 3	-29.14	2.06	-19.99	1.90	-33.31	2.04	-58.99	2.71
	Zones 2 and 3	-12.11	1.79	-10.26	1.65	-10.27	1.60	-14.02	2.02
1	All Zones	-11.46	2.48	-8.32	1.95	-12.61	2.65	-14.10	2.92
	Zone 1	-19.17	2.51	-13.01	1.76	-26.07	3.10	-24.16	3.14
	Zone 2	-25.10	2.32	-29.46	1.88	-18.01	2.03	-21.58	2.59
	Zone 3	-40.60	2.77	-27.10	2.49	-46.63	2.82	-86.08	3.70
	Zones 2 and 3	-16.97	2.46	-14.15	2.19	-14.69	2.28	-19.61	2.78
2	All Zones	-14.27	3.08	-10.58	2.42	-15.67	3.34	-17.34	3.62
	Zone 1	-24.41	3.14	-16.81	2.21	-32.84	3.89	-30.65	3.88
	Zone 2	-30.71	2.90	-35.50	2.30	-23.25	2.63	-25.95	3.23
	Zone 3	-48.37	3.36	-32.46	3.01	-53.94	3.44	-104.61	4.50
	Zones 2 and 3	-20.98	3.05	-17.71	2.68	-18.21	2.88	-24.06	3.46

Table 7. Concavity (gray) and slope values for regressions of sediment-loading rate reductions. Parameters are shown for all three lower gauges and their total (same designations as those in Table 5) in scenarios using K = 1E-7 m/s. All R^2 values for these regressions are above 0.98.

Design Depth (m)	Scenario	Concavity and slope values for Equation 12, K = 1E-7 m/s							
		T		L		C		M	
0.5	All Zones	-24.88	7.52	-26.75	7.81	-21.71	6.98	-25.21	7.59
	Zone 1	-39.82	8.20	-42.22	8.45	-40.47	8.26	-35.17	7.97
	Zone 2	-36.70	6.89	-51.25	7.12	-21.23	5.75	-32.26	7.16
	Zone 3	-46.10	6.93	-37.40	7.02	-38.64	6.16	-86.63	8.33
	Zones 2 and 3	-26.86	6.88	-28.30	7.06	-18.11	5.86	-30.36	7.35
1	All Zones	-33.45	9.41	-37.29	10.01	-28.61	8.60	-32.85	9.35
	Zone 1	-54.57	10.58	-61.63	11.30	-53.07	10.56	-43.58	9.79
	Zone 2	-43.76	8.39	-59.60	8.65	-22.64	6.69	-40.04	8.93
	Zone 3	-47.07	8.24	-39.91	8.32	-37.91	7.21	-81.40	10.15
	Zones 2 and 3	-32.46	8.32	-33.05	8.45	-20.26	6.84	-38.60	9.14
2	All Zones	-38.79	10.67	-43.28	11.47	-32.95	9.63	-38.22	10.56
	Zone 1	-62.08	12.19	-72.70	13.30	-58.26	12.04	-46.82	10.99
	Zone 2	-45.71	9.34	-55.56	9.47	-23.84	7.27	-43.14	10.11
	Zone 3	-44.66	9.06	-38.71	9.07	-36.16	7.89	-71.99	11.38
	Zones 2 and 3	-34.38	9.21	-33.08	9.22	-21.16	7.42	-42.42	10.33

Table 8. Concavity (gray) and slope values for regressions of sediment-loading rate reductions. Parameters are shown for all three lower gauges and their total (same designations as those in Table 5) in scenarios using K = 1E-6 m/s. All R^2 values for these regressions are above 0.98.

Design Depth (m)	Scenario	Concavity and slope values for Equation 12, K = 1E-6 m/s							
		T		L		C		M	
0.5	All Zones	-39.74	11.37	-45.15	12.91	-33.72	9.93	-38.26	10.76
	Zone 1	-59.88	13.25	-68.80	15.33	-58.20	12.50	-45.79	11.19
	Zone 2	-40.49	9.65	-29.35	10.14	-22.79	7.39	-41.57	10.34
	Zone 3	-34.31	9.39	-26.74	9.57	-32.69	8.02	-63.36	11.56
	Zones 2 and 3	-32.32	9.54	-27.19	9.82	-21.21	7.56	-41.73	10.55
1	All Zones	-41.23	11.62	-46.30	13.11	-34.97	10.16	-40.33	11.06
	Zone 1	-61.01	13.57	-70.72	15.68	-58.83	12.87	-45.95	11.44
	Zone 2	-40.35	9.84	-28.35	10.16	-22.31	7.49	-41.80	10.66
	Zone 3	-32.96	9.47	-26.89	9.60	-30.38	8.09	-55.90	11.79
	Zones 2 and 3	-32.55	9.69	-27.00	9.84	-20.96	7.65	-42.56	10.86
2	All Zones	-41.25	11.62	-46.32	13.12	-34.99	10.16	-40.35	11.06
	Zone 1	-60.98	13.57	-70.73	15.68	-58.73	12.88	-45.89	11.44
	Zone 2	-40.28	9.84	-28.36	10.16	-22.36	7.49	-41.68	10.66
	Zone 3	-32.70	9.47	-26.63	9.60	-30.26	8.09	-55.45	11.79
	Zones 2 and 3	-32.52	9.69	-26.99	9.84	-20.95	7.65	-42.52	10.86

Table 9. Minimum (Min.) and maximum (Max.) assessed WRS extents as percentages of the watershed area. The parameters in Tables 5-8 should not be applied to any WRS extents outside of the ranges shown here.

Placement Scenario	Total		Le Sueur		Cobb		Maple	
	Min.	Max.	Min.	Max.	Min.	Max.	Min.	Max.
All Zones	0.50%	7.50%	0.50%	7.50%	0.50%	7.50%	0.50%	7.50%
Zone 1	0.25%	3.79%	0.28%	4.25%	0.24%	3.61%	0.22%	3.36%
Zone 2	0.16%	2.36%	0.10%	1.44%	0.17%	2.62%	0.22%	3.34%
Zone 3	0.09%	1.36%	0.12%	1.84%	0.09%	1.28%	0.05%	0.80%
Zones 2 and 3	0.25%	3.72%	0.22%	3.28%	0.26%	3.89%	0.28%	4.14%

An example of how specific Q/DA bins' frequencies (F, days per year; see Equation 9) change with WRS extent is shown in Figure 17. The frequency of each bin in a WRS scenario (F_{WRS}) is normalized by the corresponding frequency in the baseline

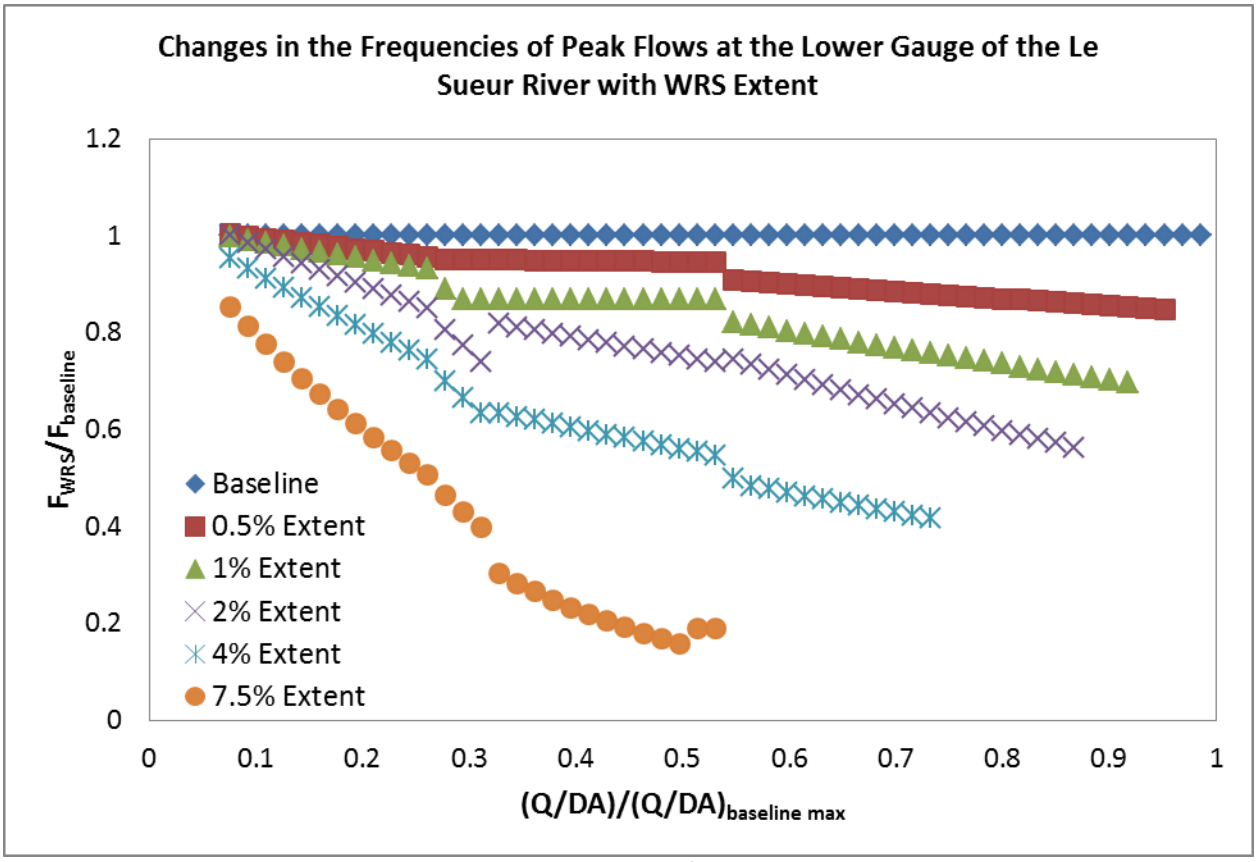

Figure 17. Frequencies (F, days per year; see Equation 9) of binned Q/DA values exceeding the threshold (0.01 $m^3/s/km^2$) at the lower gauge of the Le Sueur River relative to each value's frequency in the baseline scenario ($F_{baseline}$). Q/DA values are also normalized by the maximum baseline value, $(Q/DA)_{max}$. These WRS implementation scenarios use all zones with depths of 1m and K = 1E-6 m/s, and the extents listed in the legend are in terms of the watershed area. Trends in both the relative frequencies of specific flows and the maximum flows achieved in each extent scenario can be used in combination with the baseline scenario's exponential regressions (see Section 2.6) to predict peak flows and sediment-loading rates for arbitrary WRS extents.

scenario ($F_{baseline}$), so a lower $F_{WRS}/F_{baseline}$ value indicates a reduction in the frequency of a Q/DA value. All extents considered for the generalized WRS scenarios are shown (see Table 1), and this example uses all zones, design depths of 1 meter, and K = 1E-6 m/s. While this example yields a trend for slopes of $F_{WRS}/F_{baseline}$ vs normalized Q/DA that increase linearly with WRS extent, such clear trends are not always available. Values of $F_{WRS}/F_{baseline}$ can exhibit different trends at different discharge values, with low Q/DA values sometimes increasing while higher Q/DA values are decreasing. Trends for the

maximum Q/DA values achieved in each scenario can also vary. For example, although this relationship is not shown, the data shown in Figure 17 yield a relationship between maximum discharge achieved and WRS extent such that $Q/DA_{baseline} = -6.2901(A_{WRS}/A_{watershed})Q/DA_{baseline\ max}$ ($R^2 = 0.9994$; see Equation 11).

The strengths of regressions of $F_{WRS}/F_{baseline}$ values versus WRS extent (see Equation 10) vary considerably, and these regressions are used to generate peak flows. Appendix G shows examples demonstrating the approximate ranges of R^2 values achieved, but the actual values can be assessed through the Microsoft Excel® flow generator file available in the digital archive attached to this thesis. The linear regressions for scenarios using all zones or zone 1 with K = 1E-6 m/s and any design depth always have R^2 values above 0.7. While most of the R^2 values for scenarios using zones 2 and 3 with K = 1E-6 and any design depth are similarly high, some values approach zero. Using lower K values of 1E-7 m/s and depths of 1 or 2 meters can still offer relatively high R^2 values in scenarios using all zones, zone 1, or zones 2 and 3; most R^2 values for these scenarios exceed 0.7, but some values again approach zero (especially with zones 2 and 3). Scenarios using zone 2, zone 3, or K values of 1E-8 m/s often yield relationships that are consistently weak. Design depths often have little influence on R^2 values, but using depths of 0.5 m can offer lower values. The flow generator is more suitable for scenarios using large placement zones (i.e., all zones, zone 1, and zones 2 and 3) and K values of 1E-6 m/s, and usually K values of 1E-7 m/s. The flow generator is less suitable for small placement zones (i.e., zone 2 or zone 3)

and/or K values of 1E-8 m/s due to the low R^2 values used. Despite such weaknesses, the flow generator's peak flow volume and sediment-loading rate projections are relatively close to the SWAT-derived values they were based on.

The flow generator was used to determine peak flow volume and sediment-loading rate reductions for all generalized WRS scenarios that were then compared to their corresponding values derived from SWAT output (Figure 18). Figure 19 compares the peak flow volumes, while Figure 20 compares the sediment-loading rates. Values are shown for all three rivers in all scenarios using generalized contributing-area relationships. Each scenario has five points corresponding with extent scenarios utilizing 0.5, 1, 2, 4, and 7.5% of the subwatershed area. The solid line represents a 1:1 relationship between values derived from SWAT and generated data, while the dashed and dotted lines above the solid line represent 1:1.1 and 1:1.33 relationships. Generated peak flow volumes tend to be slightly larger than the corresponding SWAT-derived values, but almost all of these volumes occur within about 10% of each other. Sediment-loading rates exhibit much more variation, however, but largely within about 33% of each other. The generated sediment-loading rates for the gauged reach of the Le Sueur River are often smaller, roughly following the lower dashed line. Generated sediment-loading rates for the gauged reach of the Maple River are higher than SWAT-based values (near the upper dashed line) when K values and extents are low, but generally lower than SWAT-based values (between the lower dashed and dotted lines) when reductions are high due to high K values and high extents. A similar trend occurs for

sediment-loading rates for the Cobb with K = 1E-6 m/s (red), but the opposite is true for the Cobb's scenarios with K = 1E-8 m/s (yellow); higher points lie on the solid line and lower points lie just above the upper dashed line, exceeding SWAT-based values. This

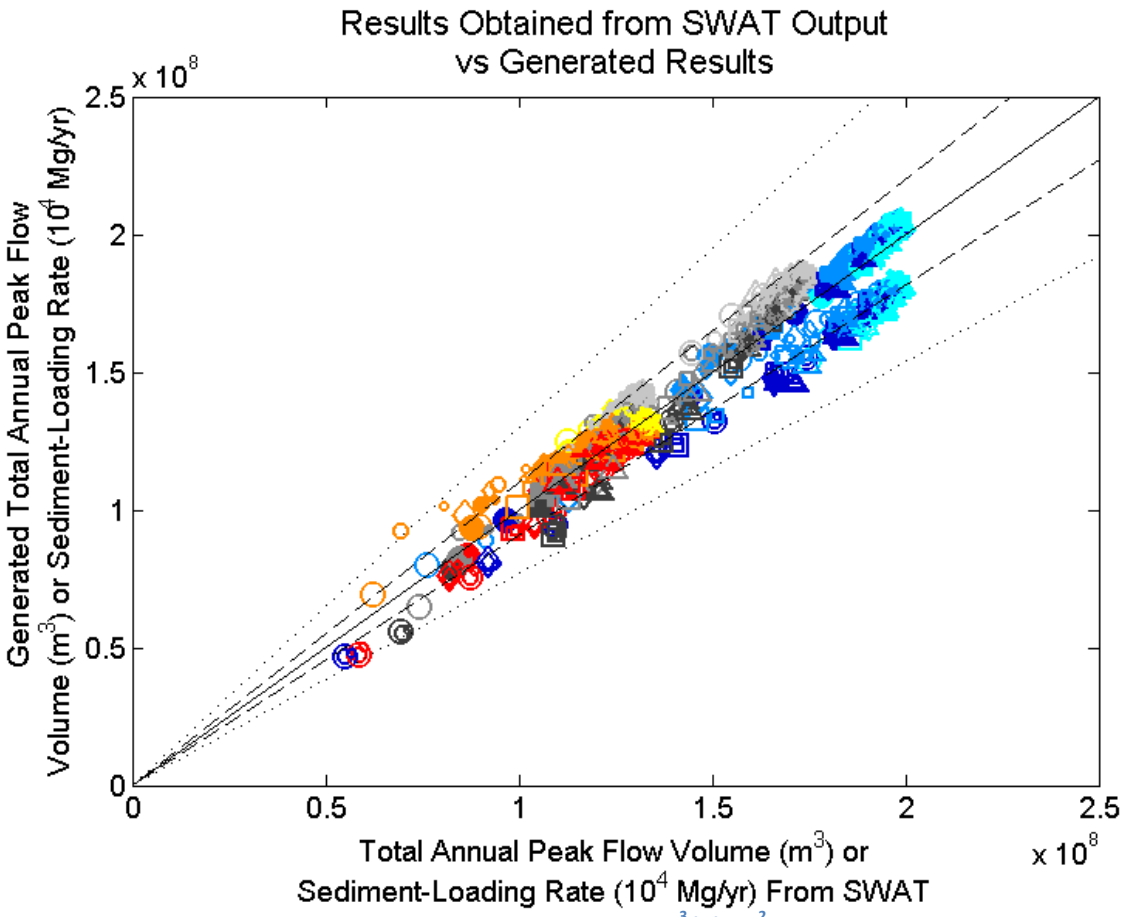

Figure 18. Total volumes of peak flows exceeding the threshold (0.01 $m^3/s/kms^2$) at the three lower gauges and sediment-loading rates for the three gauged reaches derived from both SWAT output and generated data. No legend is shown due to the immense number of scenarios included. Volumes are indicated with filled symbols while sediment-loading rates are indicated with hollow symbols. Both hydraulic conductivity and location are indicated by color. Scenarios using values of 1E-8, 1E-7, and 1E-6 m/s use light, medium and dark colors, respectively; the Le Sueur uses blue, the Cobb uses yellow to red (i.e., yellow = 1E-8 m/s, orange = 1E-7 m/s, and red = 1E-6 m/s), and the Maple uses grey. Design depth is indicated by symbol size; depths of 0.5, 1, and 2 meter(s) are represented by small, medium, and large symbols. Placement scenario is indicated by symbol shape; scenarios using all zones, zone 1, zones 2 and 3, zone 2, and zone 3 have circles, diamonds, squares, triangles, and hexagons, respectively. The solid black line indicates a 1:1 relationship between results from SWAT output and generated results while the dashed and dotted lines above the solid line represent 1:1.1 and 1:1.33 relationships and the dashed and dotted lines below the solid line represent 1.1:1 and 1.33:1 relationships. The symbol classification scheme used here is only meant to allow for the identification of outliers, as point densities are quite high.

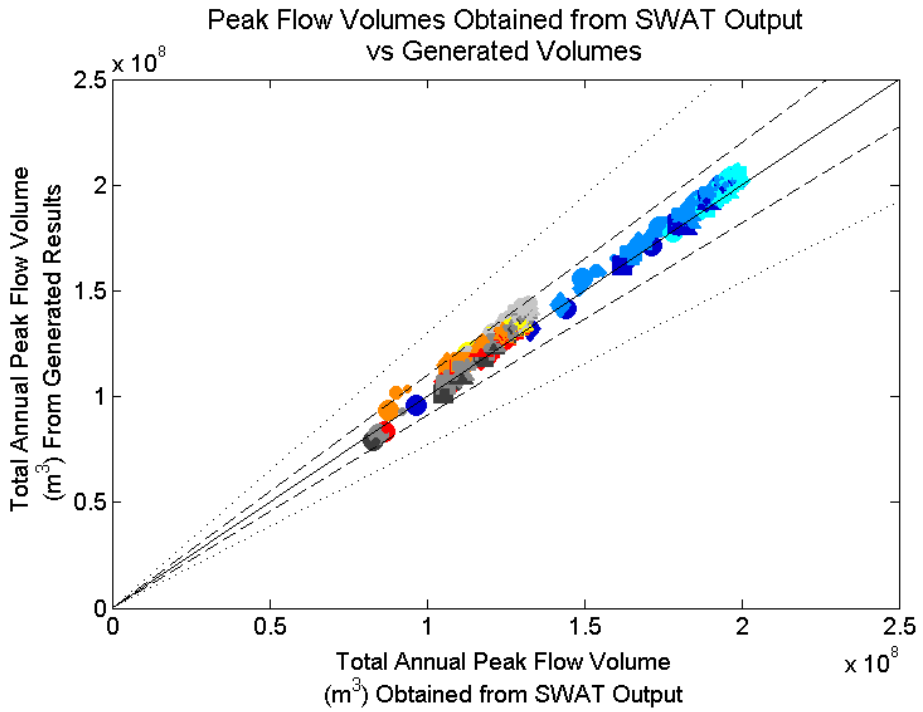

Figure 19. Version of Figure 18 showing only peak flow volumes, rather than peak flow volumes and sediment-loading rates.

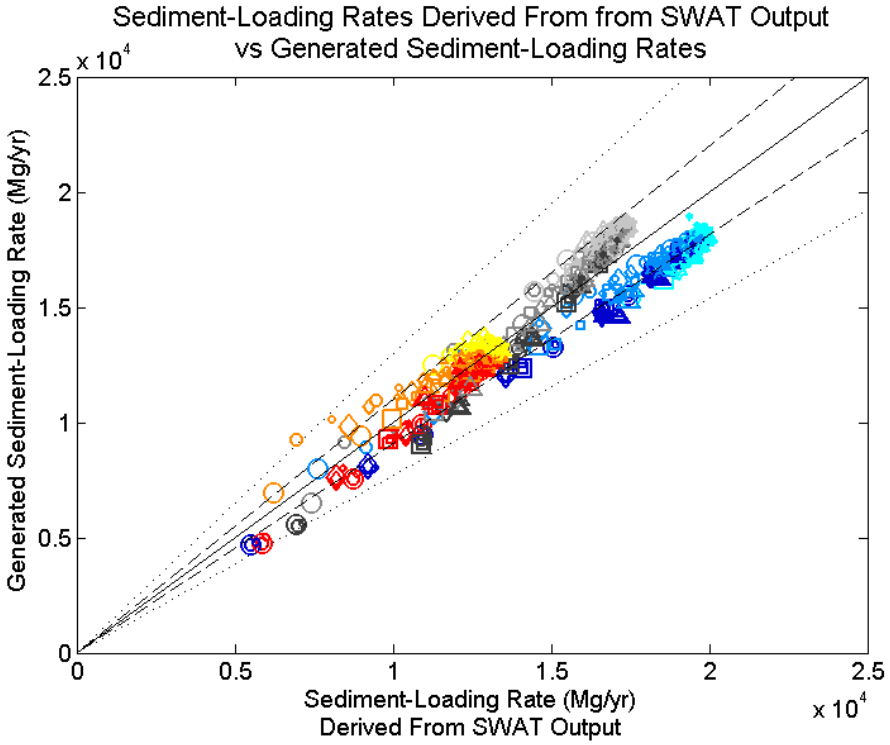

Figure 20. Version of Figure 18 showing only sediment-loading rates, rather than sediment-loading rates and peak flow volumes.

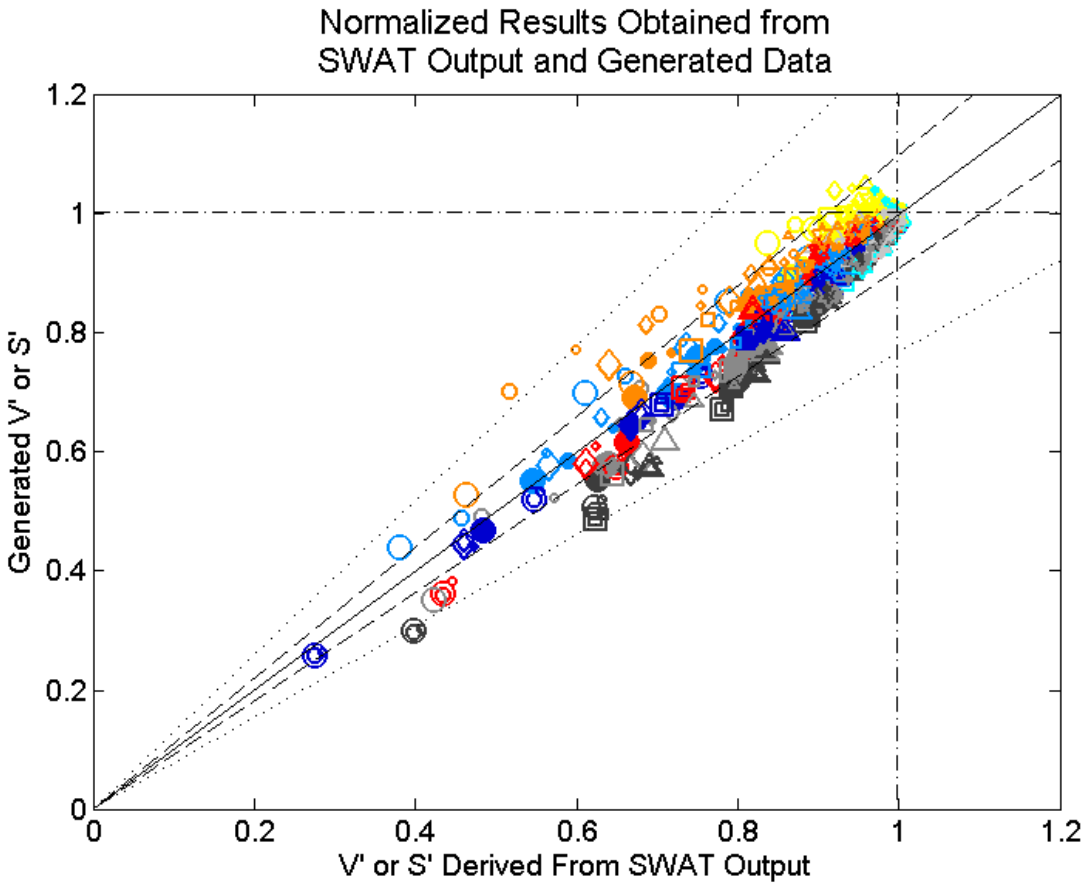

Figure 21. Generated and SWAT-derived total peak flow volumes at the three lower gauges and sediment-loading rates for the three gauged reaches normalized by the corresponding generated or SWAT-derived baseline value. This graph uses the same symbol classification scheme used in Figure 18. The solid, dashed, and dotted lines portray the same relationships used for such lines in Figure 18, while the dash-dot lines shown here clarify which scenarios exceed the baseline values (i.e., some scenarios with K = 1E-8 m/s).

trend is also exhibited by scenarios with K = 1E-7 m/s on the Cobb (orange), but higher points occur between the solid and lower dashed lines and lower points occur between the upper dashed and dotted lines. Despite these incongruities, the differences between generated and SWAT-derived values are still relatively small.

Differences in peak flow volumes and sediment-loading rates change when these values are normalized by the corresponding baseline values (Figure 21). Although some

noise is still exhibited by these data, the systematic trends noted above are somewhat alleviated. Generated values for the Maple and those for the Cobb with K = 1E-6 m/s still tend to fall beneath SWAT-based values with increasing reductions, while lower generated values for the Cobb with K = 1E-7 or 1E-6 m/s still tend to rise above SWAT-based values with increasing reductions. Generated values for the Le Sueur on Figure 21 almost achieve a 1:1 relationship with SWAT-based values. Scenarios employing K = 1E-8 m/s, especially in the Cobb subwatershed, can increase peak flow and sediment-loading rate values slightly. These increases are small in magnitude (i.e., less than 5%), however, and generally occur only in generated results.

Utilizing a lower spilling threshold can reduce the rates of reductions in V_T' with WRS extent while maintaining or increasing the rates of reductions in S_T' (see Figures 15 and 22). The examples presented in Figure 22 use all zones with depths of 1m, making the scenarios similar to those in Figure 15. The reductions in S_T' from Figure 15 are also presented in Figure 22 (plus signs) to emphasize the greater reductions in S_T' possible with a lower spilling threshold when K = 1E-8 m/s. The lower spilling threshold allows sites to overflow at a lower rate before the maximum capacity is exceeded (see Equation 3). This spilling can reduce the reductions in V', because the spilled water can contribute to the volume of peak flows in the lower watershed. The greater loss of water from the sites can empty more of their capacity between events, however, enabling them to more effectively attenuate the next flood event. The S' term is sensitive to the magnitude of specific flows, and the greater reductions in S_T' shown in

Figure 22 demonstrate that low-K sites can offer greater reductions in sediment loading when lower spilling thresholds are used. The S' reductions presented in this study may therefore be conservative, as only maximum capacities were used as spilling thresholds.

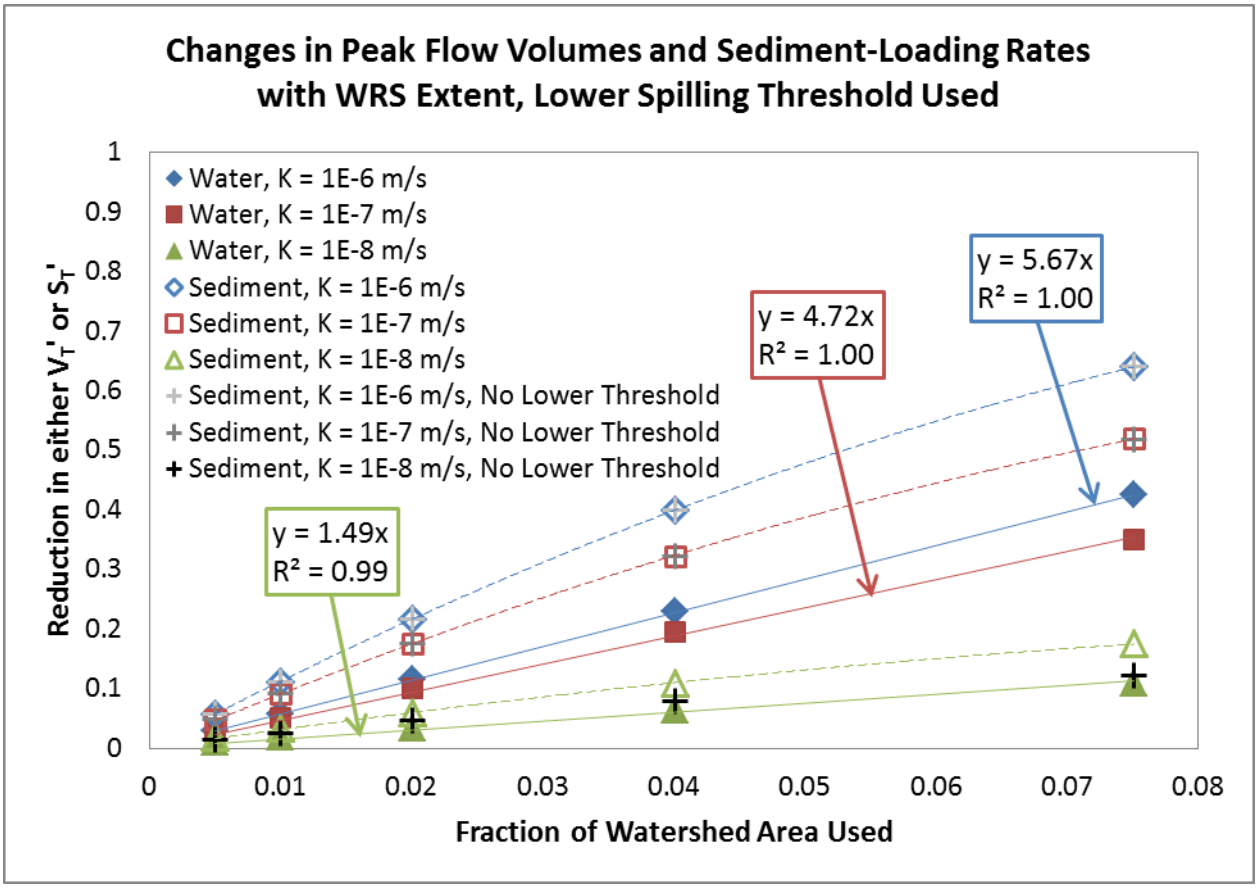

Figure 22. Examples showing the effect of a lower spilling threshold (90% of the maximum capacity) on reductions in the total peak flow volume at all three lower gauges normalized by the baseline total (V_T') and the total sediment-loading rate of all three gauged reaches normalized by the baseline total (S_T') offered by generalized WRS scenarios. These scenarios use all zones and depths of 1m, making them similar to those shown in Figure 15. The reductions in S_T' from Figure 15 are shown with plus signs of differing shades of gray. Although rates of peak flow volume reduction are lower here than in Figure 15, the sediment-loading rate reductions presented here can be higher (especially when K = 1E-8 m/s). The equations for the reductions in S_T' (dashed curves) for K = 1E-6, 1E-7, and 1E-8 m/s are $y = -41.223x^2 + 11.615x$ ($R^2 = 1$), $y = -33.286x^2 + 9.4053x$ ($R^2 = 0.9999$), and $y = -11.891x^2 + 3.2164$ ($R^2 = 0.9995$), respectively.

4: Discussion

The results presented in this study show that sites designed to increase water storage can decrease peak flow volumes and sediment-loading rates (reported here as V' and S', when normalized by baseline values) in the lower reaches of the Le Sueur watershed. These reductions are achieved at different rates with WRS extent (e.g., Tables 5-8), with certain scenarios being more effective. This section first discusses this study's major findings regarding peak flow and sediment-loading rate reductions and then the limitations of SWAT's wetlands.

4.1: Major Findings

Sites offer greater V' reductions with higher K values; higher seepage rates allow sites to more effectively empty their storages between precipitation events, enabling them to absorb more of the water associated with the upcoming event. Although the region's geomorphic history has left it with low-K sediments, achieve higher K values could be achieved through changes in site design. While V' reductions generally increase with design depth, such reductions are insensitive to depth when K values are high. Sites with K = 1E-6 m/s do not overflow very easily, as the range of design depths considered did not significantly influence results. This lack of overflowing would allow scenarios using the higher K values suggested by SSURGO data (e.g., 1E-5 m/s) to produce results identical to those of scenarios using K = 1E-6 m/s. The ability of even sites with 0.5 meter depths to avoid overflowing may be related in part to SWAT's lumping of

wetlands, however, as sites within the same subbasin can share and redistribute water in an unrealistic manner. Despite such issues, sites with K = 1E-6 m/s would still overflow less frequently due to the water loss from higher seepage rates. V' reductions do change with design depth when K is 1E-7 or 1E-8 m/s, with higher design depths providing higher peak flow reductions. For example, design depths of 2 m can allow sites with K = 1E-7 m/s to nearly match the performances of sites with K = 1E-6 m/s.

The highest rates of V' and S' reductions with WRS extent can be achieved in the Le Sueur and Cobb subwatersheds by placing sites with high K values (i.e., 1E-6 m/s) in the upper watershed (zone 1; see Figure 8). Runoff produced in the uplands of zone 1 might arrive to the lower watershed in such a manner that it tends to compose a flood event's peak. Muting the signal from zone 1 would then be the best way to reduce peak flows in the lower watershed. In contrast, runoff produced closer to the outlet (i.e., zone 3) might arrive at the lower gauges well before a flood event's peak. Such considerations are discussed in greater depth below. Unlike the Le Sueur and Cobb subwatersheds, rates of reductions are maximized in the Maple when sites with high K values are placed in zone 3. The model may be capturing unique traits of the Maple subwatershed, or the model's portrayal of the subwatershed could simply be lacking. While zone 1 still offers the highest peak flow reductions for the Le Sueur and Cobb watersheds when K = 1E-7 m/s, scenarios using K = 1E-8 m/s in any of the three subwatersheds tend to offer the highest rates of reductions when zone 3 is used. For sites with K = 1E-8 m/s, the rates of reductions offered by placement in zone 3 are only

exceeded or matched by those offered by both zones 2 and 3. These findings suggest that wetlands constructed with clay lining and low K values may reduce flooding and erosion more when placed closer to the watershed outlet. Conversely, detention basins with high K values can reduce flooding and erosion more when placed farther from the watershed outlet (except in the Maple subwatershed).

Changes in site performance with both site K values and placement in the watershed may not require significant changes in site design within the Le Sueur watershed, as the existing K values already indicate a favorable distribution. Figure 5 shows SSURGO saturated K values for the surface soil layers in the watershed to generally be higher in the uplands and lower closer to the outlet. This spatial trend allows sites to naturally have K values that allow them to perform more effectively. All three subwatersheds feature this trend, but not in a uniform manner; most of the Maple subwatershed features low K values, with only high values in the uppermost reaches, while most of the Le Sueur subwatershed features high K values, with only low values in the lowermost reaches. The distribution of K values in the Cobb subwatershed lies somewhere between these two extremes.

The fact that sites with different K values perform more effectively in different parts of the watershed might reflect the different overflowing behaviors of sites with high or low K values and spilled water's interaction with flood peak timing. If a WRS site remains relatively full with water, possibly due to low K values, the precipitation landing on the site will overflow from the site rather than infiltrating into the soil. A site with K =

1E-8 m/s might tend to overflow relatively early during a precipitation event, relative to a site with K = 1E-6 m/s. If a site with K = 1E-8 m/s overflows relatively early, then the spilled water from such a site placed in zone 3 (i.e., close to the outlet) might arrive at the outlet well before the flood event's peak occurs there. In contrast, the spilled water from a site with K = 1E-8 m/s in zone 1, the upper half of the watershed, might arrive at the outlet at a later time coinciding with the flood event's peak in the lower watershed. Although sites with low-K values can still provide peak flow reductions (e.g., Figure 15 and Tables 5-8), their greater tendency to overflow can make them less effective when placed in areas associated with the runoff composing flood peaks. With lower tendency to overflow, a site with K = 1E-6 m/s placed in the upper watershed (zone 1) can simply absorb water that would otherwise contribute to the flood's peak in the lower watershed. The complete removal of this water from the flood peak aids in reducing both flood magnitudes and the erosion of near-channel features. While this explanation fits the results presented here (e.g., Table 5), SWAT may not accurately portray such complex interactions. Even though the areas within a watershed that offer the largest contributions to flood peaks should have a high priority in WRS implementation scenarios, it may be best at times to place sites susceptible to overflowing elsewhere in the watershed.

The areas in the Le Sueur watershed associated with water composing flood events' peaks at the lower gauges seem to occur in zone 1, the upper watershed. This characterization is not applicable to all watersheds, as the areas associated with peaks

are dictated by the unique configuration and characteristics of a watershed. The nearby Blue Earth watershed may have its flood events more strongly associated with its upper reaches, as the watershed has a fan-shape and the outlet is located at the tip of the "fan." The Watonwan watershed, which is also adjacent to the Blue Earth watershed, may have its peak flows associated with the middle section of the watershed, as the lower and upper watershed are relatively small in comparison. The Blue Earth, Le Sueur, and Watonwan watersheds form the Greater Blue Earth watershed, and the need for peak flow and sediment-loading rate reductions in all three watersheds may require additional studies assessing the individual traits of both the Blue Earth and Watonwan watersheds. The areas associated with a flood event's peak could be determined through the application of spectral analysis to water composing a flood event's peak, either through the use of tracers in real watersheds or the tracking of individual water packets in a numerical model.

Increasing WRS extent is most cost-effective when extents are relatively low, as both V' and S' reductions level off as WRS extent increases. The downwards concavity exhibited by each of the regressions for sediment-loading rate reductions in Figure 15 is fairly representative of such relationships. Increasing the WRS extent and capacity can allow sites to attenuate a precipitation event that would have previously overwhelmed the sites. Increases in sites' capacity for flood attenuation offer lower reductions as WRS extent increases, however, as the flows the sites become capable of withstanding become less and less frequent. The downwards concavity shown in Figure 15 is

introduced by the low frequencies of high-magnitude events, and this concavity is quite apparent in placement scenarios using zones with large areas (i.e., not zone 2 or zone 3). Larger placement zones can achieve higher WRS areas with the extents considered for generalized WRS scenarios (see Table 1), and such high WRS extents can better withstand high-magnitude events. Zone 2 and zone 3 are relatively small, making extents defined as percentages of the zones' areas similarly small. With such small ranges of WRS extents, the reductions for scenarios using these zones more linear. Although the regressions for V' reductions have very high R^2 values (e.g., Figure 15 and Table 5), the extent to which the data deviate from linear relationships is caused by slight downwards concavity, particularly when K = 1E-8 m/s.

The S' reductions presented here represent only the input from bluffs along the three gauged reaches considered here, and these reductions must be considered in the larger context of the watershed's sediment budget. The sediment budget for the outlet of the Le Sueur watershed from 2000 to 2010 was 225,000 Mg/yr (Belmont et al., 2011). Of this 225,000 Mg/yr, 107,000 Mg/yr (48%) is contributed by bluffs within the knickzone of the watershed. The gauged reaches considered here occupy only a portion of this knickzone, and the bluffs along these reaches contribute 68,300 Mg/yr (see Table 3; Bevis, 2015). This 68,300 Mg/yr is the only portion of the sediment budget considered in this study, and it represents 64% of the 107,000 Mg/yr from bluffs within the knickzone and 30% of the 225,000 Mg/yr at the outlet. The reductions in S' achieved will also be met by other reductions not considered in this study. For example, bluffs

downstream of the lower gauges will experience lower erosion rates with peak flow reductions and streambank erosion within the entire knickzone will be reduced. The erosion of the uplands and ravines will not be reduced through the reduction of peak flows in the lower watershed, but the sediment loading reductions presented in this study need to be regarded as only a portion of the benefits offered by WRS implementation scenarios.

The flow generation procedures described in this study were used to create a Microsoft Excel® file capable of instantly producing normalized (i.e., V' and S') and non-normalized peak flow and sediment-loading rate projections for all three lower gauges. Despite the weaknesses of many of the regressions used to generate flows (see Appendix G), the generation procedures used here still replicate SWAT output fairly accurately. Most of the scenarios that had weaker trends in $F_{WRS}/F_{baseline}$ values were also those that produced low V' and S' reductions due to low extents or K values (e.g., using zone 2, zone 3, or K = 1E-8 m/s); even if trends were weak for these scenarios, the typically small range of $F_{WRS}/F_{baseline}$ values achieved did not allow for drastic changes. Despite consistently strong relationships, scenarios using all zones or zone 1 with K = 1E-7 or 1E-6 m/s comprise most of the outliers in Figures 18 and 21. These scenarios produced significant reductions in V' and S', and the large range of $F_{WRS}/F_{baseline}$ values achieved allowed for large reductions and greater deviations from results based on SWAT output. Although the time-consuming use of SWAT was required for the data generation procedures used here, flows at all three lower gauges in any of the 225

scenarios considered (i.e., 5 extents, 3 K values, 3 depths, and 5 placement scenarios) can be reproduced immediately in the flow generator file. Furthermore, different scenarios can be employed within each of the three subwatersheds, allowing a total of 675 potential scenarios. These possible scenario numbers only consider the five extents used for generalized WRS scenarios (Table 1), even though arbitrary extents within this range can be assessed. While the data generation procedures used here are empirical, rather than theoretical, and currently limited to only the three lower gauges within the Le Sueur watershed, the produced relationships between scenarios may aid in creating more generalized approaches to modeling flow reduction through WRS implementation. With a more generalized approach, flow reductions could be modeled at gauges in the nearby Blue Earth and Watonwan watersheds.

The data generation procedures used here will be incorporated into a decision-analysis model. This model will portray the effects of a large variety of management options in the Le Sueur watershed, including grassed waterways, different tillage practices, and bluff toe protection. The reductions in S' offered by WRS implementation scenarios may be combined with those offered by bluff toe protection (e.g., reduce the length of active bluffs used to calculate sediment-loading rates for a certain number of years), and these reductions may also be combined with reductions in the sediment delivery ratios for agricultural fields in the uplands through management options like grassed waterways and different tillage practices. A model offering such a suite of

options may further aid regional stakeholders in selecting management options that best address the issues faced.

4.2: Issues with SWAT

While SWAT is a powerful tool capable of effectively portraying the complex movements of water within a watershed, there are issues with SWAT's treatment of wetlands and these issues must be considered in the interpretation of SWAT output. The first issue discussed is the lumping of all wetlands within each subbasin, while the second is the loss of all water exiting wetlands through seepage.

The lumping of all wetlands within each subbasin in a SWAT model can allow for behaviors that are unrealistic. The most prominent of these behaviors is the implied redistribution of water amongst wetlands in a subbasin, no matter how far apart they are or how they are situated in relation to each other. The small site prioritizations in the initial WRS scenarios were not considered further, as the large number of small sites distributed throughout each subbasin intercepted most of the subbasin's runoff. This interception provided high contributing areas that did not decrease with decreasing WRS extent; only one of the small sites needed to remain on each flow path to maintain flow interception. Any losses in contributing area related to outlets being forced further upstream were also generally made up in reductions of the WRS area used, as this area was subtracted from the flow accumulation of all non-redundant outlets in order to produce a contributing area. This study attempted to lessen the influence of SWAT's

lumping of wetlands by favoring large-site prioritizations; while large sites are still lumped, they are not as widely distributed within each subbasin.

Issues related to wetland lumping could be avoided entirely by using only one wetland in each subbasin. The wetlands to be simulated would need to identified before the model's construction, so that the subbasin delineation produced could favor their use. Such an approach could not be used in this study due to the coarse resolution of the 30-subbasin model and the need for a wide variety of WRS implementation scenarios. Any sites located on a subbasin's main channel would also need to be simulated as a reservoir, rather than a wetland, in order to allow for inputs from the channel network. The 175 subbasin SWAT model offers a spatial resolution that could allow for this approach, but each subbasin would still feature multiple sites. One site would need to be selected for each subbasin, and different prioritization schemes could require different selections of sites for each subbasin. The contributing areas for each selection would also need to be measured; the contributing-area relationship used in this study is only suitable for coarse spatial resolutions. Futhermore, this relationship should not be applied to a different geomorphic setting without data demonstrating its suitability.

The second issue with SWAT's wetlands is the treatment of seepage losses. All water that leaves SWAT's wetlands through seepage is lost from the system, and this loss of water may significantly influence results. This issue ultimately reflects SWAT's overly simplistic treatment of groundwater; only two groundwater units are available,

shallow and deep units, and the deep unit that wetlands contribute to through seepage does not contribute any water back into the watershed. The loss of water could be corrected by (1) increasing each subbasin's daily water yield by the product of the K value used and the current extent of the subbasin's wetlands and (2) routing the adjusted water yield values through the watershed with a Muskingum-Cunge routing model. SWAT does not report the extents of its subbasin-level wetlands, however, so this adjustment could not be performed in this study. If the water lost from sites through seepage arrives in the lower watershed during a period with flows beneath the discharge threshold, then the seepage water would not influence the results presented here. If sites have very high seepage rates and insufficiently short water retention times, then seepage water may contribute appreciably to flows over the threshold in the lower watershed. The current version of SWAT does not allow for these considerations to be assessed, but one could instead consider simple approaches to residence times. A 1 meter column of water in a site with a constant seepage rate of 1E-6 m/s would have an average residence time of about 6 days and a maximum of about 12 days, ignoring evapotranspiration effects. Once the water has drained through the wetland bottom, it still needs time to travel through the subsurface to the channel network before it would impact a flood peak. A flood peak featuring Q/DA values above the discharge threshold in the lower watershed would need to last for 6 to 12 days for most of the site's water to exit through seepage. The addition of the time necessary for the water to arrive at

the channel network could aid in desynchronizing the peak flows in the lower watershed and the arrival of the seepage water to the lower watershed.

5: Conclusion

This study has shown that sites designed to increase water storage can reduce peak flows and sediment-loading rates in the Le Sueur watershed. Placing sites with high hydraulic conductivity values in the upper half of the watershed generally provides the highest reductions, but there are exceptions to this generality. Data obtained from the complex Soil and Water Assessment Tool (SWAT) were used to create a simplified empirical model capable of generating peak flow and sediment-loading rates for the lower reaches of the watershed. This model is being incorporated into another model that portrays a wide variety of management options designed to address the challenges faced in the Minnesota River Basin. Such models have the potential to demonstrate the costs and benefits of potential management scenarios and hopefully motivate real action. Without meaningful action, the problems faced in southern Minnesota may continue to worsen until drastic action is forced upon unwilling land owners. Instead of facing such a crisis, farmers are now able to help shape and adopt practices that address the issues faced and are beneficial to their businesses and livelihoods.

References

Babbar-Sebens, M., Barr, R. C., Tedesco, L. P., & Anderson, M. (2013). Spatial identification and optimization of upland wetlands in agricultural watersheds. *Ecological Engineering*, *52*, 130-142.

Belmont, P., Gran, K. B., Schottler, S. P., Wilcock, P. R., Day, S. S., Jennings, C., Lauer, J., Viparelli, E., Willenbring, J., Engstrom, D., & Parker, G. (2011). Large shift in source of fine sediment in the Upper Mississippi River. *Environmental science & technology*, *45* (20), 8804-8810.

Bevis, M. (2015). *Sediment budgets indicate Pleistocene base level fall drives erosion in Minnesota's greater Blue Earth River basin* (Master's thesis, UNIVERSITY OF MINNESOTA).

Bullock, A., & Acreman, M. (1999). The role of wetlands in the hydrological cycle. *Hydrology and Earth System Sciences*, *7* (3), 358-389.

Day, S. S., Gran, K. B., Belmont, P., & Wawrzyniec, T. (2013). Measuring bluff erosion part 2: pairing aerial photographs and terrestrial laser scanning to create a watershed scale sediment budget. *Earth Surface Processes and Landforms*,*38*(10), 1068-1082.

Engstrom, D. R., Almendinger, J. E., & Wolin, J. A. (2009). Historical changes in sediment and phosphorus loading to the upper Mississippi River: mass-balance reconstructions from the sediments of Lake Pepin. *Journal of Paleolimnology*, *41* (4), 563-588.

Goolsby, D. A., Battaglin, W. A., Aulenbach, B. T., & Hooper, R. P. (2000). Nitrogen flux and sources in the Mississippi River Basin. *Science of the Total Environment*, *248* (2), 75-86.

Gran, K. B., Belmont, P., Day, S. S., Jennings, C., Johnson, A., Perg, L., & Wilcock, P. R. (2009). Geomorphic evolution of the Le Sueur River, Minnesota, USA, and implications for current sediment loading. *Management and restoration of fluvial systems with broad historical changes and human impacts: Geological Society of America Special Paper*, *451*, 119-130.

Gran, K., Belmont, P., Day, S., Jennings, C., Lauer, J. W., Viparelli, E., Wilcock, P., & Parker, G. (2011). An integrated sediment budget for the Le Sueur River Basin. *MPCA Report wq-iw7-29o*.

Gran, K. B., Finnegan, N., Johnson, A. L., Belmont, P., Wittkop, C., & Rittenour, T. (2013). Landscape evolution, valley excavation, and terrace development following abrupt postglacial base-level fall. *Geological Society of America Bulletin*, *125* (11-12), 1851-1864.

Kelley, D. W., & Nater, E. A. (2000). Historical sediment flux from three watersheds into Lake Pepin, Minnesota, USA. *Journal of Environmental Quality*, *29* (2), 561-568.

Kuehner, K. J. (2004, November). An historical perspective of hydrologic changes in Seven Mile Creek watershed. In *Proceedings of the American Society of Agricultural Engineers (ASAE) conference. St. Joseph, Michigan, USA: ASAE*.

Lenhart, C. F., Verry, E. S., Brooks, K. N., & Magner, J. A. (2011). ADJUSTMENT OF PRAIRIE POTHOLE STREAMS TO LAND-USE, DRAINAGE AND CLIMATE CHANGES AND CONSEQUENCES FOR TURBIDITY IMPAIRMENT. *River Research and Applications*, *28*(10), 1609-1619.

Martinez-Martinez, E., Nejadhashemi, A. P., Woznicki, S. A., & Love, B. J. (2014). Modeling the hydrological significance of wetland restoration scenarios.*Journal of environmental management*, *133*, 121-134.

Minnesota Pollution Control Agency (2014). Minnesota's Impaired Waters List. Retrieved from http://www.pca.state.mn.us/index.php/water/water-types-and-programs/minnesotas-impaired-waters-and-tmdls/impaired-waters-list.html

Mitsch, W. J., & Day Jr, J. W. (2006). Restoration of wetlands in the Mississippi–Ohio–Missouri (MOM) River basin: experience and needed research. *Ecological Engineering*, *26* (1), 55-69.

Neitsch, S. L., Arnold, J. G., Kiniry, J. R., & Williams, J.R. (2009). Soil and Water Assessment Tool Theoretical Documentation Version 2009. Temple, TX: Grassland Soil and Water Research Laboratory. *Agricultural Research Service, Blackland Research Center, Texas Agricultural Experiment Station*.

Novotny, E. V., & Stefan, H. G. (2007). Stream flow in Minnesota: Indicator of climate change. *Journal of Hydrology*, *334* (3), 319-333.

Rabalais, N. N., Turner, R. E., & Scavia, D. (2002). Beyond Science into Policy: Gulf of Mexico Hypoxia and the Mississippi River Nutrient policy development for the Mississippi River watershed reflects the accumulated scientific evidence that the increase in nitrogen loading is the primary factor in the worsening of hypoxia in the northern Gulf of Mexico. *BioScience*, *52* (2), 129-142.

Schottler, S. P., Ulrich, J., Belmont, P., Moore, R., Lauer, J. W., Engstrom, D. R., & Almendinger, J. E. (2013). Twentieth century agricultural drainage creates more erosive rivers. *Hydrological Processes. Wiley Online Library. DOI*, *10*.

Wang, X., Yang, W., & Melesse, A. M. (2008). Using hydrologic equivalent wetland concept within SWAT to estimate streamflow in watersheds with numerous wetlands. *Transactions of the ASAE (American Society of Agricultural Engineers)*, *51*(1), 55.

Wang, X., Shang, S., Qu, Z., Liu, T., Melesse, A. M., & Yang, W. (2010). Simulated wetland conservation-restoration effects on water quantity and quality at watershed scale. *Journal of environmental management*, *91* (7), 1511-1525.

Appendix

Appendix A: SWAT Model Setup

ArcSWAT Version 2012.10_1.15 was used to setup the 30-subbasin Le Sueur watershed SWAT model and SWAT2012 Rev. 627 executable was used to simulate streamflow. A 10 m DEM obtained from the National Elevation Dataset distributed by USGS was used to characterize topography and to delineate watershed subbasins and reaches. The ArcSWAT interface was used to enforce (i.e., burn in) the National Hydrography Dataset (NHD) streamlines as the model's stream network. The total area of the watershed was computed by ArcSWAT's automatic watershed delineation dialog as 2894 km^2, with the watershed outlet identified as the confluence of the Le Sueur and Blue Earth Rivers. The watershed's elevations range from 232 to 417 m above sea level. A watershed delineation threshold of 2200 ha resulted in 30 subbasins within the Le Sueur watershed. Land use was initialized using a 2006 Cropland Data Layer (CDL). Soil information for the watershed was specified using SSURGO data obtained through the web soil survey from NRCS for the study area and clipped using ArcSWAT. Multiple HRU delineation criteria were specified, with thresholds of 49% landuse, 0% soil, and 0% slope, resulting in 2103 Hydrologic Response Units (HRUs). Six climate stations were used to populate the model with daily weather data obtained from the global weather data for SWAT database.

The flow years were separated into two parts comprised of wet, normal and dry years, which were further divided into calibration and validation datasets such that all three types were present in both datasets. Calibration was attempted at a daily time The 175-subbasin SWAT model was created with SWAT 2012 version 635. Subbasins were delineated using a 1500 ha threshold. Simulations ran from 2004 to 2010, with no data recorded for the first two years to allow for adjustment from initial conditions. The NSE values for the 175-subbasin model (Table 12) are considerably higher than those for the 30-subbasin model. Although the highly-resolved model more effectively captures

Table 10. Calibrated parameter values for the 30 subbasin SWAT model.

Parameter	Default Value	Calibrated Value
TIMP	1	0.25
EPCO	1	0
SURLAG	4	1
Channel Routing	Variable Storage	Muskingum
DDRAIN_BSN	Inactive	1200
TDRAIN_BSN	Inactive	48
TDRAIN_BSN	Inactive	24
DEP_IMP	6000	2000
CH_N1	0.014	0.368
CH_N2	0.04	0.03
ALPHA_BF	0.048	Max: 0.1585, Min: 0.0046
DEEPST	2000	1000
CN2	NA	±10%

Table 11. Nash-Sutcliff Efficiency (NSE) coefficients describing the goodness of fit for the 30 subbasin SWAT model.

Stream gage	Nash-Sutcliff Efficiency
Le Sueur River at St. Clair, CSAH28	-0.17
Le Sueur River nr Rapidan, CR8	-0.02
Le Sueur River nr Rapidan, MN66	-0.27
Little Beauford Ditch nr Beauford, MN22	0.03
Little Cobb River nr Beauford, MN	0.05
Big Cobb River nr Beauford, CR16	0.01
Maple River nr Sterling Center, CR18	0.20
Maple River nr Rapidan, CR35	0.15

the behaviors exhibited by the gauging record (Figure 11), the model was not available when this study began. Peak flow and sediment-loading rate projections from each model do not differ by orders of magnitude (Table 4), however, and projections are largely evaluated here after normalization by baseline values.

Table 12. Nash-Sutcliff Efficiency (NSE) coefficients for the 175 subbasin SWAT model of the Le Sueur Watershed.

Stream Gauge	Seasonal NSE	Overall NSE
Le Sueur River at St. Clair, CSAH28	0.64	0.65
Le Sueur River near Rapidan, CR8	0.79	0.57
Le Sueur River near Rapidan, MN66	0.89	0.72
Little Beauford Ditch near Beauford, MN22	0.60	0.68
Little Cobb River near Beauford, MN	0.75	0.63
Big Cobb River near Beauford, CR16	0.69	0.48
Maple River near Sterling Center, CR18	0.82	0.76
Maple River near Rapidan, CR35	0.65	0.68

Appendix B: SWAT's Hydrological Functions

This section discusses the modeling framework of SWAT, focuses on the hydrological functions pertinent to wetlands, and largely paraphrases the SWAT theoretical documentation created by Neitsch et al. (2009). Note that this documentation is for SWAT 2009, while SWAT 2012 is largely used in this study; no theoretical documentation for SWAT 2012 is available, and any important distinctions between the versions are noted. SWAT 2005 is described by Neitsch et al. (2005) and was used for sensitivity analyses performed in the Seven Mile Creek Watershed. Many models can be treated as "black boxes" (i.e., tools that are fed input and produce output, yet are not understood) by users, despite the fact that understanding the manner in which results are obtained is essential to the interpretation of those results. A presentation of SWAT's operation is therefore important to the context of this study.

In SWAT, a watershed is partitioned into a number of subbasins (Figure 23). Each subbasin consists of a number of spatially lumped (i.e., not spatially explicit) Hydrologic

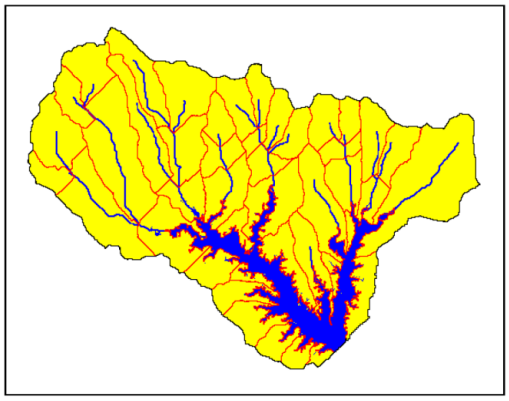

Figure 23. Image showing an example of subbasin delineation in the Lake Fork Watershed. From Neitsch et al. (2009).

Response Units (HRUs). HRUs are land segments with certain land cover, soil, slope, and management combinations. Varying numbers of HRUs within subbasins can be produced by dictating different land use, soil, and slope thresholds. For example, setting a high land use threshold (e.g., 99% over subbasin area) will allow only the most prevalent land use to be represented. Only one HRU for each subbasin could be generated by using similarly high thresholds for soil and slope classes, while smaller HRUs could be defined by using lower thresholds for these classes. Setting delineation thresholds of 0% would make HRUs for each unique combination of soil, slope, and land use in the subbasin. Such an exhaustive approach, however, can increase both model run times and computational requirements without appreciable changes in modeling results. Since HRUs are spatially inexplicit, they do not interact with each other; the runoff from each HRU is predicted individually and used to obtain the total runoff from all HRUs, before this total runoff is input into the channel network of the watershed. Note that this distinction prevents water from flowing between HRUs and allows HRUs representing areas that are not adjacent to channels to contribute their runoff (surficial and subsurface) directly into channels.

The hydrological functions in SWAT are separated into two phases: the land phase, which controls the amount of water, sediment, nutrients, and pesticides input into the channel network from the surrounding land (i.e., HRUs in each subbasin), and the routing phase, which consists of the movement of those inputs through the channel

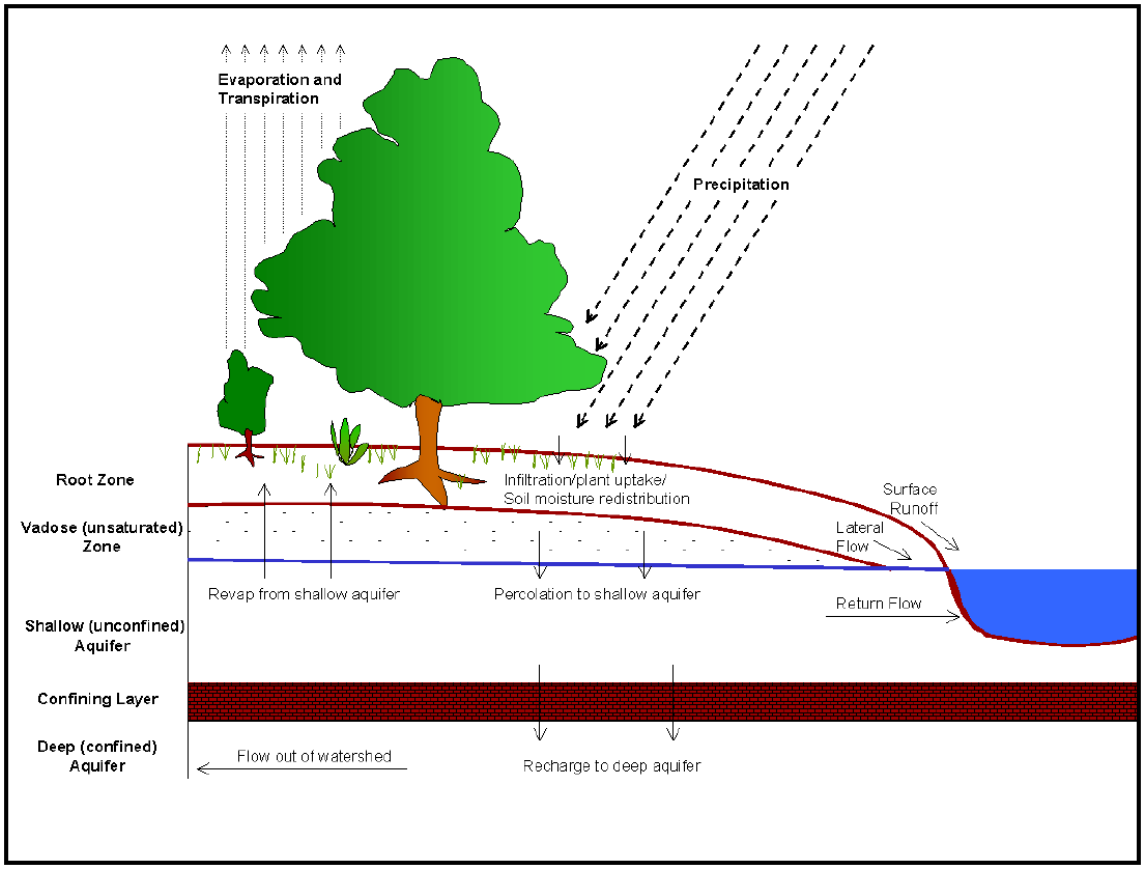

Figure 24. Image demonstrating the processes involved in the land phase of SWAT's hydrological cycle. From Neitsch et al. (2009).

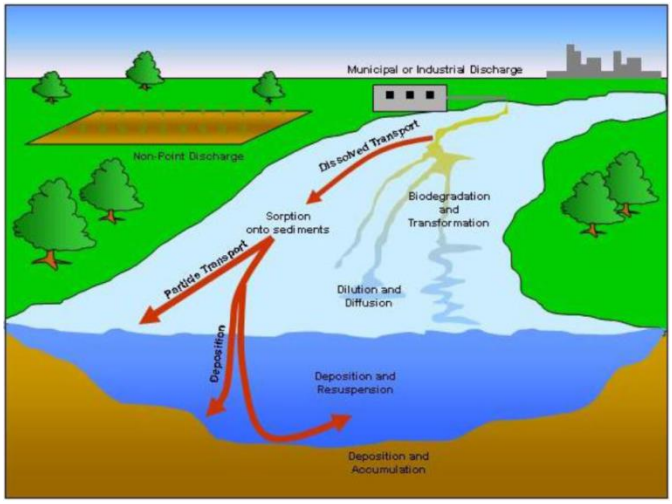

Figure 25. Image showing the processes involved in the routing phase of SWAT's hydrological cycle. From Neitsch et al. (2009).

network. Figure 24 depicts the land phase while Figure 25 depicts the routing phase. During the land phase, the hydrological cycle is based on the water balance equation:

$$SW_t = SW_0 + \sum_{i=1}^{t}\left(R_{day} - Q_{surf} - E_a - w_{seep} - Q_{gw}\right) \quad (13)$$

where SW_t is the final soil water content (mm H_2O), SW_0 is the initial soil water content o day i (mm H_2O), t is time (days), R_{day} is the amount of precipitation on day i (mm H_2O), Q_{surf} is the amount of surface runoff on day i (mm H_2O), E_a is the amount of evapotranspiration on day i (mm H_2O), w_{seep} is the amount of water entering the vadose zone from the soil profile on day i (mm H_2O), and Q_{gw} is the amount of return flow on day i (mm H_2O).

Before the components of the water balance equation can be calculated, however, the climatic inputs of the watershed must be processed. SWAT requires daily precipitation, maximum/minimum air temperatures, solar radiation, wind speed, and relative humidity inputs. These inputs may be obtained from records of observed data or generated during the simulation. These climatic inputs control the upper steps shown in Figure 26, a diagram of the command loop used to model the land phase of the hydrological cycle in SWAT.

The lower steps in Figure 26 consider the fate of precipitation falling upon an HRU; this fate is controlled by the pathways available for water's movement in SWAT. These pathways are depicted in Figure 27. Note that interception by vegetation is not shown, as it is considered in the calculation of surface runoff when using the curve number method. Although the curve number method is commonly used, the Green &

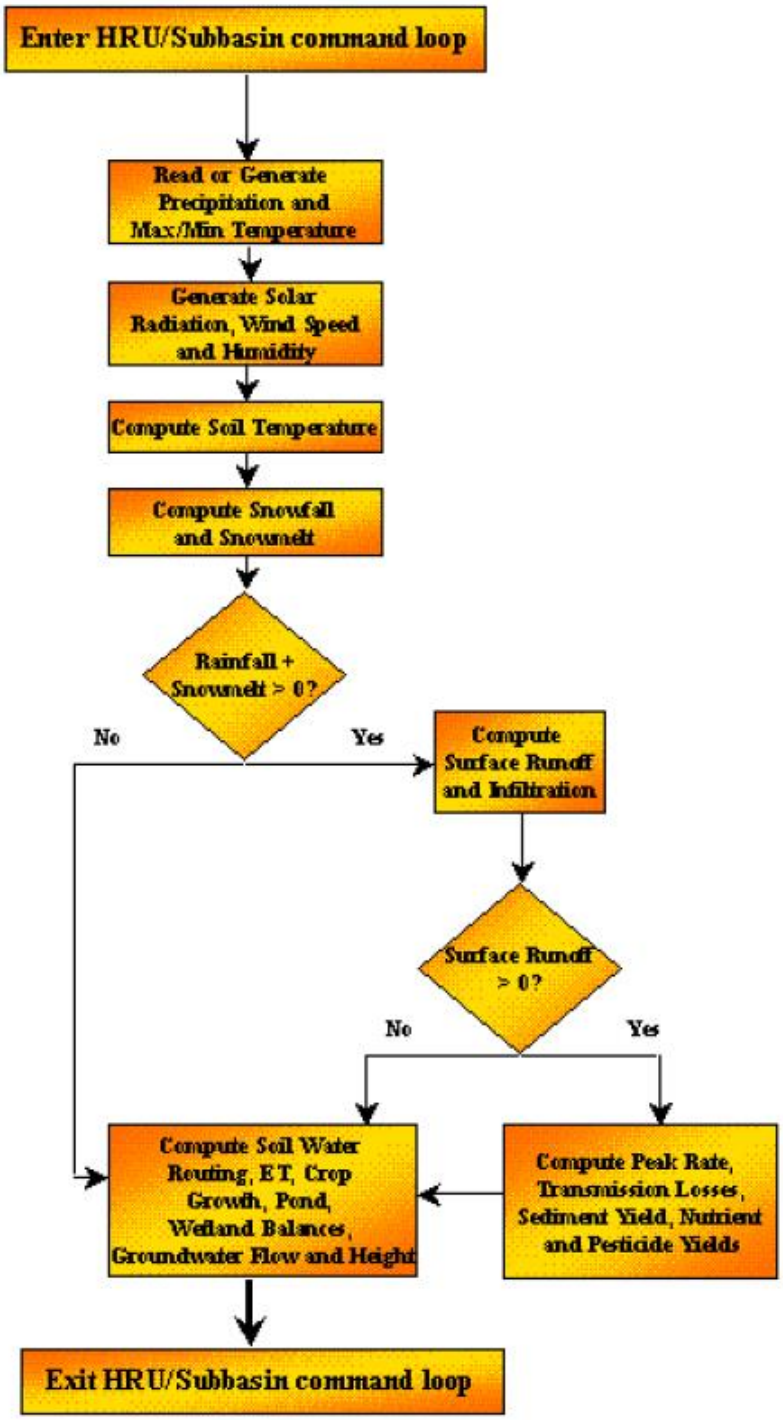

Figure 26. Representation of the HRU/Subbasin command loop used in SWAT. From Neitsch et al. (2009).

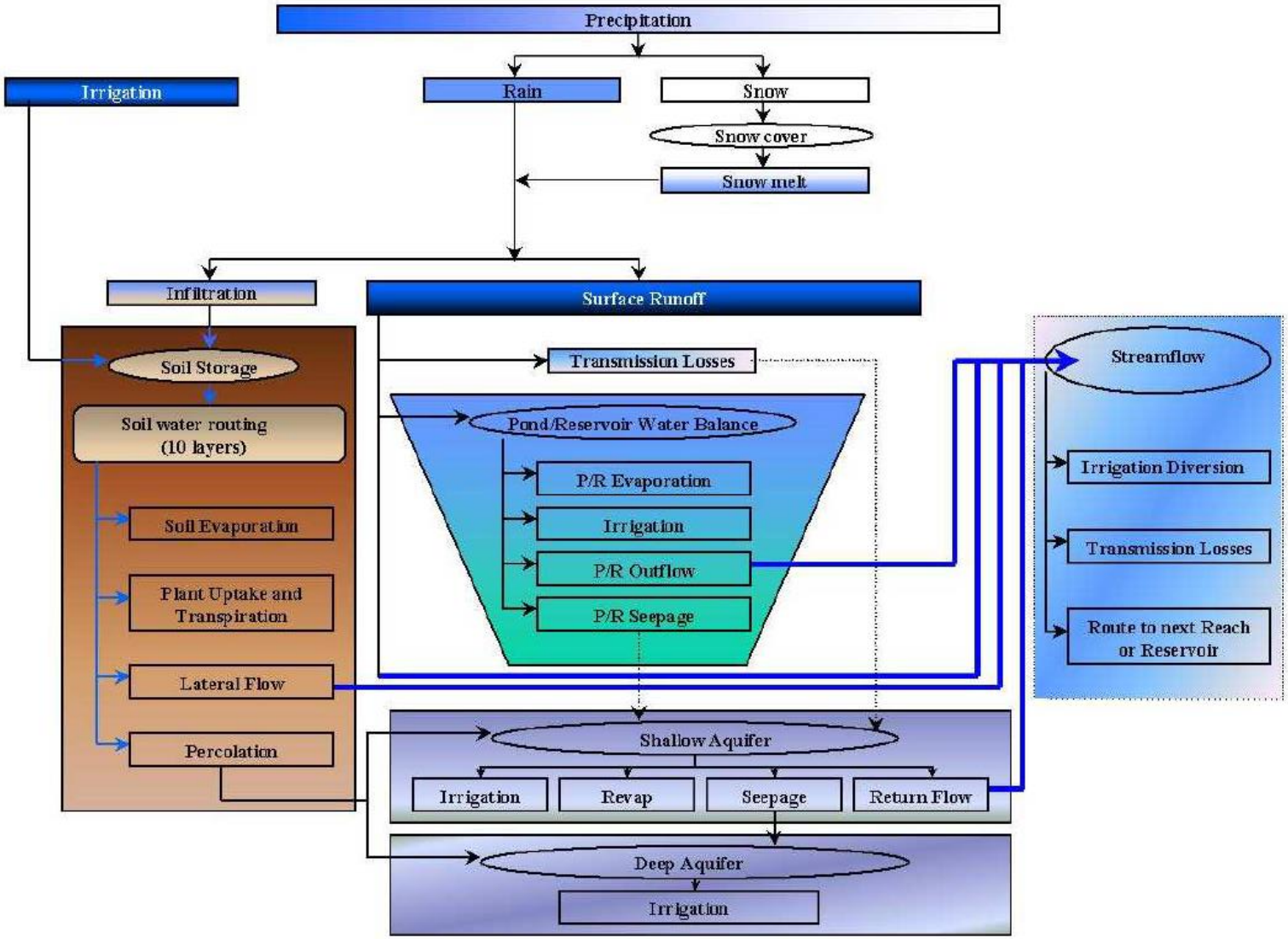

Figure 27. Representation of the pathways available for water's movement in SWAT. From Neitsch et al. (2009).

Ampt method of infiltration and runoff modeling is also available. The latter method calculates canopy storage separately. The curve number method operates on a daily time-step, and is therefore unable to directly model infiltration; infiltration is taken as the difference between the rainfall input and surface runoff calculated. The Green & Ampt method does model infiltration directly, but requires subdaily precipitation data. The models used in this study employ the curve number method. While surface runoff volumes for each HRU can be calculated with either the curve number method or the Green & Ampt method, peak runoff rates for each HRU are calculated with a modification of the rational method.

Water that has infiltrated into soils from either precipitation or irrigation sources will be redistributed through the soil profile. This redistribution is caused by differences in water content in the profile, and will cease once uniformity is reached. SWAT simulates redistribution with a storage routing technique; downward flow occurs when a soil layer's field capacity is exceeded and the layer below is not saturated. Percolation (i.e., downward flow) rates are controlled by the saturated conductivity of the soil layer and are brought to zero in a layer when that layer is at or below 0°C. Lateral subsurface (depths of 0-2m) flow is considered simultaneously with redistribution and is calculated with a kinematic storage model accounting for hydraulic conductivity, slope, and soil water content.

SWAT separates groundwater systems into two aquifers. The first, shallower unit is an unconfined aquifer capable of contributing water to streams within the watershed.

The second, deeper unit is a confined aquifer that contributes water to streams outside of the watershed. Any water percolating into the deep aquifer is therefore lost from the model. A fraction of the total daily recharge can be input to the deep aquifer; this fraction is removed from the water percolating past the bottom of the root zone. The remaining water is input to the unconfined aquifer, and can be lost to streams, the overlying soil profile during dry conditions, and plants. Both the shallow and deep aquifer can lose water to pumping.

SWAT allows for four types of water bodies: reservoirs, ponds, wetlands, and potholes. These water bodies differ in their input and output of water as well as their place within the scale of the watershed. Reservoirs are located on the main channel network of the watershed and receive water from upstream reaches. Ponds and wetlands are not located on the channel network, and receive water from a fraction of their subbasin's total discharge. This fraction is meant to represent the water body's contributing area; obtaining a physically representative value for this contributing area is an important challenge, as previously noted. Ponds and wetlands only differ in their outflow, as ponds change their outflow to pursue a targeted storage volume while wetlands do not. In this sense, ponds are meant to maintain a more consistent form and presence while wetlands are allowed to alter their own appreciably. These differences are explored further below. The fourth type of water body, potholes, occur on the HRU level, rather than the subbasin level. An individual HRU can be designated as a pothole, and a fraction of the discharge from specific HRUs in the same subbasin can be routed

into this pothole. Potholes can therefore be made to reflect the physical drainage area of a water body more directly than a pond or wetland. The large numbers of HRUs and subbasins in a SWAT model, however, can render a reliance on potholes unrealistic or inefficient. All types of water bodies can gain and lose water from direct precipitation onto or evaporation from their surfaces, respectively. Their surface areas also change as an exponential function of their volumes. All types of water bodies can also lose water through seepage.

SWAT's wetlands are used in this study to simulate distributed stream flow management systems. Ponds are not used, as the simulated control systems will alter their contained volumes freely and without a target value. The water balance of a wetland is simulated with Equation 1 (section 2.1).

Many of the water balance components shown in Equation 1 depend on the surface area of the water body. The surface area of a subbasin's wetlands is updated daily as:

$$SA = \beta_{sa} \cdot V^{expsa} \tag{14}$$

where SA is the surface area (ha), β_{sa} is a coefficient, V is the volume of water at the end of the day (m^3 H_2O), and *expsa* is an exponent. The *expsa* and β_{sa} of wetlands are calculated daily as:

$$expsa = \frac{\log_{10}(SA_{mx}) - \log_{10}(SA_{nor})}{\log_{10}(V_{mx}) - \log_{10}(V_{nor})} \tag{15}$$

$$\beta_{sa} = \left(\frac{SA_{mx}}{V_{mx}}\right)^{expsa} \tag{16}$$

where SA_{mx} is the surface area when filled to the maximum water level (ha), SA_{nor} is the surface area of when filled to the normal water level (ha), V_{mx} is the volume of water in the wetland when filled to the maximum water level (m^3 H_2O), and V_{nor} is the volume of water in the wetland when filled to the normal water level (m^3 H_2O).

The volume of precipitation falling directly onto the surface of a wetland over the course of a day is calculated as:

$$V_{pcp} = 10 \cdot R_{day} \cdot SA \tag{17}$$

where V_{pcp} is the volume of precipitation gained during the day (m^3 H_2O), R_{day} is the precipitation during the day (mm H_2O), and SA is the surface area (ha).

Wetlands' inputs of surficial runoff, groundwater, and lateral flow from the rest of the subbasin are governed by the term V_{flowin}, calculated as:

$$V_{flowin} = fr_{imp} \cdot 10 \cdot (Q_{sur} + Q_{gw} + Q_{lat}) \cdot (Area - SA) \tag{18}$$

where V_{flowin} is the total volume of water added through surficial runoff, groundwater, and lateral flow during the day (m^3 H_2O), fr_{imp} is the fraction of the subbasin draining into the water body (equivalent to WET_FR), Q_{surf} is the total surface runoff produced in the subbasin during the day (mm H_2O), Q_{gw} is the total groundwater flow produced in the subbasin during the day (mm H_2O), *Area* is the area of the subbasin (ha), and SA is the wetland's surface area on that day (ha). Wetlands' inputs from Q_{surf}, Q_{gw}, and Q_{lat} are removed from their subbasin's total output to the main channel. Wetlands therefore act as a kind of buffer between the HRUs and main channel of each subbasin.

The daily evaporation from a wetland is calculated as:

$$V_{evap} = 10 \cdot \eta \cdot E_0 \cdot SA \quad (19)$$

where V_{evap} is the volume evaporated during the day (m^3 H_2O), η is an evaporation coefficient, E_0 is the potential evapotranspiration during the day (mm H_2O), and *SA* is the surface area (ha). Note that η is represented by the input parameter WETEVCOEFF. The default value of η is 0.6, but it may range from 0 to 5 in SWAT 2009 and SWAT 2012. SWAT 2005 does not allow this parameter to be changed from its default value. Certain types of wetlands might tend towards certain WETEVCOEFF values. If such values could be determined, modelers could further refine the hydrological behavior of wetlands. Only one evaporation coefficient can be enforced on the lumped wetlands of each subbasin, however, restricting the extent to which individual wetlands can be specialized. This obstacle could be met through the use of more subbasins in the watershed, but many attempts at the estimation of WETEVCOEFF values are unlikely to be sufficiently accurate, but such inaccuracies could prevent results from being suitable in the context of real management scenarios. SWAT's wetlands do not include the simulation of plants that could enhance water loss through transpiration, and this study uses a WETEVCOEFF value of 1.

The water lost from seepage through a wetland's bottom is calculated daily as:

$$V_{seep} = 240 \cdot K_{sat} \cdot SA \quad (20)$$

where V_{seep} is the volume lost through seepage during the day (m^3 H_2O), K_{sat} is the effective saturated hydraulic conductivity of the wetland's bottom (mm/hr), and *SA* is the surface area of the wetland (ha). It is implied that the coefficient is 24 hrs·10. Water

that leaves a wetland through seepage enters the lower aquifer and is therefore lost from the model. Note that if *SA* is taken as the surface area of the top of the wetland, this construction assumes that the wetland's bottom is similar in surface area to its top. Real wetlands are unlikely to meet this assumption, and may instead have greater surface areas on their bottoms. This distinction may be slight, however, and one could account for it by using a slightly higher K_{sat} value. The K_{sat} value of a wetland is controlled by the input parameter WET_K, and only one conductivity value can be enforced on the lumped wetlands of each subbasin. Although WET_K should vary with the sediments under wetlands, deriving exact values each subbasin's WET_K value is impeded by the highly variable nature of conductivity measurements, variations in effective conductivity with water content (i.e., pressure head on the bottom), and the large extent of many SWAT models. Determining the effective hydraulic conductivity of the bottom of a specific subbasin's lumped wetlands and then taking a slightly higher value to account for the shapes of the component wetlands is an unrealistic modeling approach. Fortunately, the uplands of each study area considered here may be much more homogeneous over space than many areas due to Minnesota's glacial history. The uplands of the Le Sueur watershed are dominated by glacial lacustrine sediments; glacial Lake Minnesota covered the western two-thirds of the watershed, leaving up to 3 m of flat glaciolacustrine silts and clays (Gran et al., 2013). The uplands of the Seven Mile Creek Watershed, another subwatershed of the Minnesota River Basin located north of glacial Lake Minnesota's former location, are dominated by several types of glacial clay

loam sediments (Kuehner, 2004). This study uses a wide range of hydraulic conductivity values that are feasible within the study area (Table 1).

Outflow from a wetland occurs when the water volume exceeds the normal storage volume and is calculated with Equations 2-4 (section 2.1). Note that outflow begins when wetlands exceed their normal storage volumes, but that this outflow occurs at one tenth of the difference between the current volume and the normal storage volume. When wetlands exceed their maximum storage volumes, all of the excess volume is released. Neitsch et al. (2009) does not specify the basis of this relationship. Obtaining exact surface areas and volumes for the normal and maximum water levels of nonexistent wetlands could be subject to many inaccuracies. In this study, wetlands are defined within topographic depressions (i.e., areas where flow direction routines cannot “escape” and produce a pathway to the channel network, indicating that water will accumulate; DEM resolution is important, as is discussed above) or in areas that would become isolated from the channel network through ditch plugging and other means of intervention. The identification of potential wetland sites used here provides surface areas and average depths, which are used to obtain volumes, but does not attempt to provide lower areas and volumes at which the wetlands would begin spilling at one tenth of the usual rate. Since the sites used here are existing or potential depressions, water may not escape appreciably until the maximum volume is reached. This study takes the normal and maximum water levels to

be equal to each other (i.e., WET_NVOL=WET_MXVOL and WET_NSA=WET_MXSA), so that any excess water is simply spilled.

Appendix C: Flow Generation Procedures

This section outlines the flow generation procedures used in this study. The figures shown are an example for one lower gauge in one scenario (Le Sueur with all zones used, depths of 1 m, and K = 1E-6 m/s), but the same process was applied to all generalized WRS scenarios. First, SWAT discharge data from the generalized WRS scenarios are normalized by drainage area (Q/DA), binned every 0.0025 $m^3/s/km^2$ beginning at 0.01 $m^3/s/km^2$, and plotted against their average occurrences per year (Figure 28). Q/DA values are then normalized by the maximum value at the lower gauge in the baseline scenario, $(Q/DA)_{baseline\ max}$. Since both axes are now dimensionless, exponential regressions can be fit to the data. The data are evaluated at different ranges: 0.01 to 0.05 $m^3/s/km^2$, 0.04 to 0.1 $m^3/s/km^2$, and 0.06 $m^3/s/km^2$ to the maximum value. Ranges overlap in order to increase continuity between ranges. Figures 30-32 show the exponential regressions fit to each of the ranges in this scenario, but the coefficient and exponent (γ and δ; see Equation 9) and R^2 values for all scenarios' exponential regressions are included in the flow generator file available in the digital archive attached to this thesis. Figure 33 shows the regressions for three extent scenarios (0, 2, and 7.5%). Only three extents are shown so that the transitions between ranges are more visible. These regressions are then pieced together by switching from one to the next at a point where they overlap (normalized Q/DA values of about 0.31 and 0.55) in order to yield continuous frequencies for all Q/DA values (Figure 34). Each bin's frequency is then normalized by the bin's frequency in the baseline scenario; doing

so for the data in Figure 34 produces those in Figure 17. Peak flows are then generated by (1) evaluating linear trends in the frequencies of Q/DA values relative to the baseline scenario ($F_{WRS}/F_{baseline}$) with WRS extent along "vertical slices" (i.e., specific normalized Q/DA bins) in data sets like Figure 17, (2) evaluating linear trends between the maximum Q/DA values and WRS extent (Figure 35), and (3) using a selected WRS extent in combination with the linear regressions created to solve for both the frequencies of specific Q/DA bins and the maximum Q/DA value achieved.

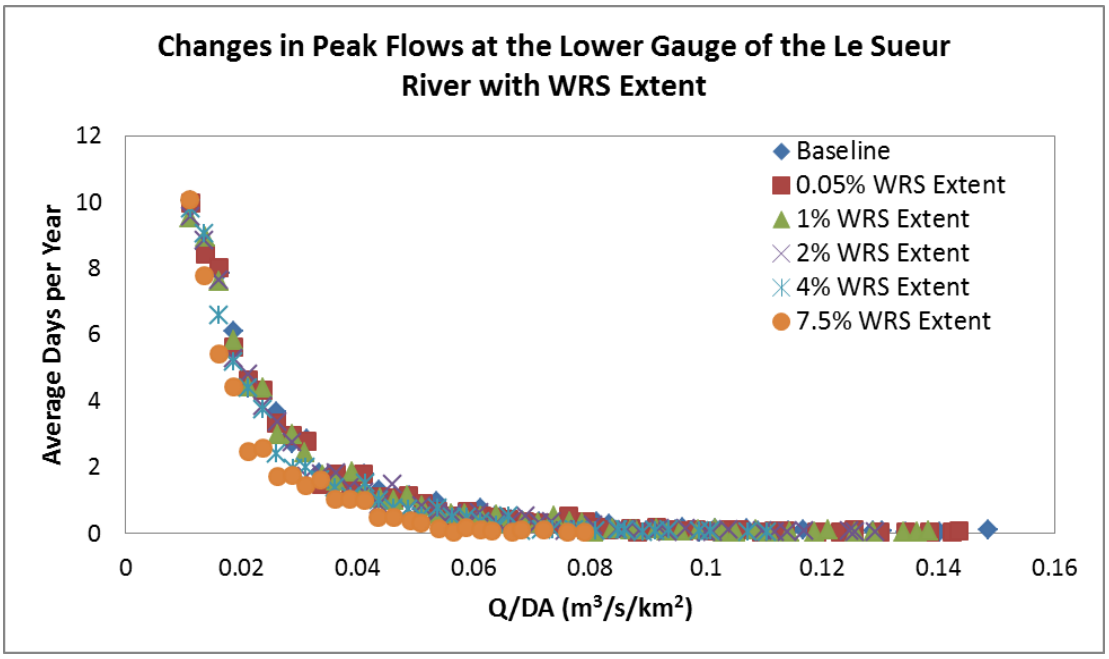

Figure 28. Average days per year for binned discharge per unit area values (Q/DA) at the lower gauge of the Le Sueur River with all zones used, depths of 1 m, and K = 1E-6 m/s. The extents listed in the legend are in terms of both the zone and watershed areas, since all zones are used.

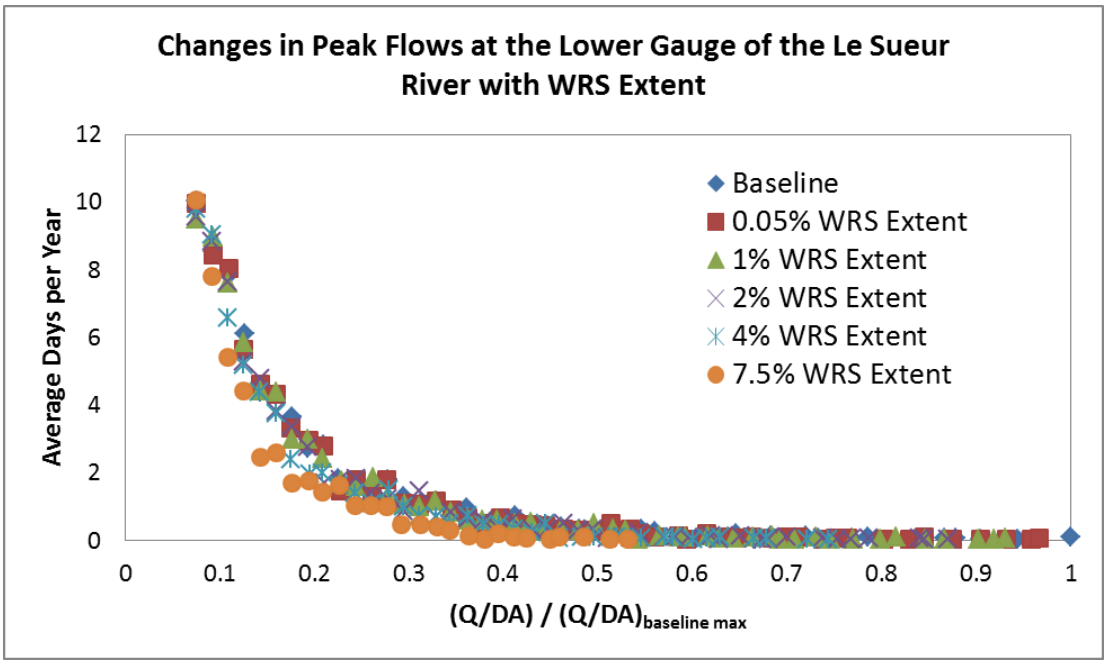

Figure 29. Version of Figure 25 after Q/DA values have been normalized by the maximum value achieved in the baseline scenario, $(Q/DA)_{baseline\ max}$.

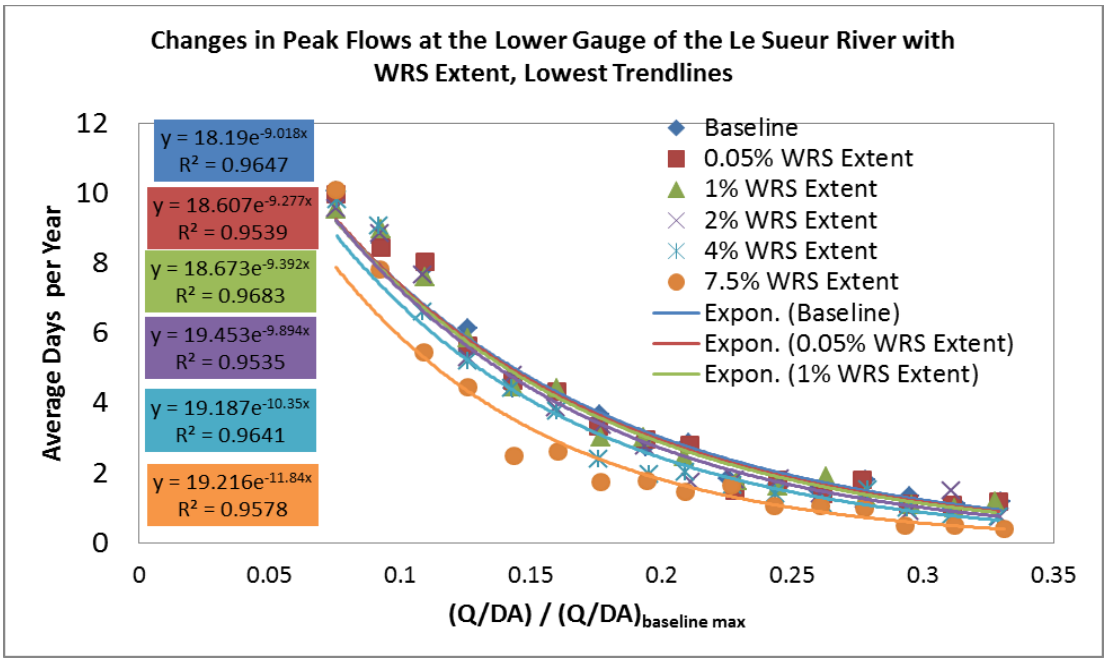

Figure 30. Average days per year for the lowest range of normalized Q/DA values at the Le Sueur River's lower gauge in the scenario considered here. Trendline labels are color coded.

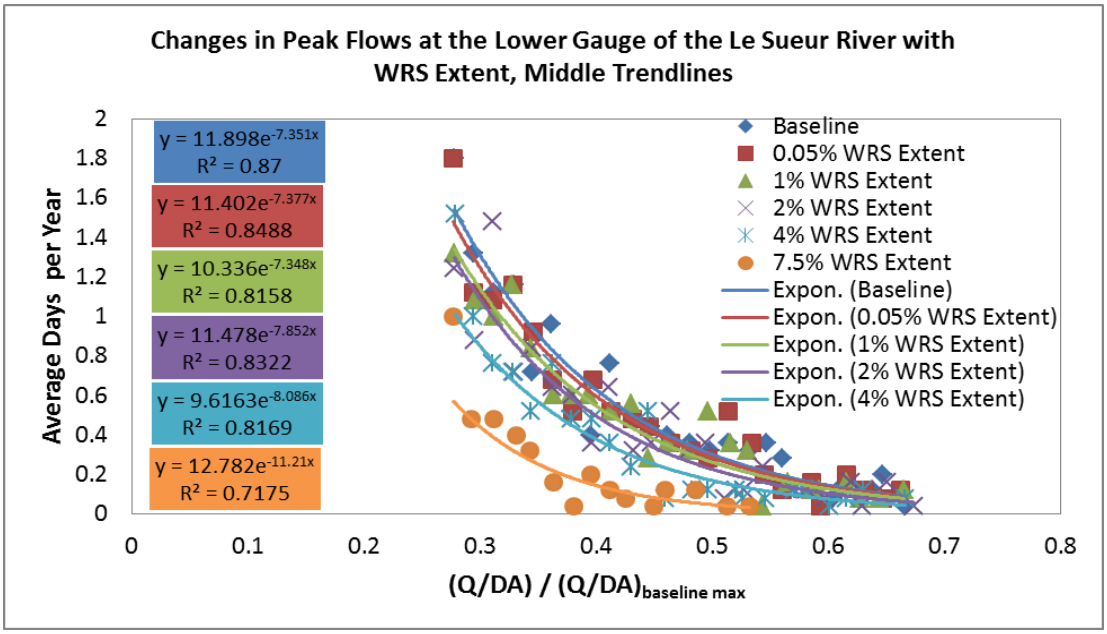

Figure 31. Average days per year for the middle range of normalized Q/DA values at the Le Sueur River's lower gauge in the scenario considered here. Trendline labels are color coded.

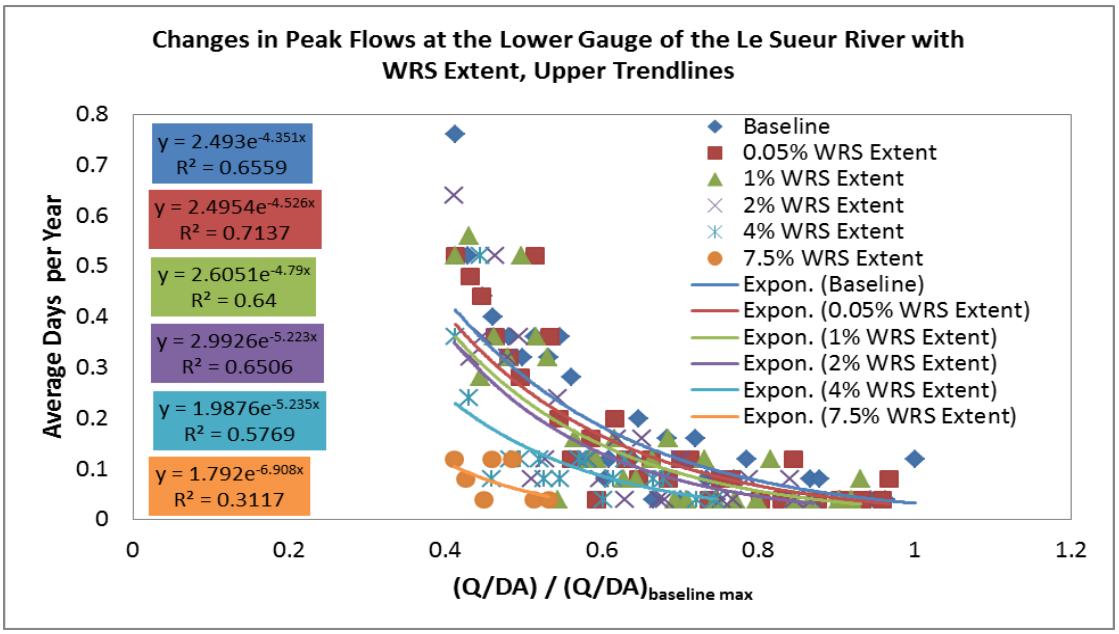

Figure 32. Average days per year for the highest range of normalized Q/DA values at the Le Sueur River's lower gauge in the scenario considered here. Trendline labels are color coded.

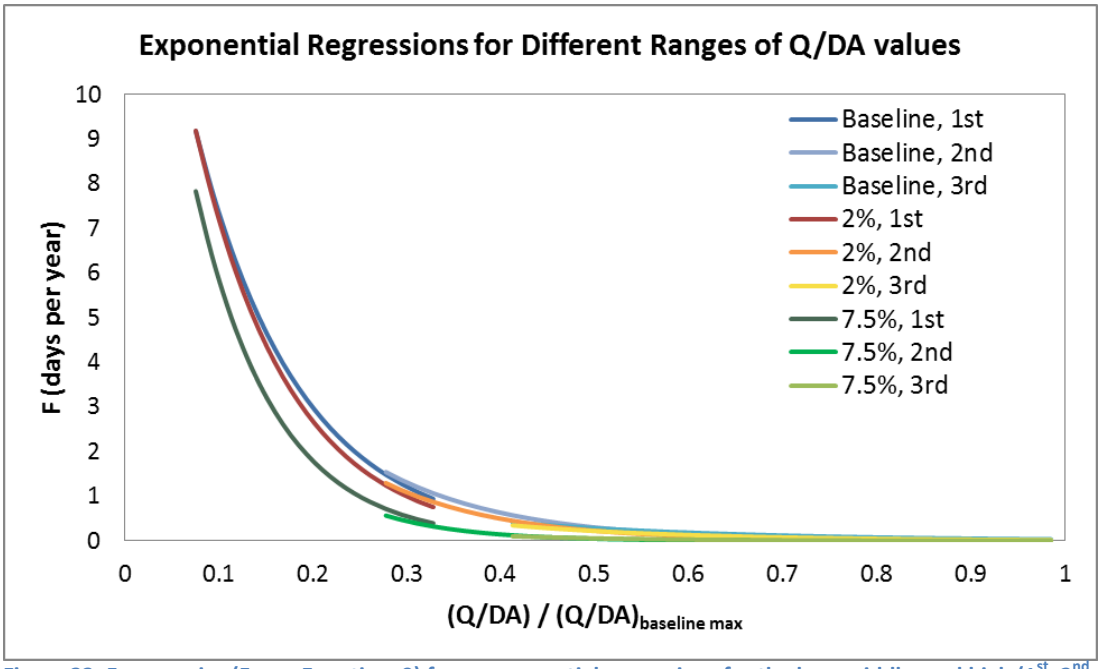

Figure 33. Frequencies (F; see Equatio n 9) from exponential regressions for the low, middle, and high (1st, 2nd, and 3rd) ranges of normalized Q/DA values. Only three scenarios (i.e., baseline, 2% of watershed used, and 7.5% of watershed used) are shown in order to clarify the transitions between regressions.

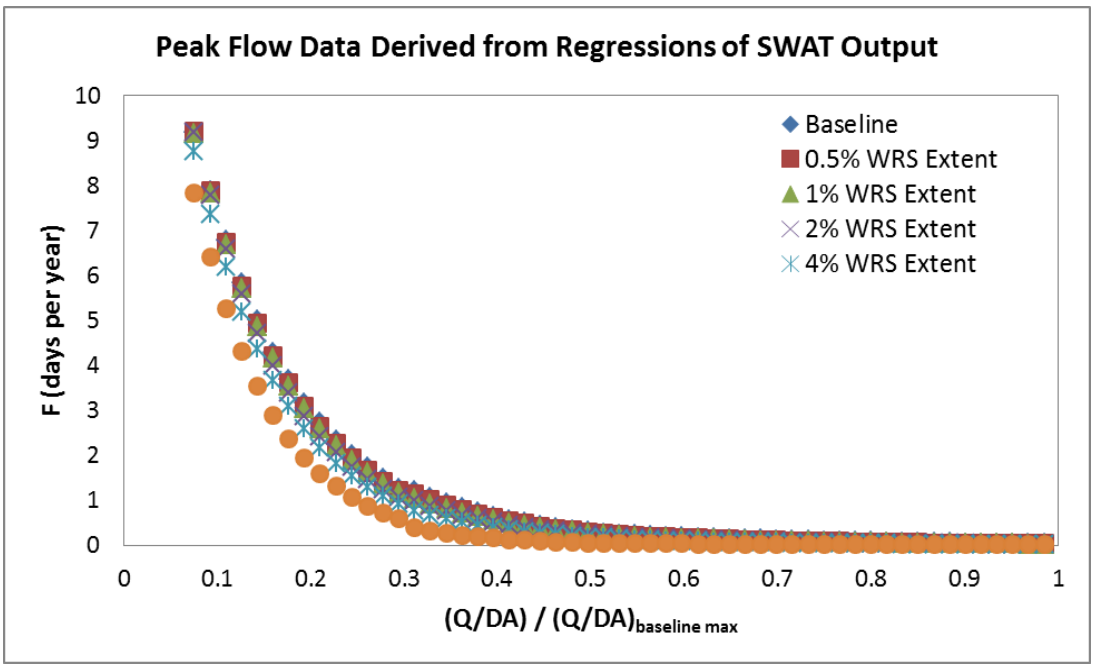

Figure 34. Frequencies (F; see Equation 9) for specific normalized Q/DA values obtained from exponential trendlines fit to SWAT output. The prediction of F values switches from using one regression to the next at points where the regressions overlap (normalized Q/DA values of about 0.31 and 0.55). When each F value on this figure is normalized by the corresponding F value in the baseline scenario, the data shown in Figure 14 are produced.

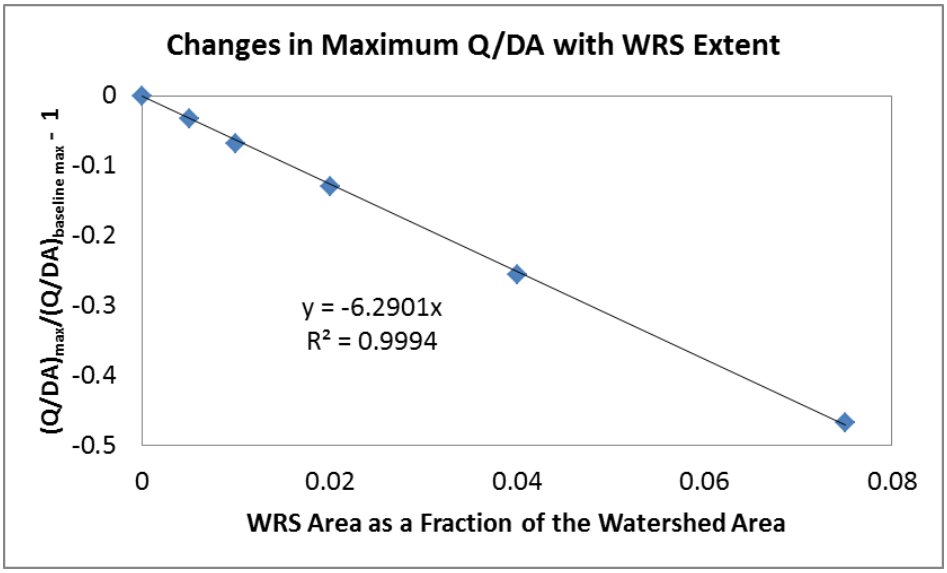

Figure 35. The linear regression of the maximum normalized Q/DA values achieved (see Figure 14) versus WRS extent in the scenario considered here. A value of one was removed from all normalized maximum Q/DA values because the Excel function LINEST was used to evaluate slopes; LINEST calculates a slope for a linear regression using a fixed intercept of zero. Calculations made with this relationship corrected for the adjustment.

Appendix D: 30 subbasin SWAT model's performance

The performance of the 30 subbasin SWAT model at the watershed outlet varies considerably by season (Figure 36). Seasons are defined here as groups of months: May-June, July-August, September-October, November-February, and March-April. The model correctly portrays that the highest flows occurring from March to June, although the top 30% of projected March-April flows are considerably higher than those from gauging records. In contrast, the upper 30% of the model's May-June flows closely match the corresponding gauged flows. This period of high performance at the outlet is important, as the May-June period often features the highest flows and turbidity levels (Belmont et al., 2011). The 30 subbasin SWAT model does, however, portray flows at the outlet going to zero with a high frequency. This lack of flow might be related to the need for the model to capture peak flows; the model was made to be so responsive, or "flashy," that the bottom 70% of summer flows (i.e., July-October) falls to zero. This lack of aptitude for capturing base flows is somewhat alleviated by the fact that this study focuses solely on peak flows; see the exceedance probabilities for the threshold of 0.01 $m^3/s/km^2$ shown in Table 2.

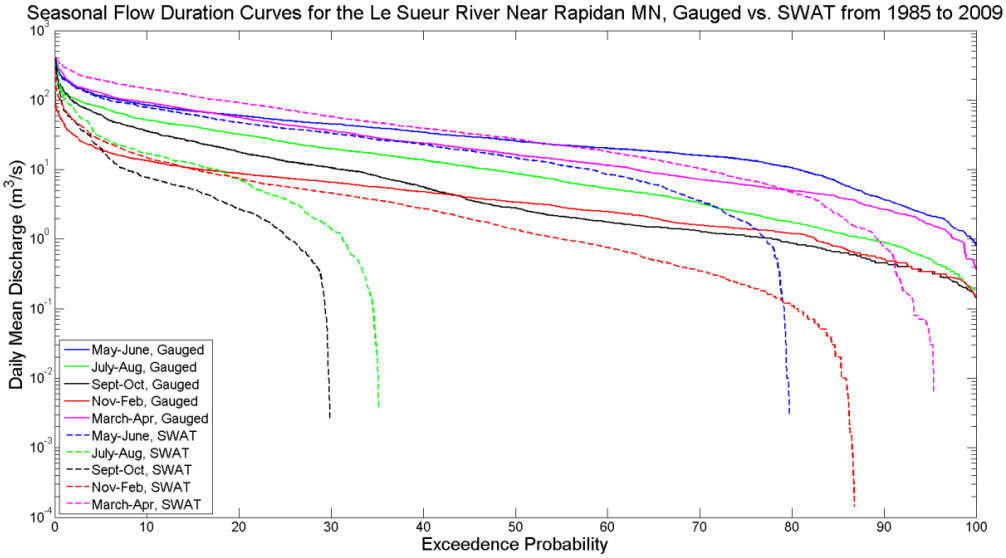

Figure 36. Seasonal SWAT-predicted and gauged flows at the watershed outlet. The 30 subbasin SWAT model used here does not capture baseflows well (e.g., flows frequently drop to zero in July-October), but it more effectively captures peak flows in spring the and early summer (i.e., March-June).

Appendix E: Results for each river in the initial WRS scenarios

This section provides peak flow volume and sediment-loading rates, normalized by baseline values (V' and S'), for Le Sueur, Cobb, and Maple Rivers in the initial WRS scenarios. Peak flows are those exceeding the threshold of 0.01 $m^3/s/km^2$ at one of the lower gauges, and all sediment-loading rates are for near-channel features along each river's gauged reach (see Figure 5). See section 2.4 for more details regarding the calculation of V' and S' parameters.

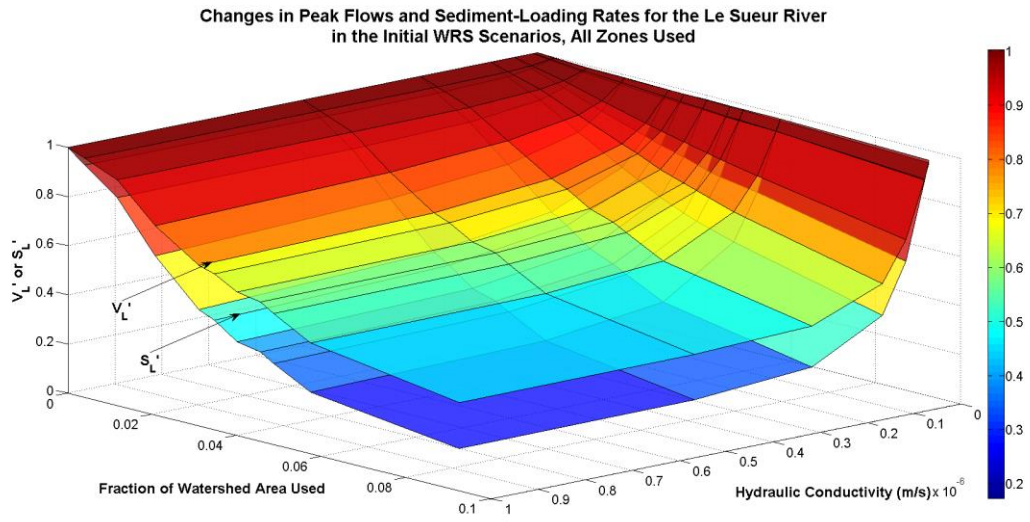

Figure 37. Changes in peak flow volumes at the Le Sueur River's lower gauge normalized by the baseline total (V_L') and sediment-loading rates of the Le Sueur River's gauged reach normalized by the baseline rate (S_L') with both WRS extent and hydraulic conductivity. These initial WRS scenarios use all zones.

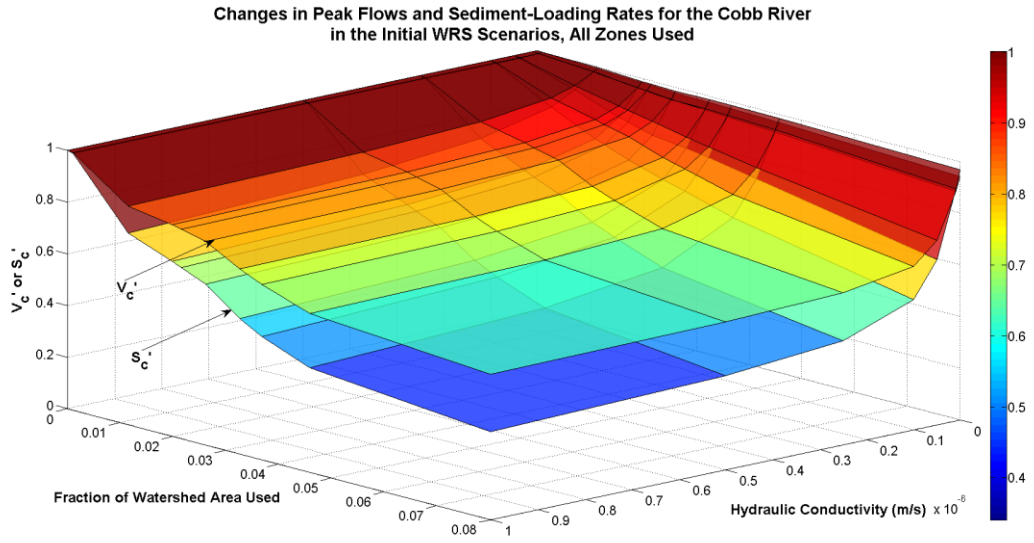

Figure 38. Changes in peak flow volumes at the Cobb River's lower gauge normalized by the baseline total (V_C') and sediment-loading rates of the Cobb River's gauged reach normalized by the baseline rate (S_C') with both WRS extent and hydraulic conductivity. These initial WRS scenarios use all zones.

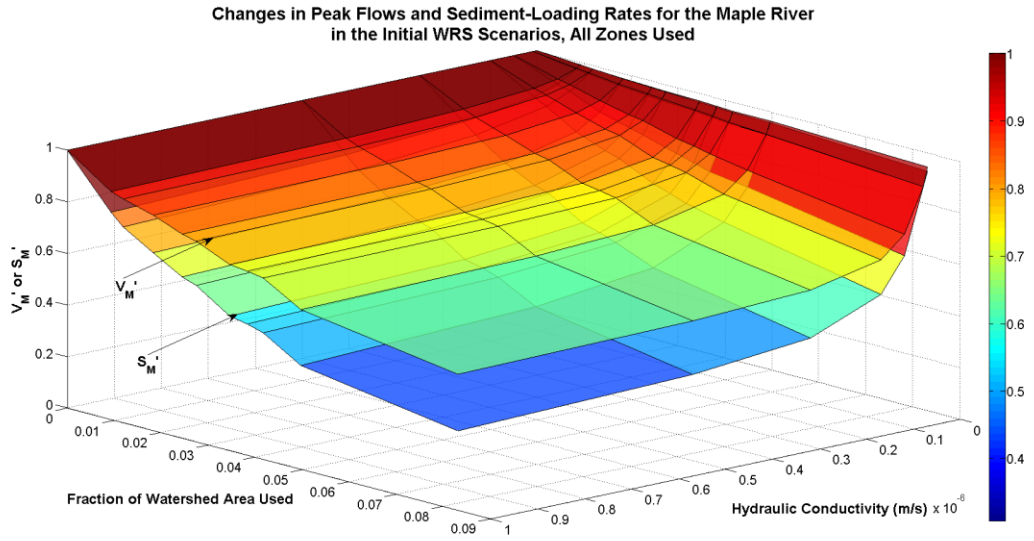

Figure 39. Changes in peak flow volumes at the Maple River's lower gauge normalized by the baseline total (V_M') and sediment-loading rates of the Maple River's gauged reach normalized by the baseline rate (S_M') with both WRS extent and hydraulic conductivity. These initial WRS scenarios use all zones.

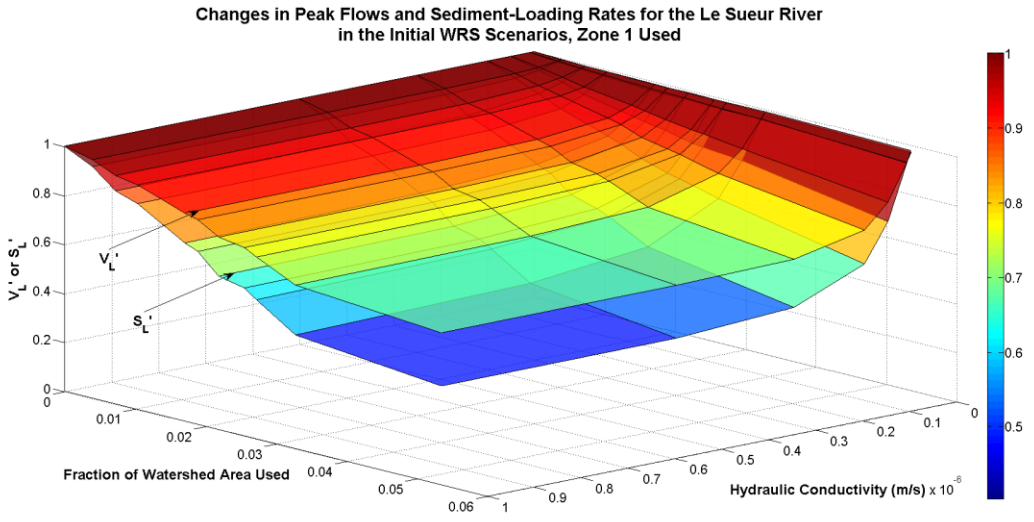

Figure 40. Changes in peak flow volumes at the Le Sueur River's lower gauge normalized by the baseline total (V_L') and sediment-loading rates of the Le Sueur River's gauged reach normalized by the baseline rate (S_L') with both WRS extent and hydraulic conductivity. These initial WRS scenarios use zone 1.

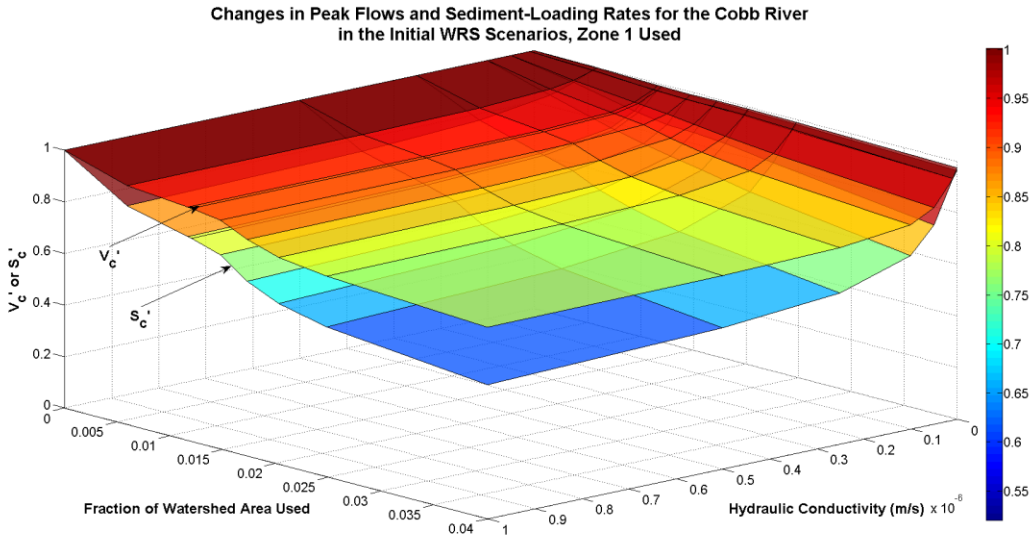

Figure 41. Changes in peak flow volumes at the Cobb River's lower gauge normalized by the baseline total (V_C') and sediment-loading rates of the Cobb River's gauged reach normalized by the baseline rate (S_C') with both WRS extent and hydraulic conductivity. These initial WRS scenarios use zone 1.

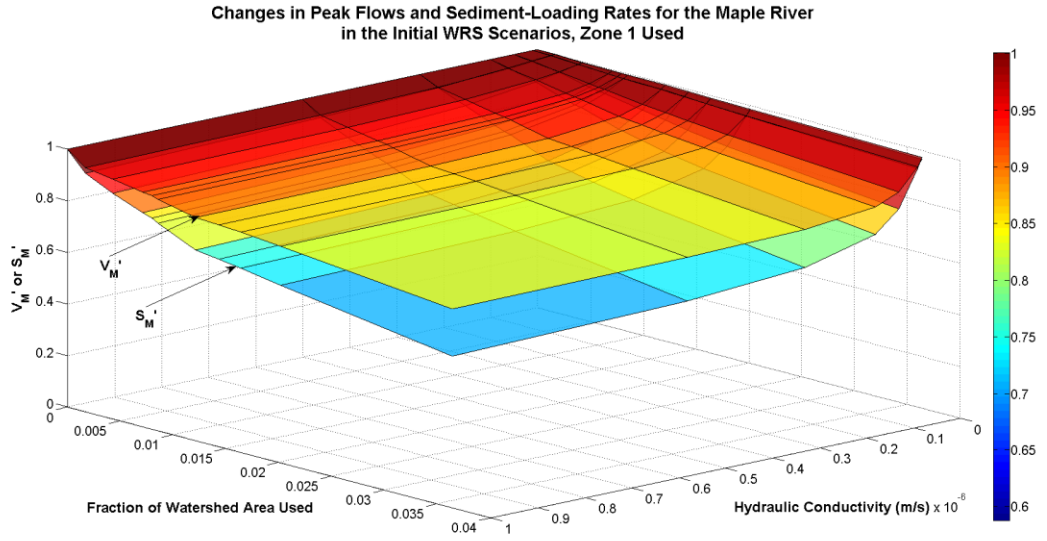

Figure 42. Changes in peak flow volumes at the Maple River's lower gauge normalized by the baseline total (V_M') and sediment-loading rates of the Maple River's gauged reach normalized by the baseline rate (S_M') with both WRS extent and hydraulic conductivity. These initial WRS scenarios use zone 1.

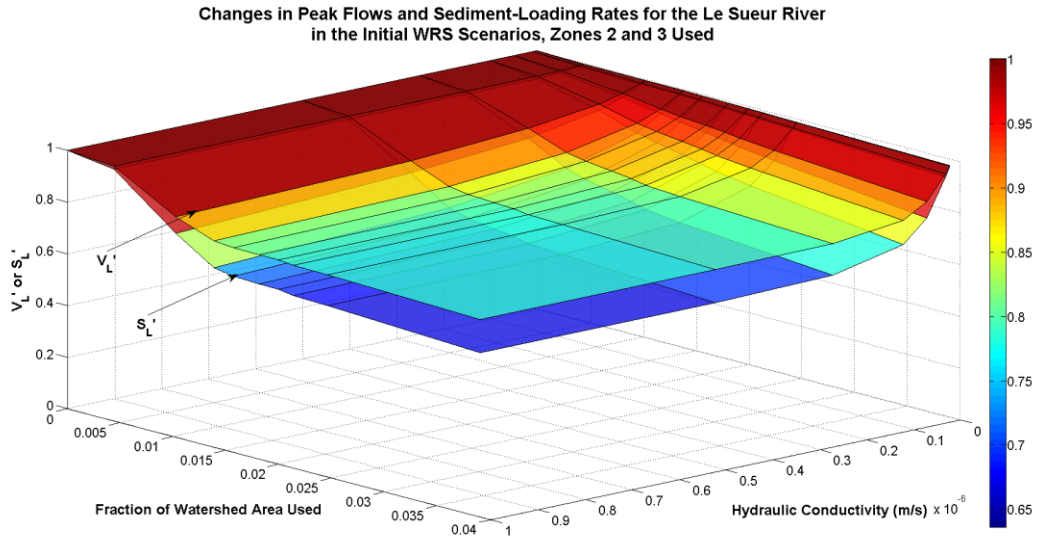

Figure 43. Changes in peak flow volumes at the Le Sueur River's lower gauge normalized by the baseline total (V_L') and sediment-loading rates of the Le Sueur River's gauged reach normalized by the baseline rate (S_L') with both WRS extent and hydraulic conductivity. These initial WRS scenarios use zones 2 and 3.

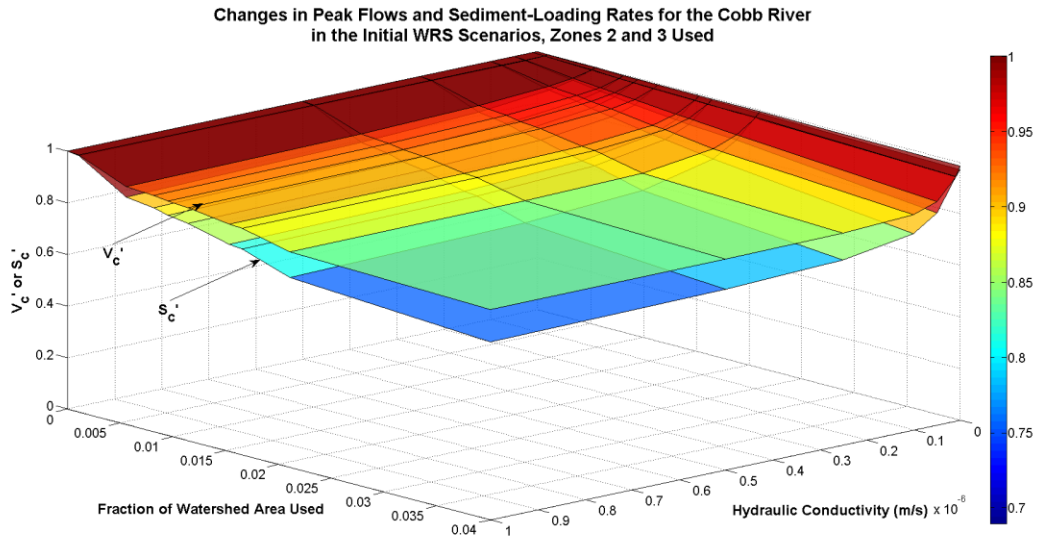

Figure 44. Changes in peak flow volumes at the Cobb River's lower gauge normalized by the baseline total (V_C') and sediment-loading rates of the Cobb River's gauged reach normalized by the baseline rate (S_C') with both WRS extent and hydraulic conductivity. These initial WRS scenarios use zones 2 and 3.

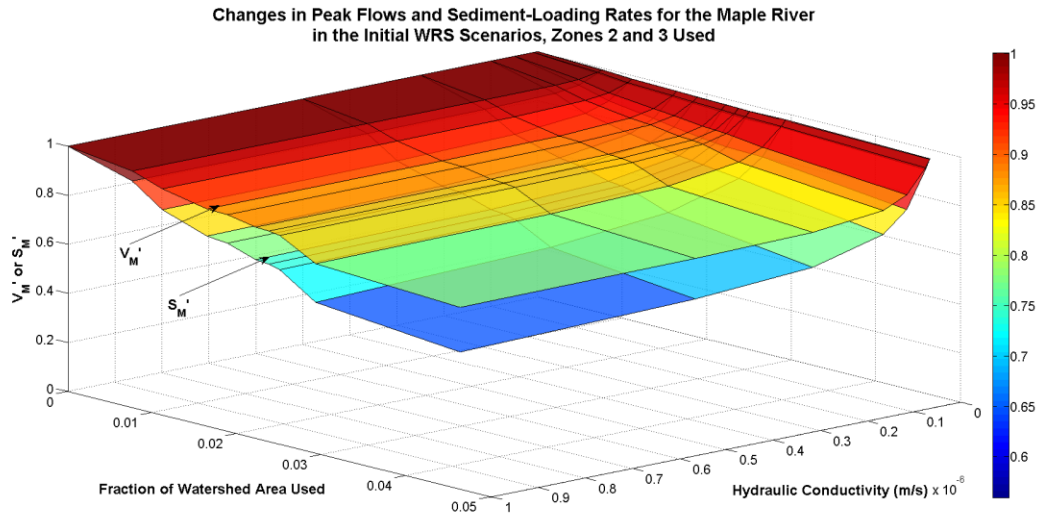

Figure 45. Changes in peak flow volumes at the Maple River's lower gauge normalized by the baseline total (V_M') and sediment-loading rates of the Maple River's gauged reach normalized by the baseline rate (S_M') with both WRS extent and hydraulic conductivity. These initial WRS scenarios use zones 2 and 3.

Appendix F: Sediment reductions in the generalized WRS scenarios

This section presents normalized (S') and non-normalized sediment-loading rate reductions in the generalized WRS scenarios created using the concavity and slope values for regressions of S' reductions with WRS extent (see Tables 6-8), the WRS extent ranges shown in Table 9, and the baseline sediment-loading rates presented in Table 3. Values were calculated for WRS extents sampled every 0.1% of the watershed area. Reductions are first presented (Figures 46-57) as normalized values with the same range of S' values (0 to 1) to allow for comparison between graphs. Non-normalized values are then presented (Figures 58-69). Only scenarios using depths of 1 meter are shown to limit the number of graphs presented.

Scenarios using zone 1 offer the highest reductions for the all three gauged reaches, the Le Sueur River's gauged reach, and Cobb River's gauged reach when K = 1E-6 or 1E-7 m/s. Scenarios using zone 3 offer the highest reductions for all scenarios within the Maple as well as all scenarios using K = 1E-8 m/s.

Non-normalized reductions for the Cobb River's gauged reach are relatively low because of the low sediment-loading rate predicted for the river's gauged reach in the baseline scenario. The rate may be low because of the confluence of the Big Cobb River between the upper and lower gauges.

Reductions in S'

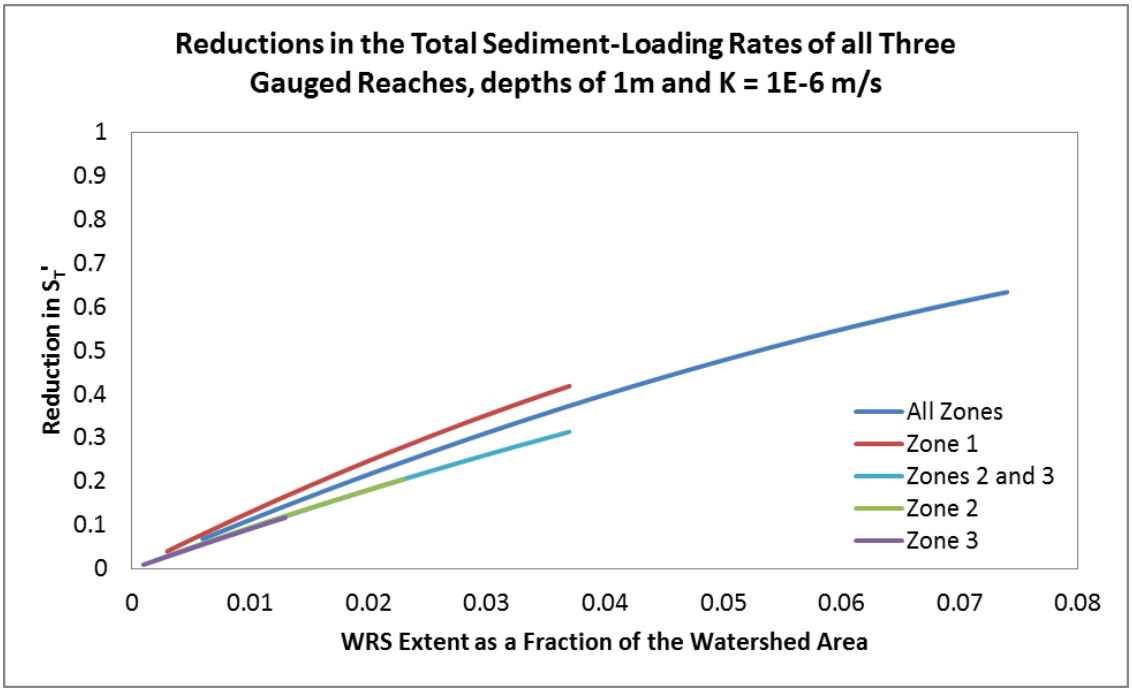

Figure 46. Reductions in S_T' with depths of 1 m and K = 1E-6 m/s.

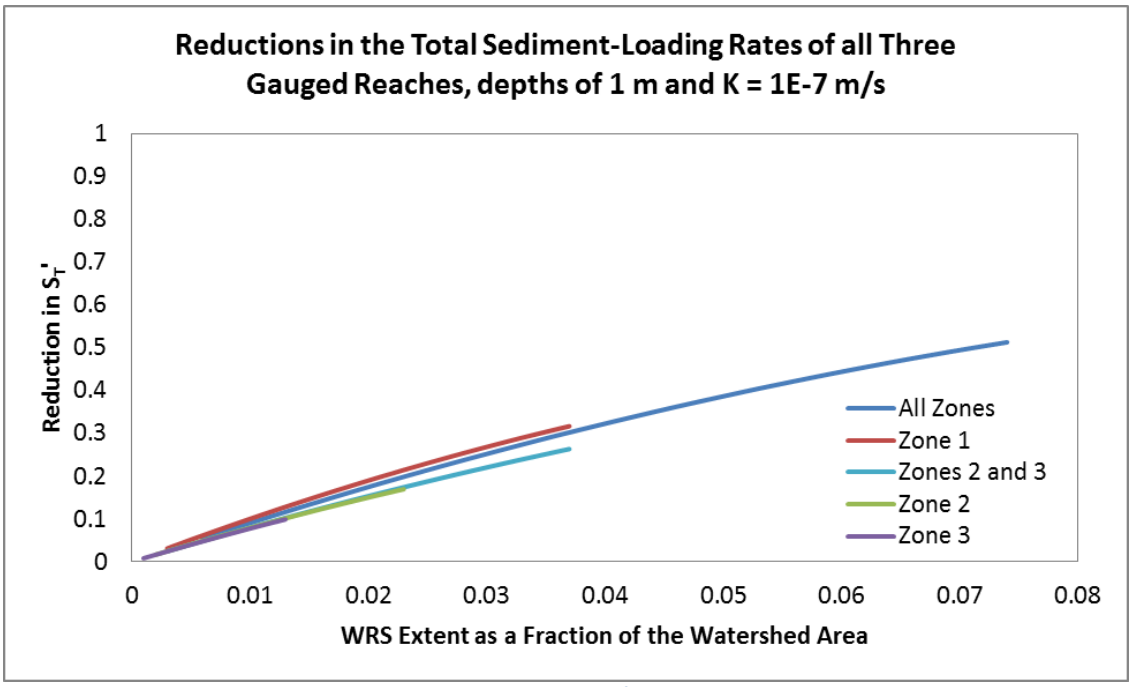

Figure 47. Reductions in S_T' with depths of 1 m and K = 1E-7 m/s.

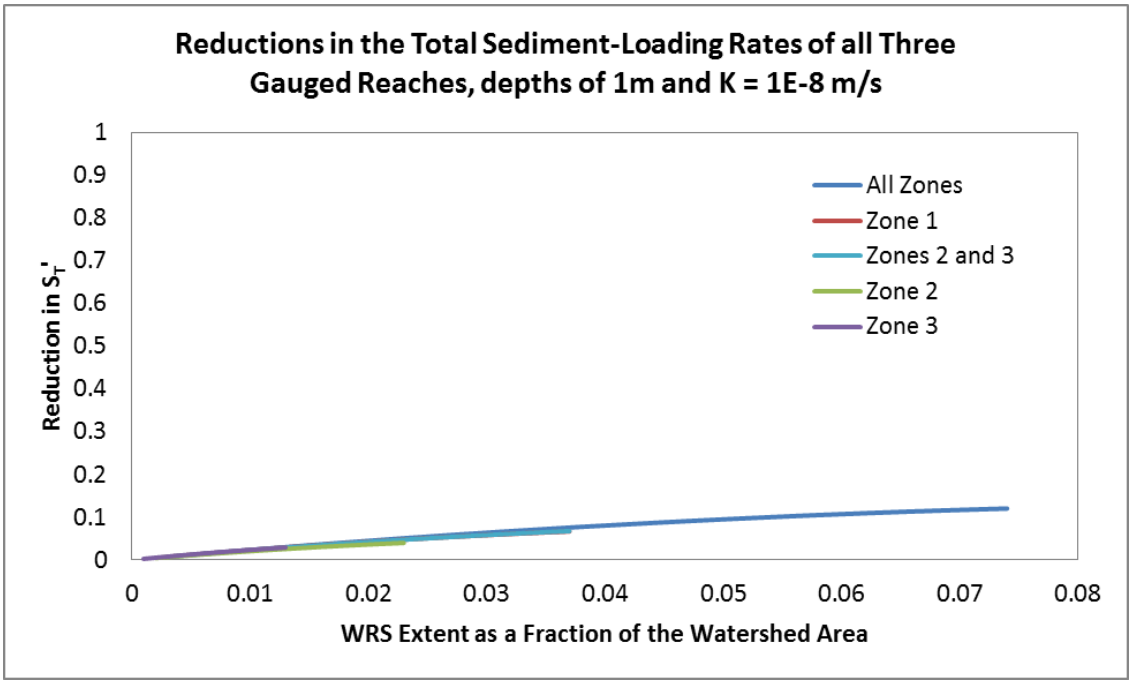

Figure 48. Reductions in S_T' with depths of 1 m and K = 1E-8 m/s.

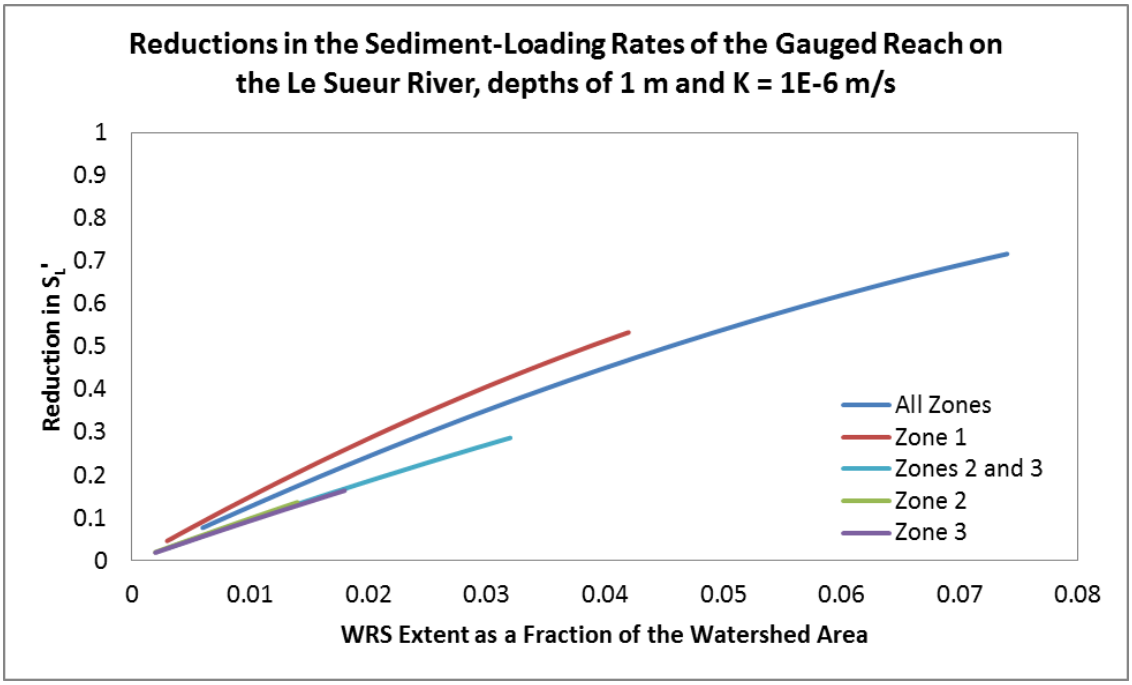

Figure 49. Reductions in S_L' with depths of 1 m and K = 1E-6 m/s.

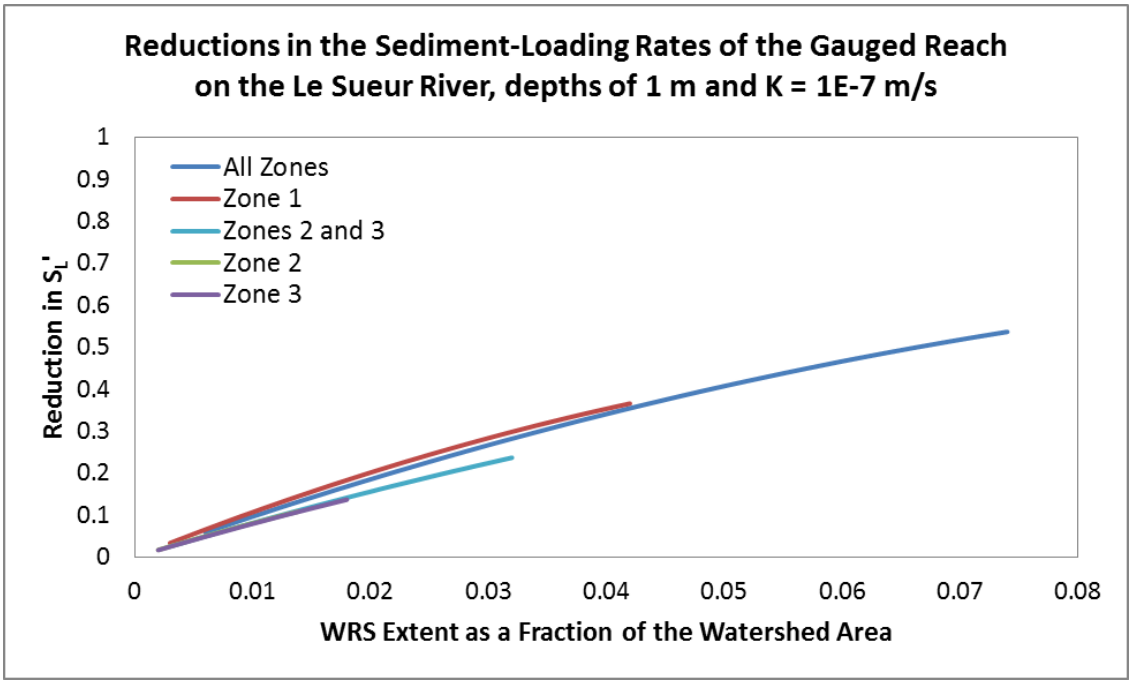

Figure 50. Reductions in S_L' with depths of 1 m and K = 1E-7 m/s.

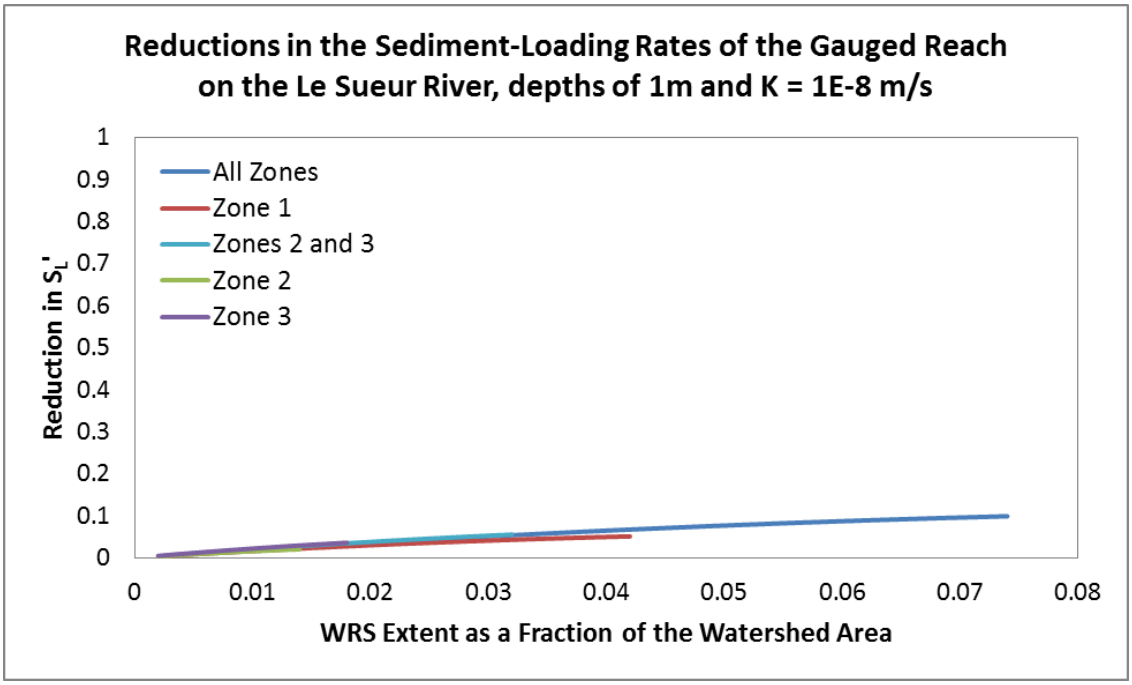

Figure 51. Reductions in S_L' with depths of 1 m and K = 1E-8 m/s.

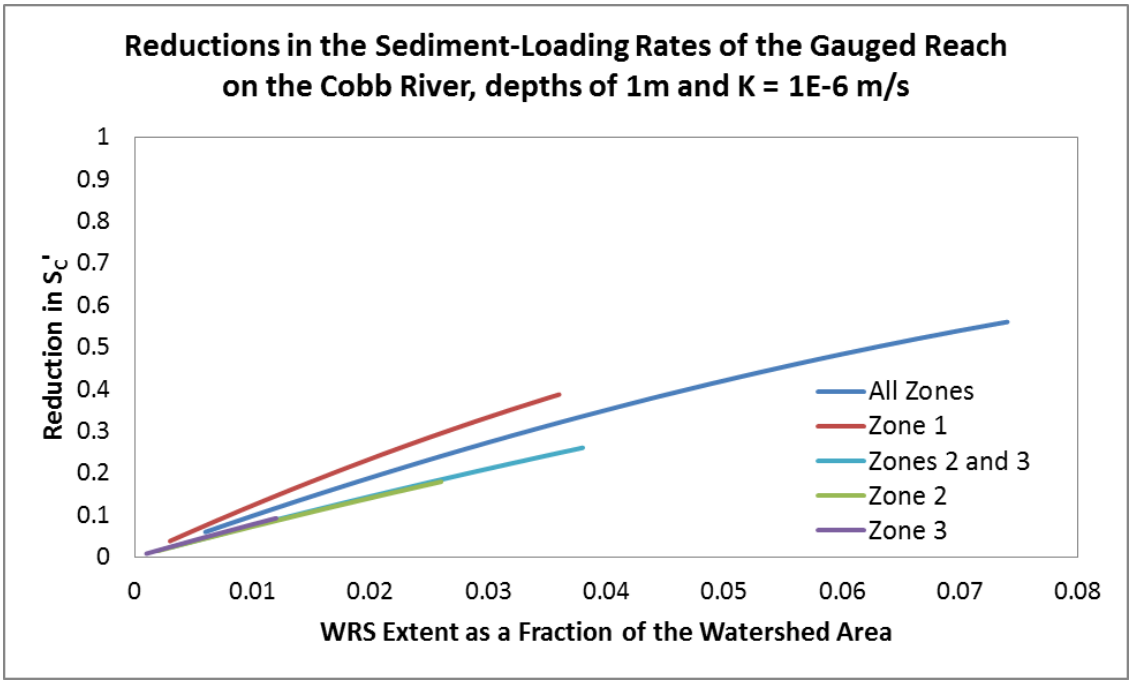

Figure 52. Reductions in S_C' with depths of 1 m and K = 1E-6 m/s.

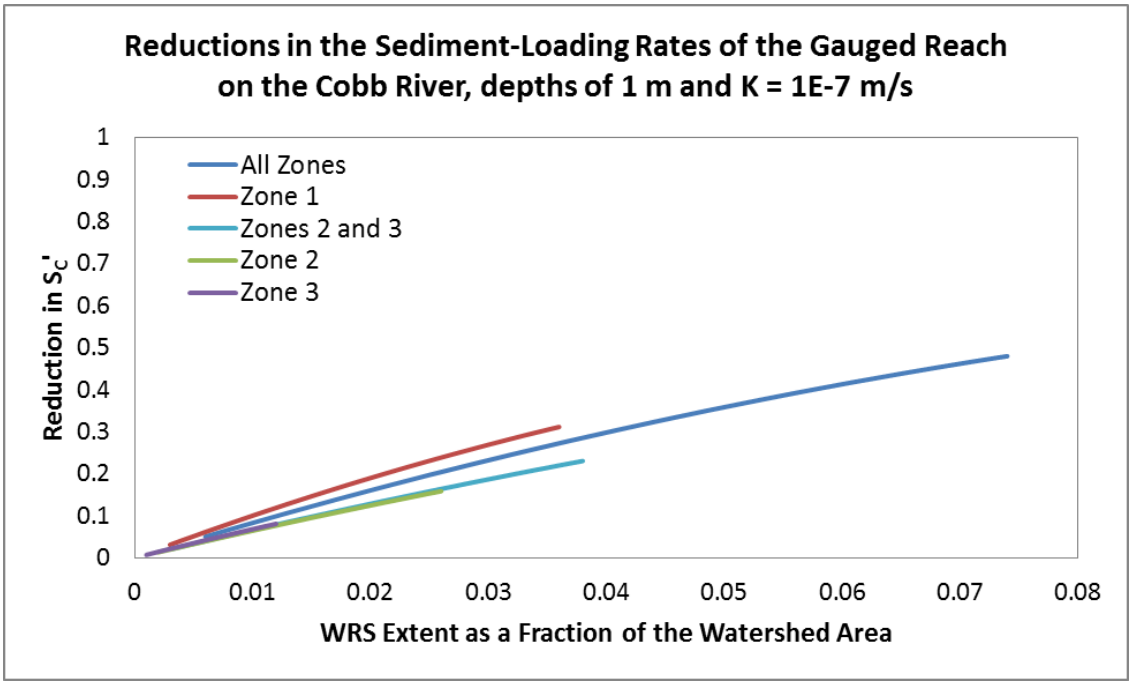

Figure 53. Reductions in S_C' with depths of 1 m and K = 1E-7 m/s.

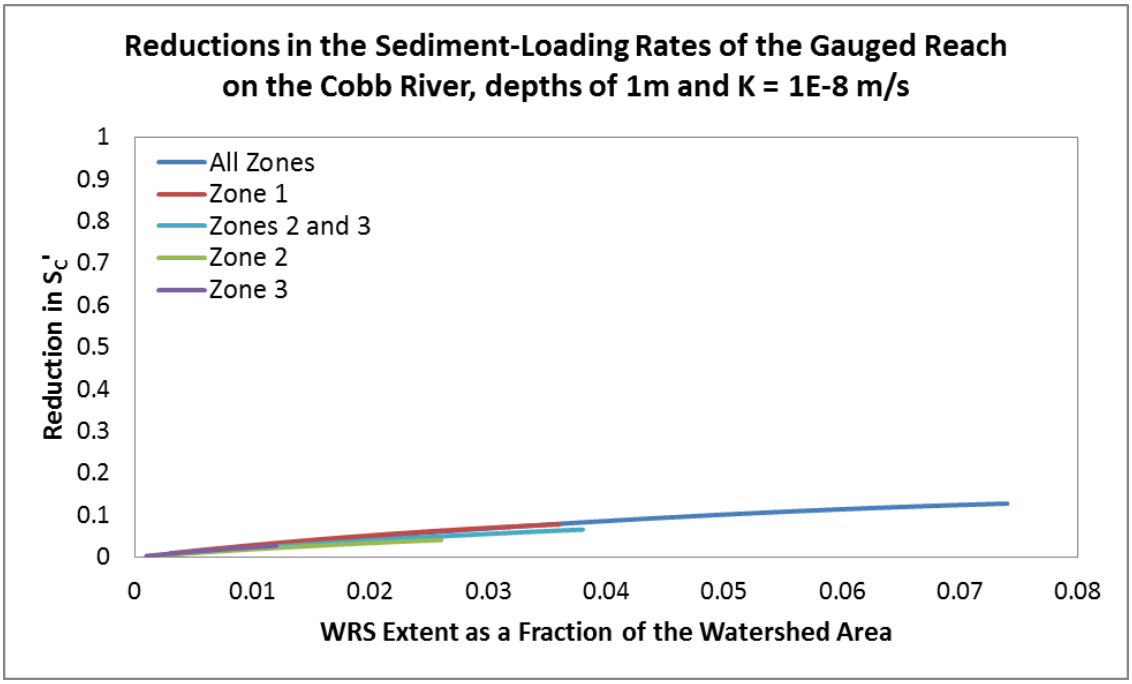

Figure 54. Reductions in S_C' with depths of 1 m and K = 1E-8 m/s.

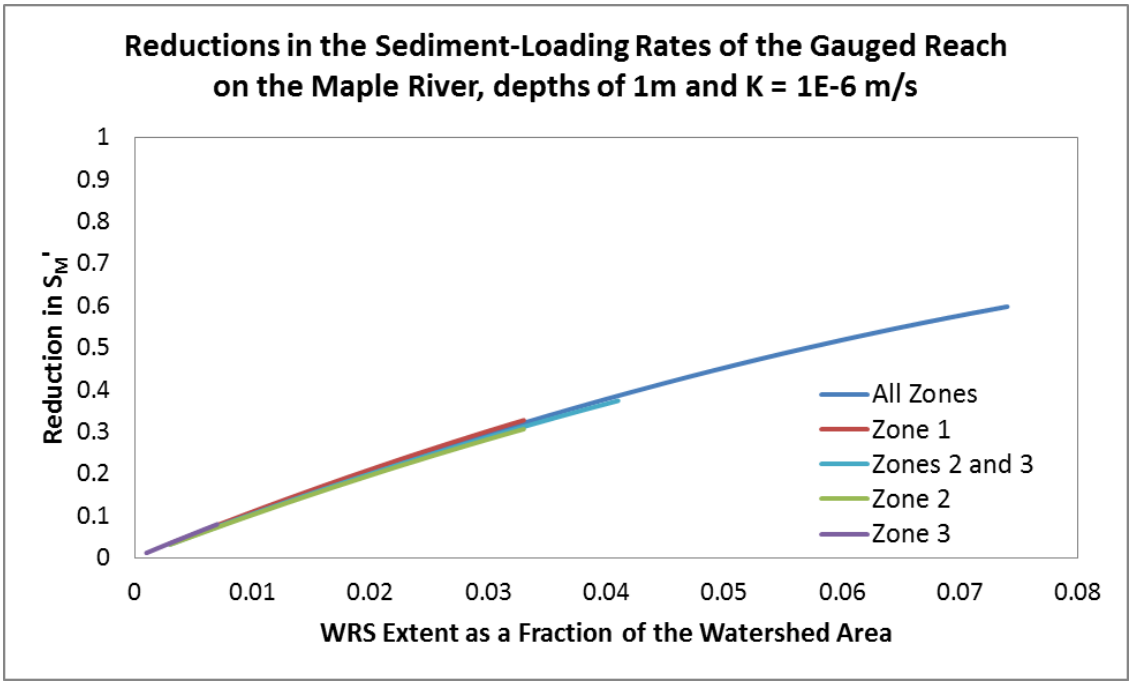

Figure 55. Reductions in S_M' with depths of 1 m and K = 1E-6 m/s.

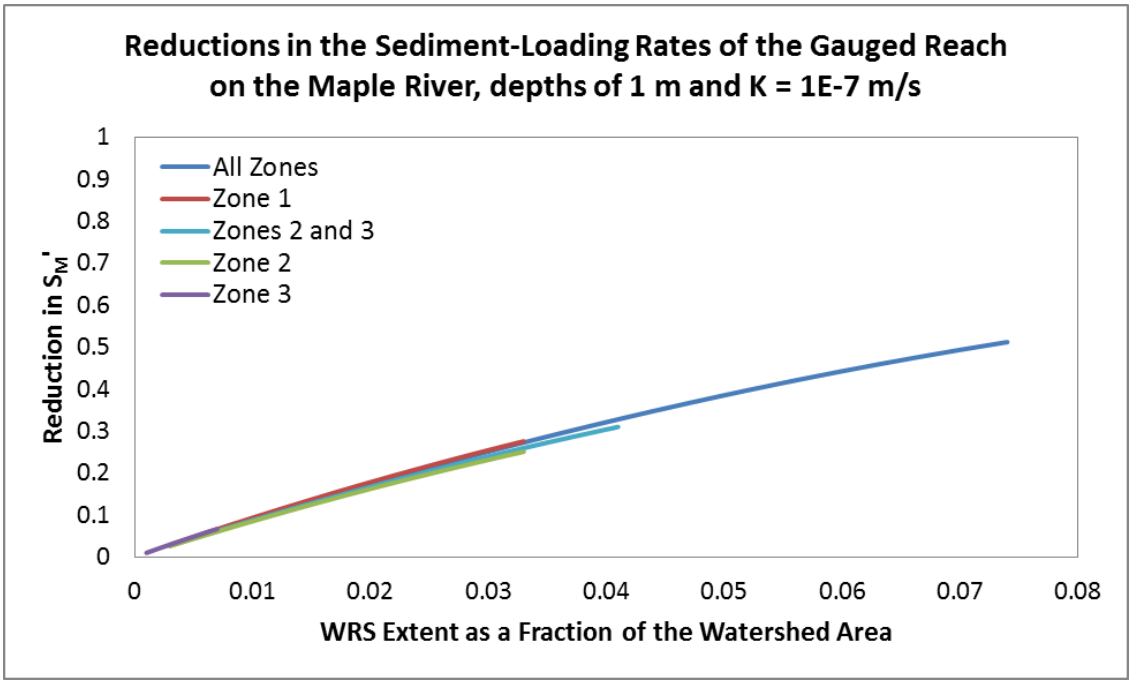

Figure 56. Reductions in S_M' with depths of 1 m and K = 1E-7 m/s.

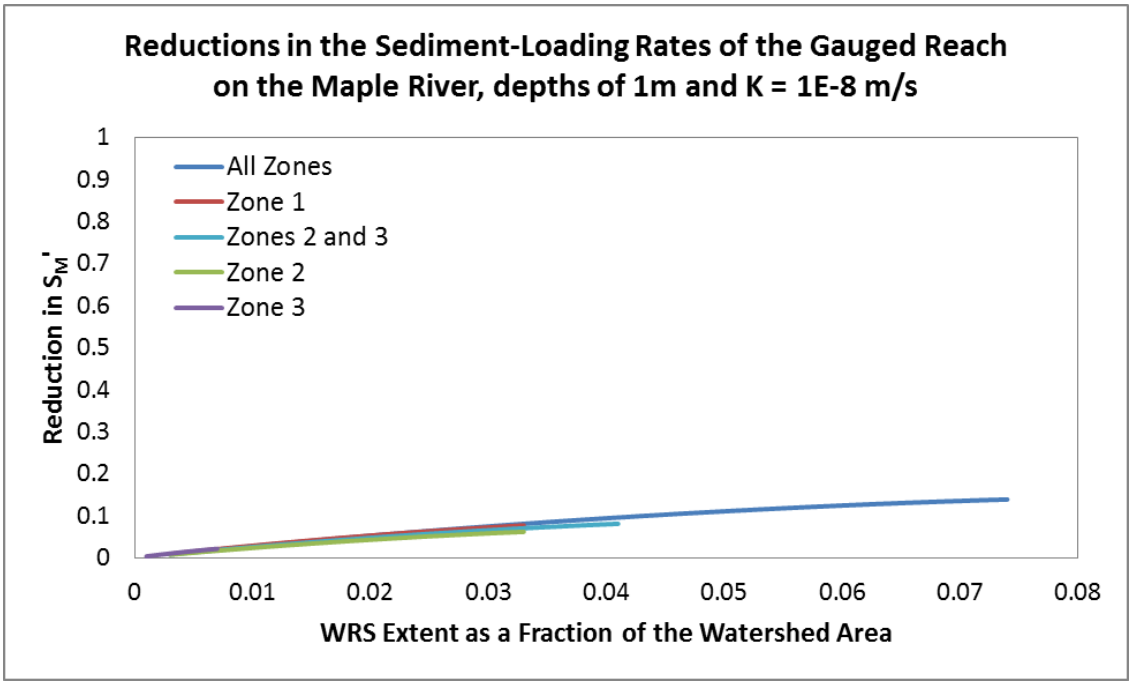

Figure 57. Reductions in S_M' with depths of 1 m and K = 1E-8 m/s.

Non-normalized sediment-loading rate reductions

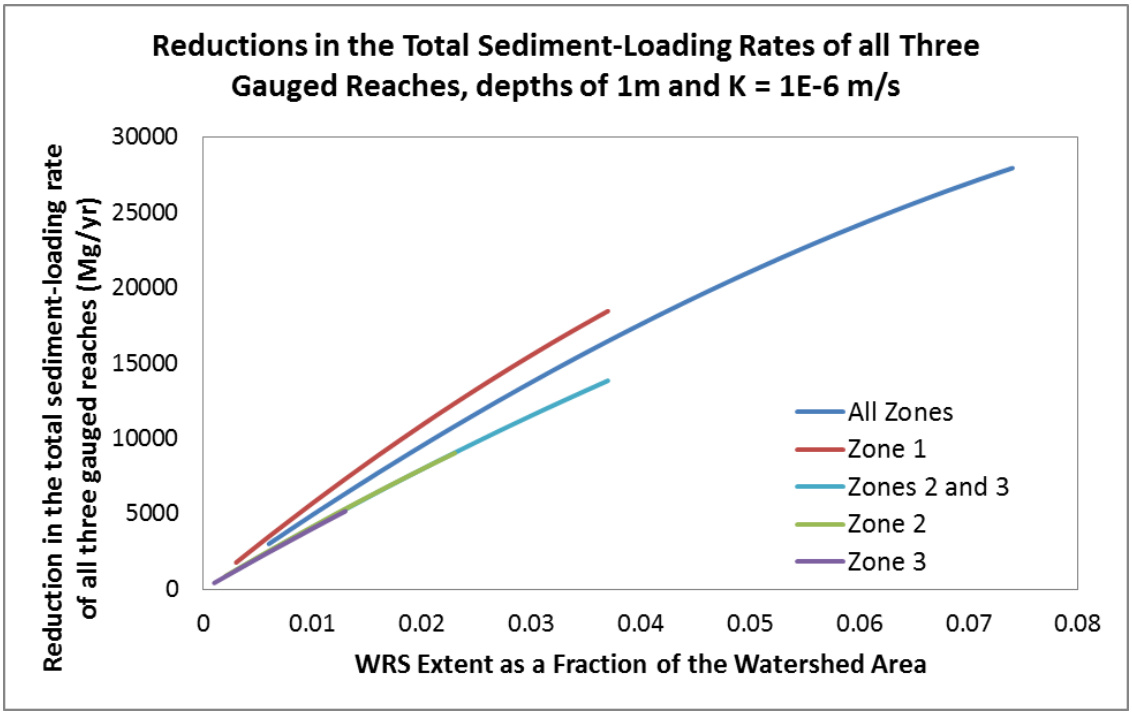

Figure 58. Reductions in the total sediment-loading rate of all three gauged reaches with depths of 1 m and K = 1E-6 m/s.

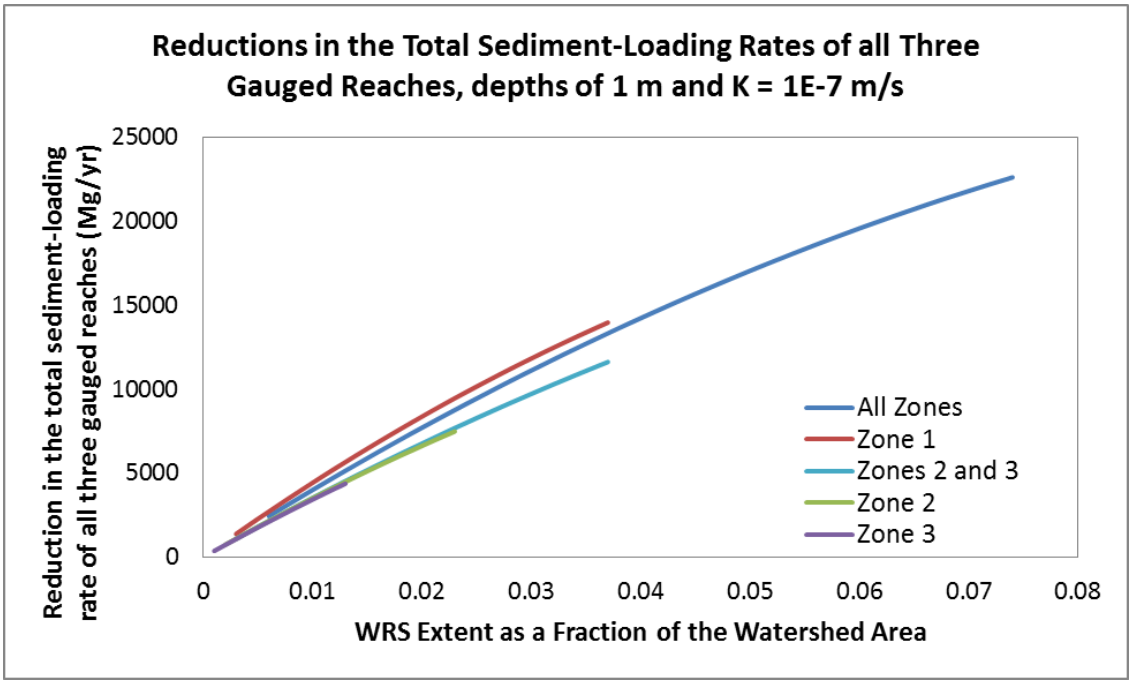

Figure 59. Reductions in the total sediment-loading rate of all three gauged reaches with depths of 1 m and K = 1E-7 m/s.

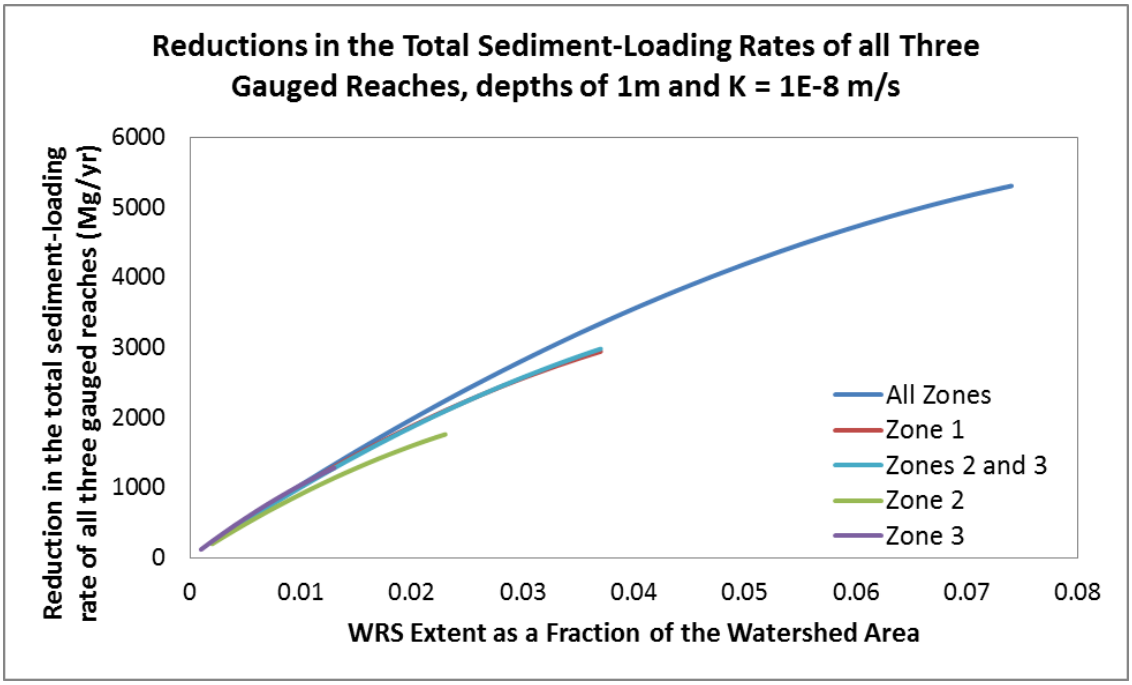

Figure 60. Reductions in the total sediment-loading rate of all three gauged reaches with depths of 1 m and K = 1E-8 m/s.

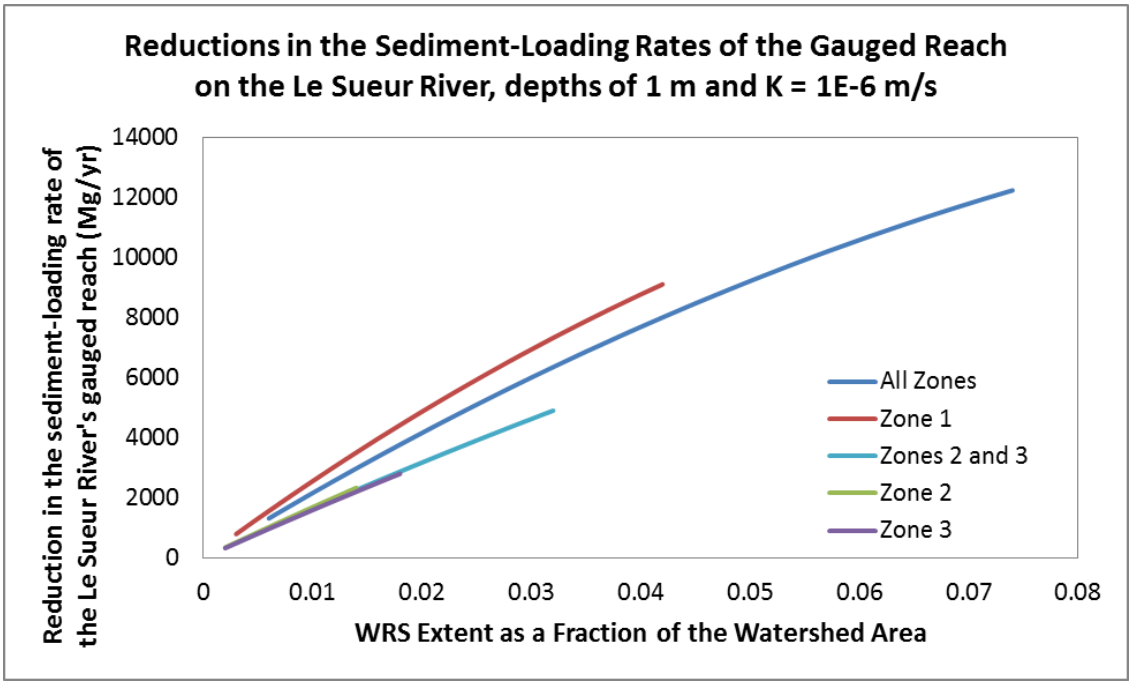

Figure 61. Reductions in the sediment-loading rate of the Le Sueur River's gauged reach with depths of 1 m and K = 1E-6 m/s.

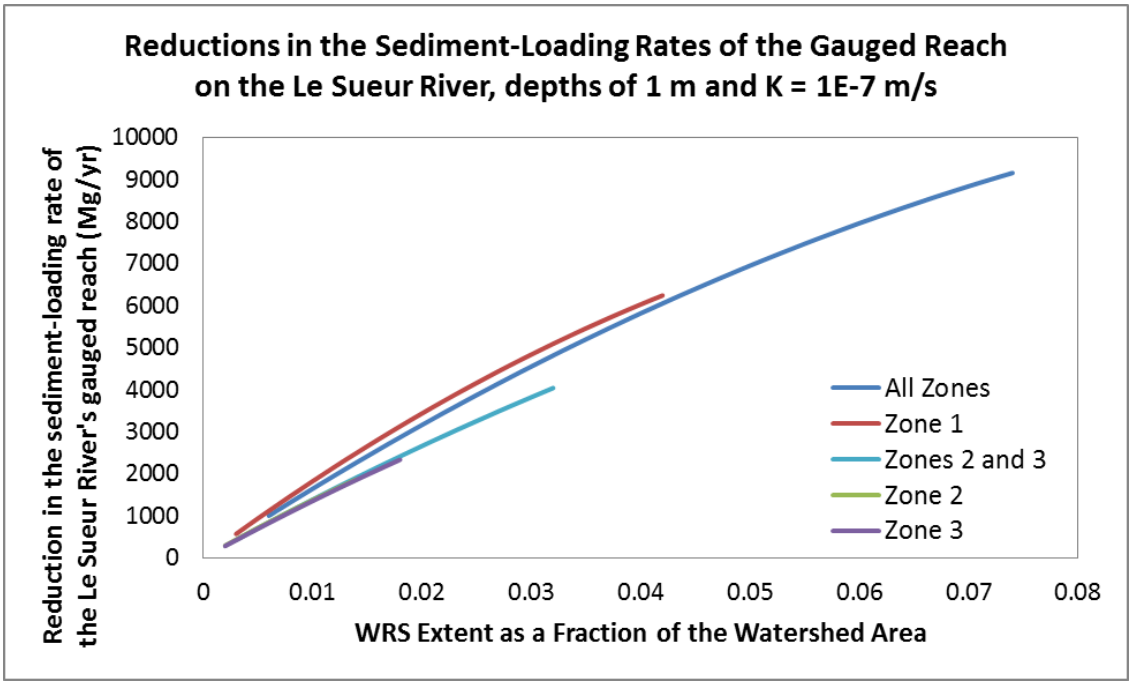

Figure 62. Reductions in the sediment-loading rate of the Le Sueur River's gauged reach with depths of 1 m and K = 1E-7 m/s.

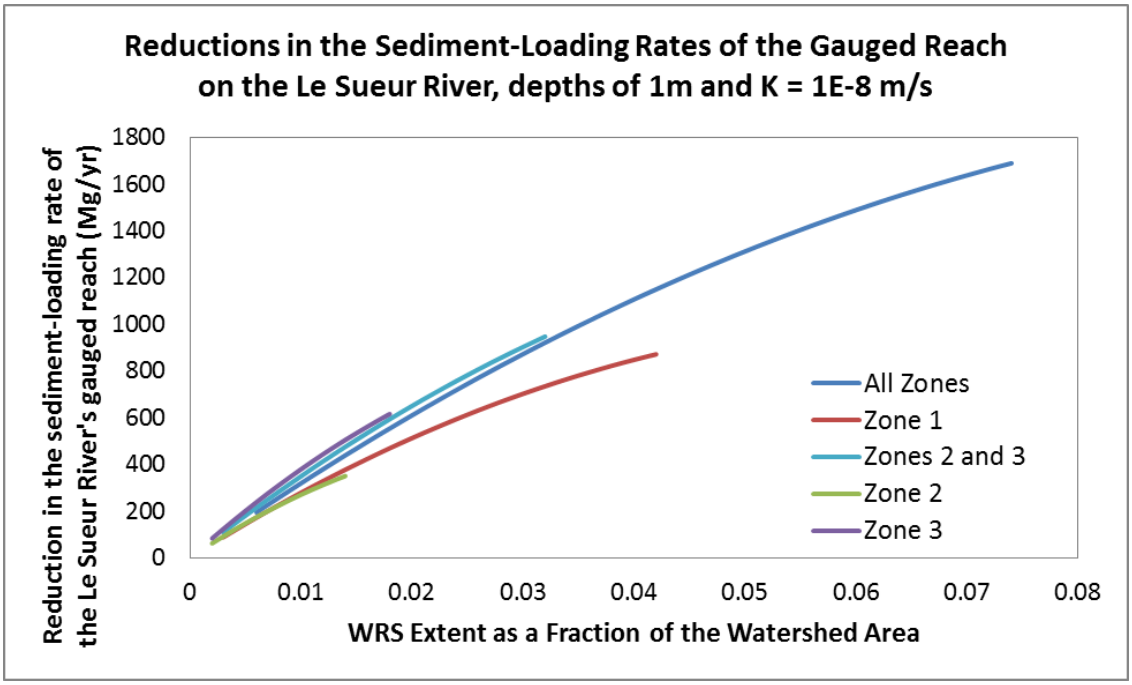

Figure 63. Reductions in the sediment-loading rate of the Le Sueur River's gauged reach with depths of 1 m and K = 1E-8 m/s.

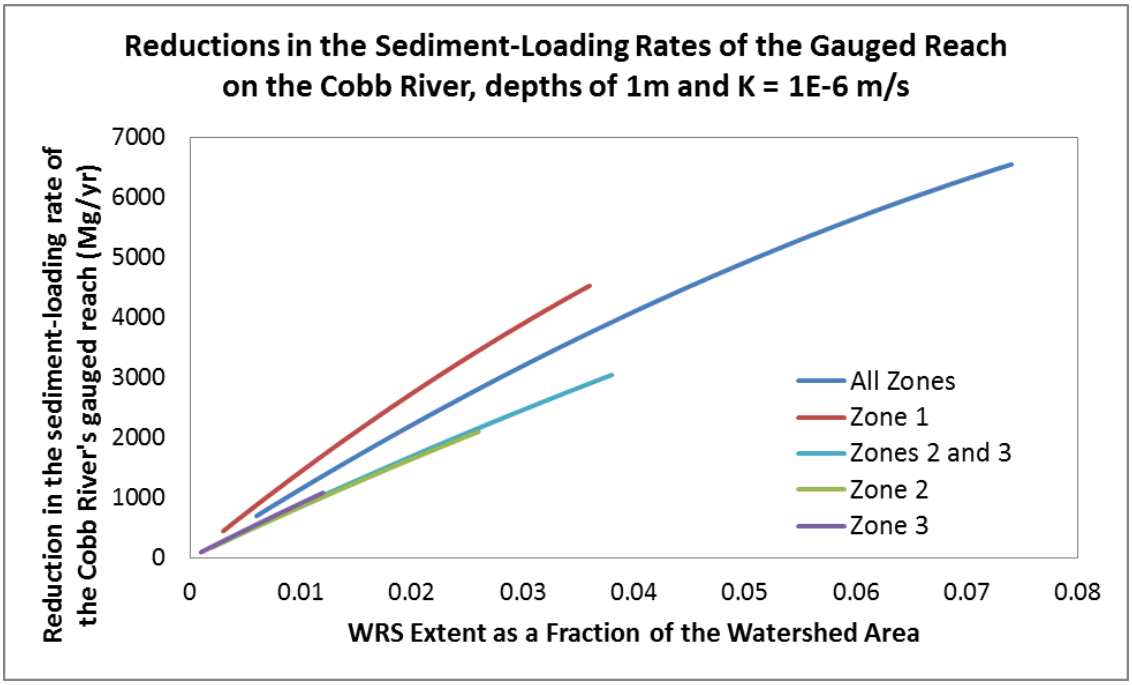

Figure 64. Reductions in the sediment-loading rate of the Cobb River's gauged reach with depths of 1 m and K = 1E-6 m/s.

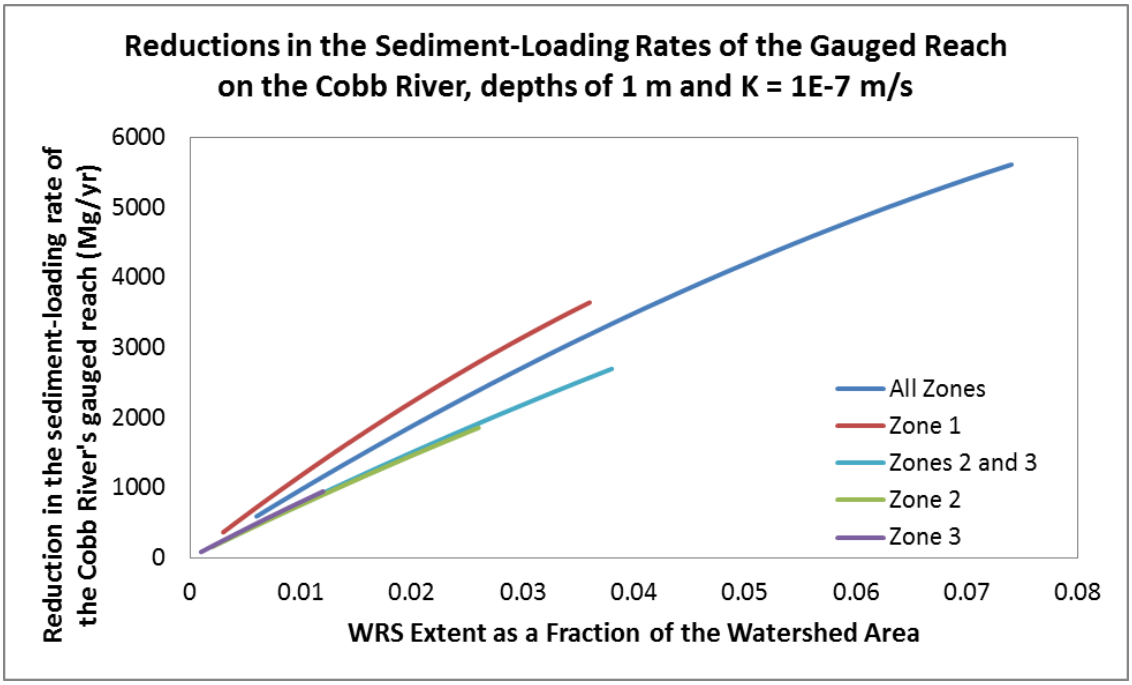

Figure 65. Reductions in the sediment-loading rate of the Cobb River's gauged reach with depths of 1 m and K = 1E-7 m/s.

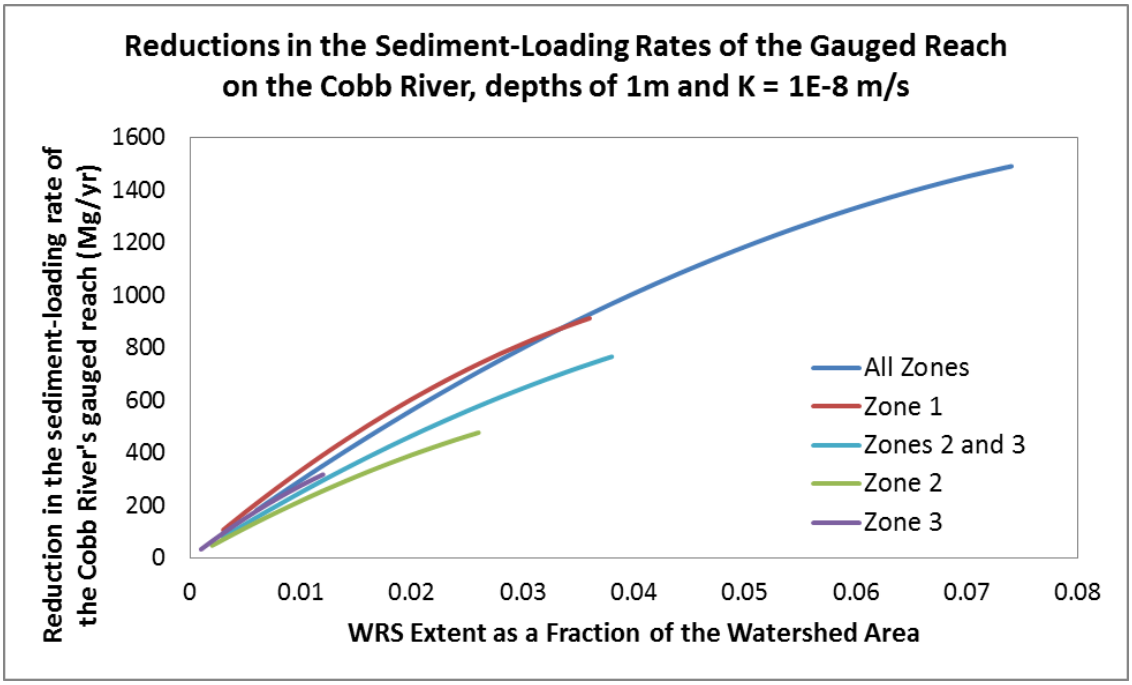

Figure 66. Reductions in the sediment-loading rate of the Cobb River's gauged reach with depths of 1 m and K = 1E-8 m/s.

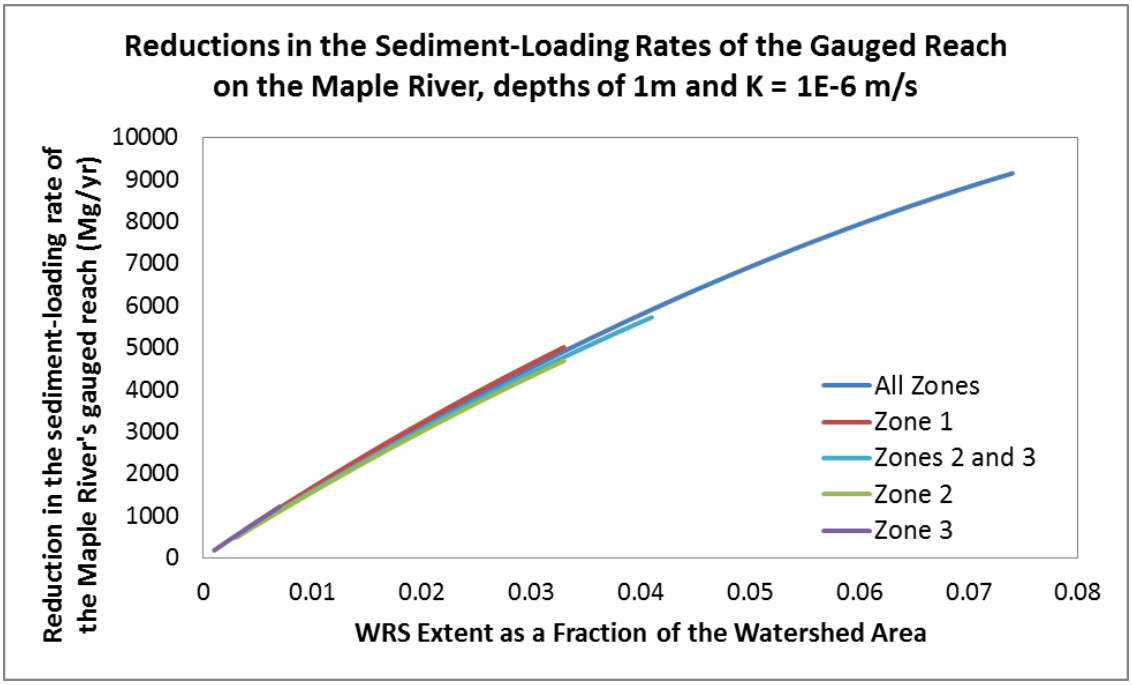

Figure 67. Reductions in the sediment-loading rate of the Maple River's gauged reach with depths of 1 m and K = 1E-6 m/s.

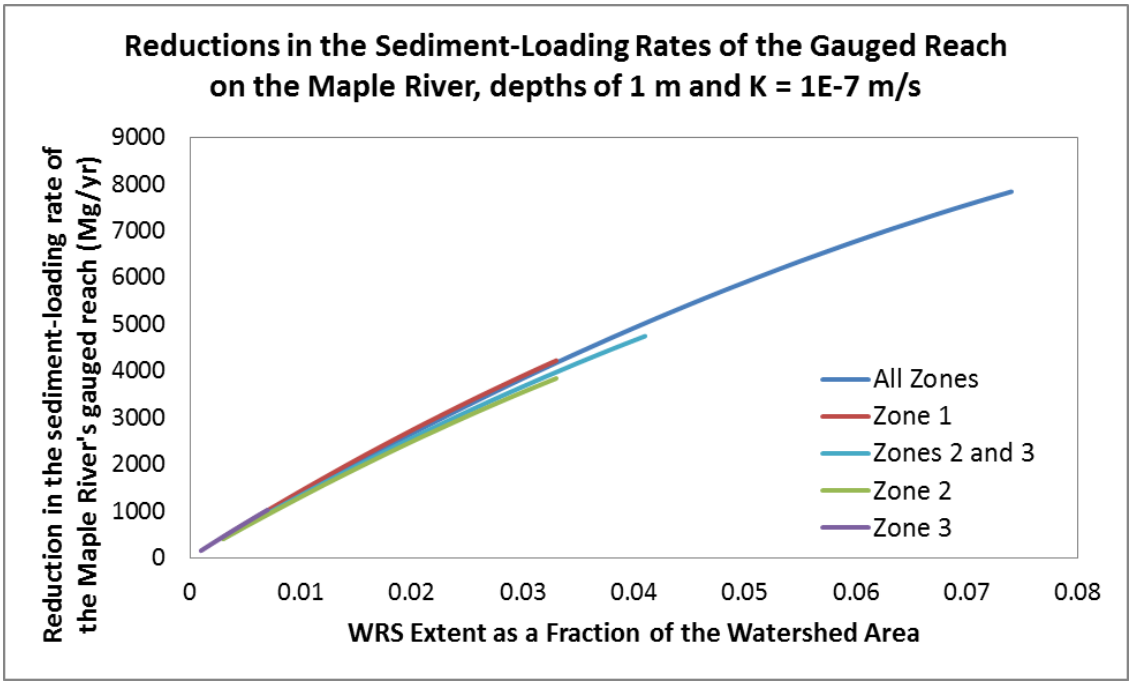

Figure 68. Reductions in the sediment-loading rate of the Maple River's gauged reach with depths of 1 m and K = 1E-7 m/s.

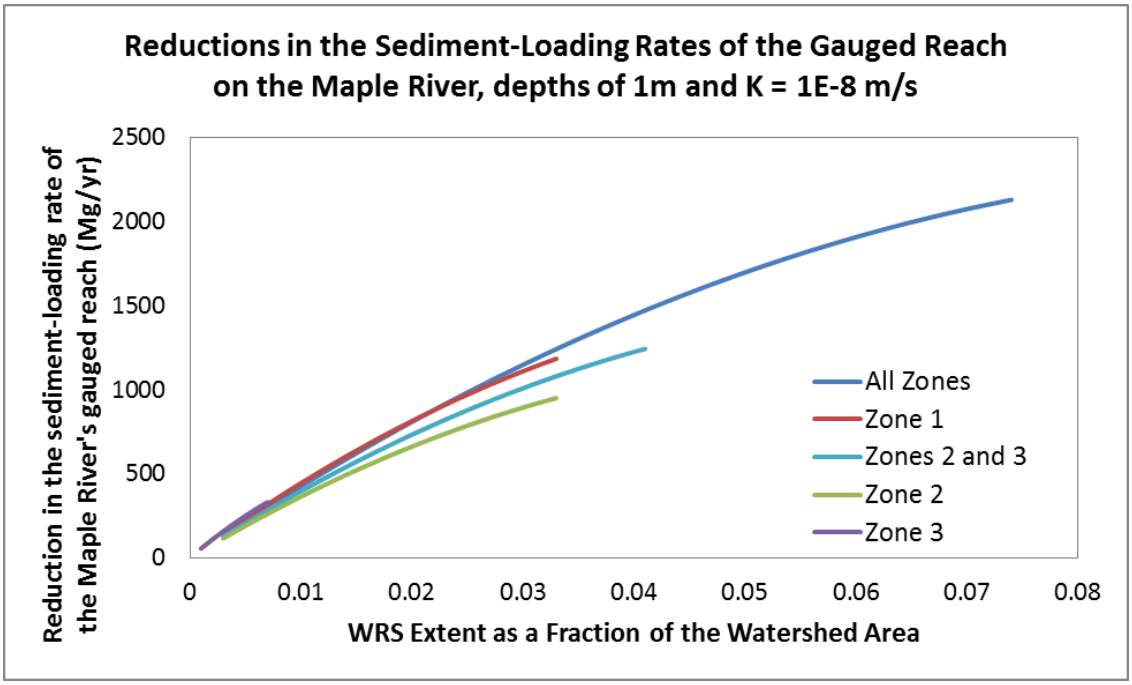

Figure 69. Reductions in the sediment-loading rate of the Maple River's gauged reach with depths of 1 m and K = 1E-8 m/s.

Appendix G: Strengths of the regressions used for flow generation

This section provides examples of the approximate R^2 values for the linear regressions used to generate peak flows. These are "approximate" values because the actual regressions used enforce a fixed intercept (through the LINEST function) so that the baseline scenario is always preserved as the starting point. These R^2 values are slightly higher than the actual values, as the "natural" intercepts are used. Actual R^2 values cannot be presented in part because Excel provides erroneous R^2 values (i.e., less than zero) for many scenarios employing a fixed intercept. These R^2 values are presented to demonstrate the general strengths of different scenarios. For example, scenarios using high hydraulic conductivity (K) values and larger placement selections like all zones, zone 1, or zones 2 and 3 tend to have higher R^2 values (e.g., Figures 70-72). Scenarios using moderate K values and large placement selections tend to have moderate R^2 values (e.g., Figure 73-75), while those using low K values (e.g., Figures 76-78) and/or small placement selections like zone 2 or zone 3 (e.g., Figures 79 and 80) tend to have very low R^2 values. Design depth does not always have an appreciable influence on R^2 values, but using very low depths (i.e., 0.5 m) can sometimes decrease such values, especially when small zones or low K values are used. The flow generator model works well for scenarios using large placement selections (i.e., all zones, zone 1, and zones 2 and 3) with high K values. The model should not be used for scenarios using low K values and/or small placement selections (i.e., zone 2 and zone 3). Despite the

weak relationships used, all peak flow volumes and sediment-loading rates are reproduced relatively accurately (see Figures 18-21).

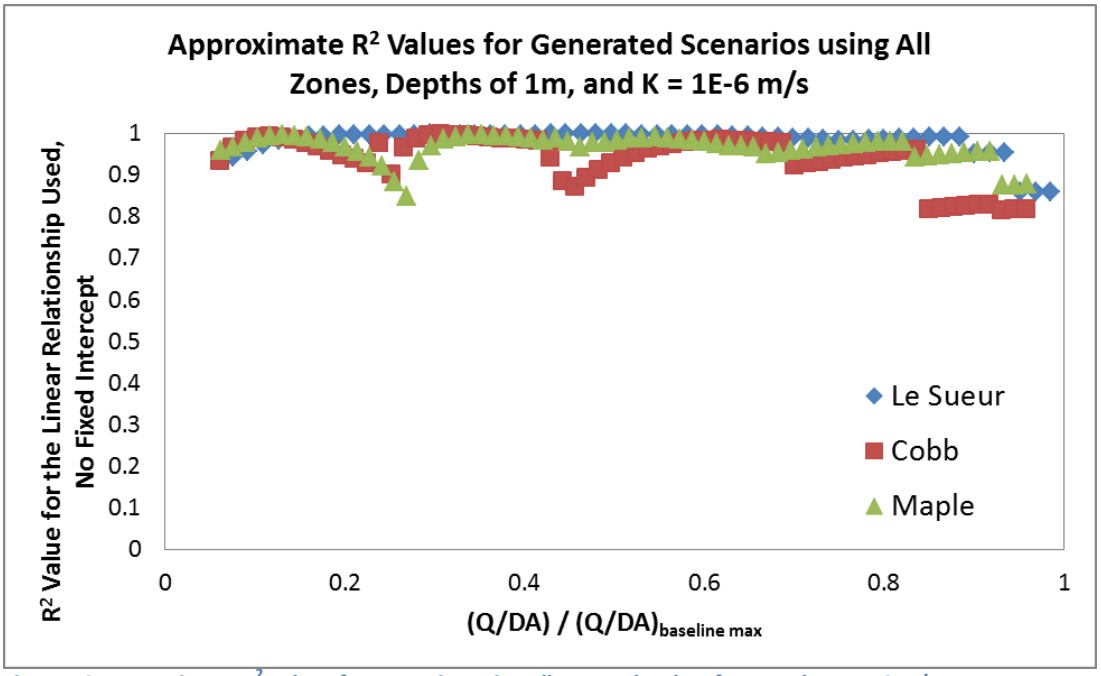

Figure 70. Approximate R^2 values for scenarios using all zones, depths of 1m, and K = 1E-6 m/s.

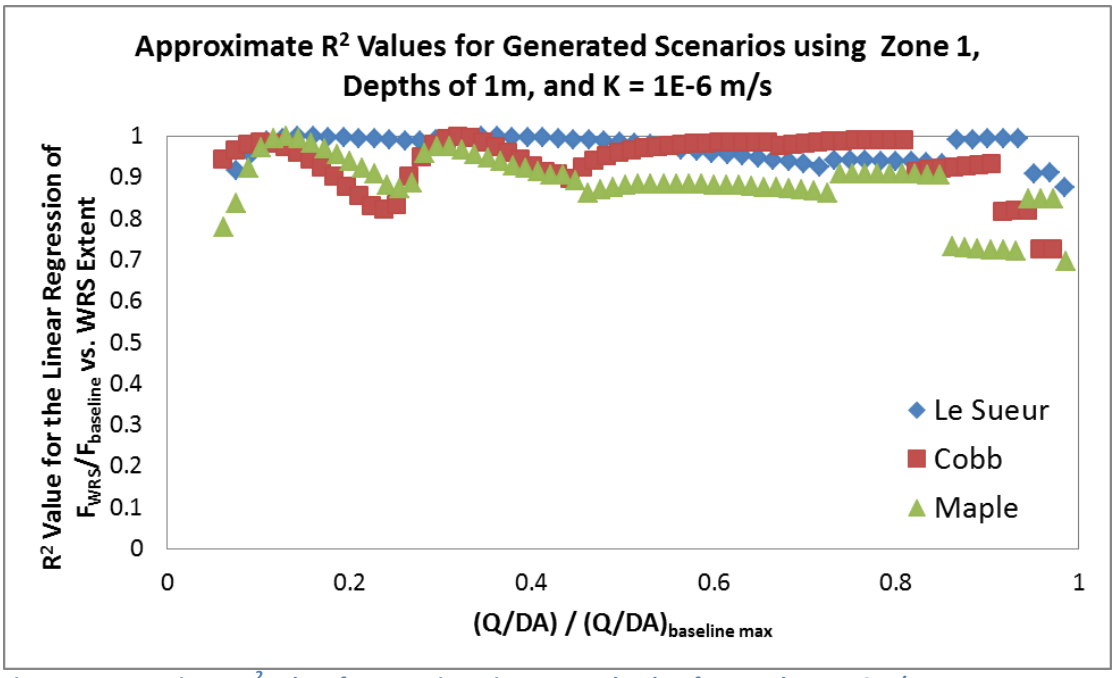

Figure 71. Approximate R^2 values for scenarios using zone 1, depths of 1m, and K = 1E-6 m/s.

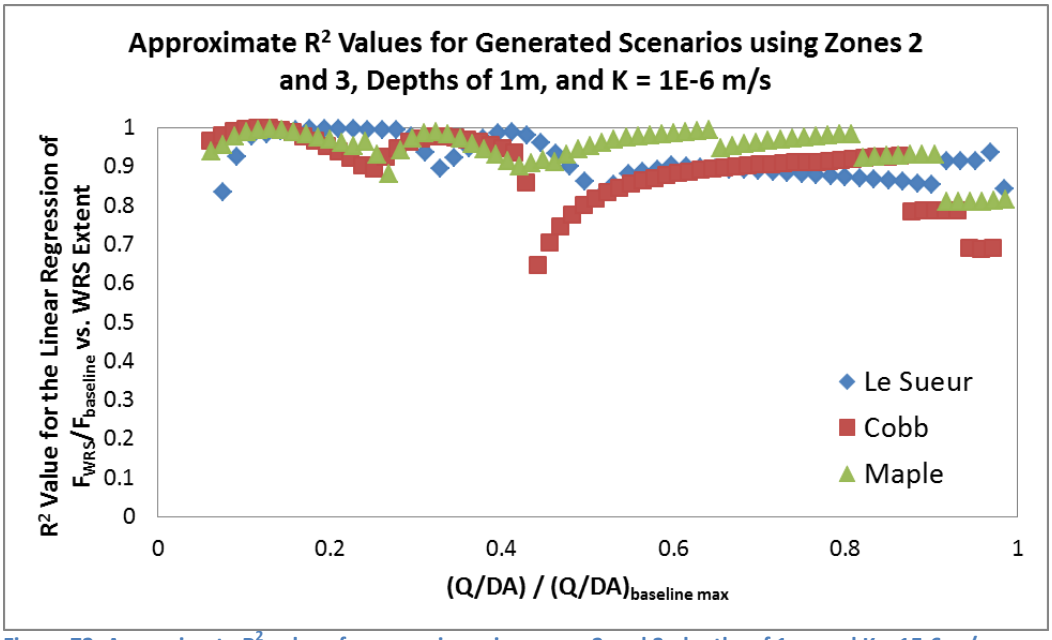

Figure 72. Approximate R^2 values for scenarios using zones 2 and 3, depths of 1m, and K = 1E-6 m/s.

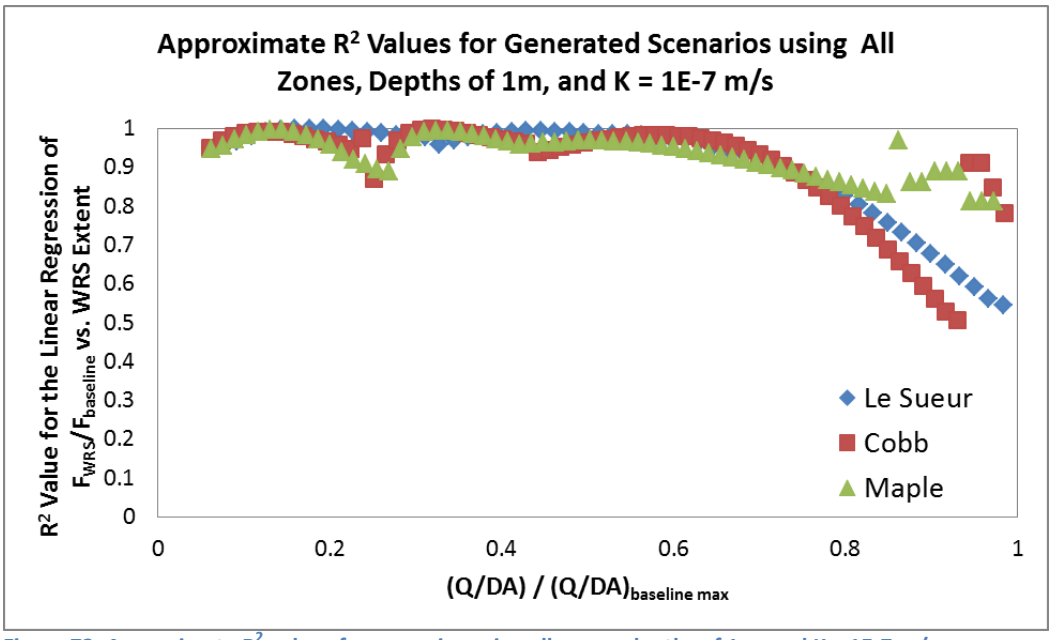

Figure 73. Approximate R^2 values for scenarios using all zones, depths of 1m, and K = 1E-7 m/s.

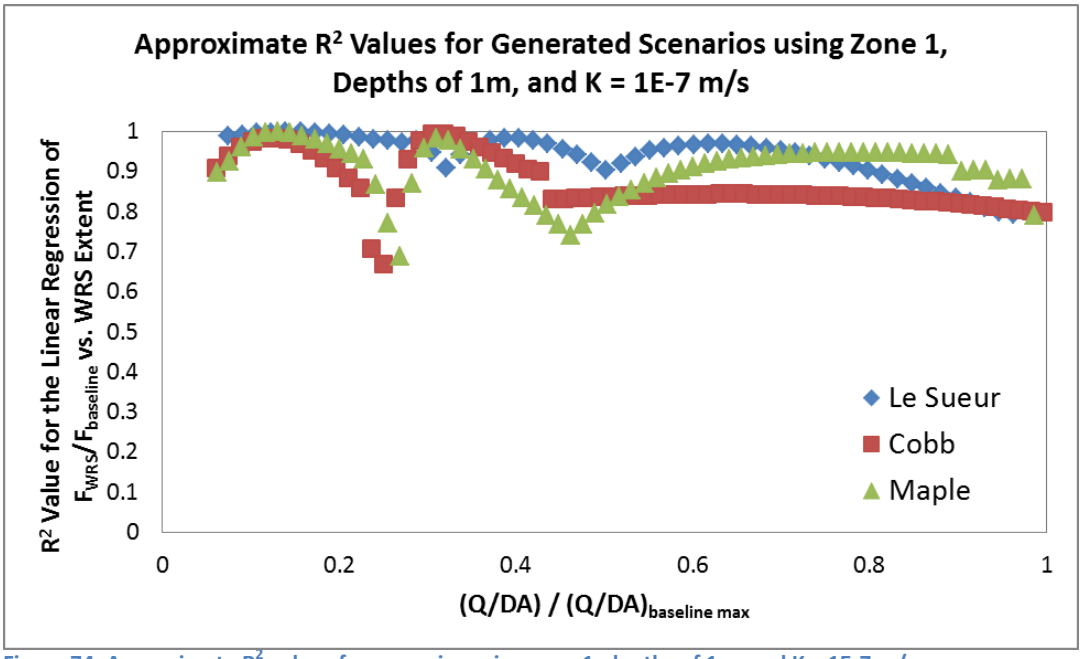

Figure 74. Approximate R^2 values for scenarios using zone 1, depths of 1m, and K = 1E-7 m/s.

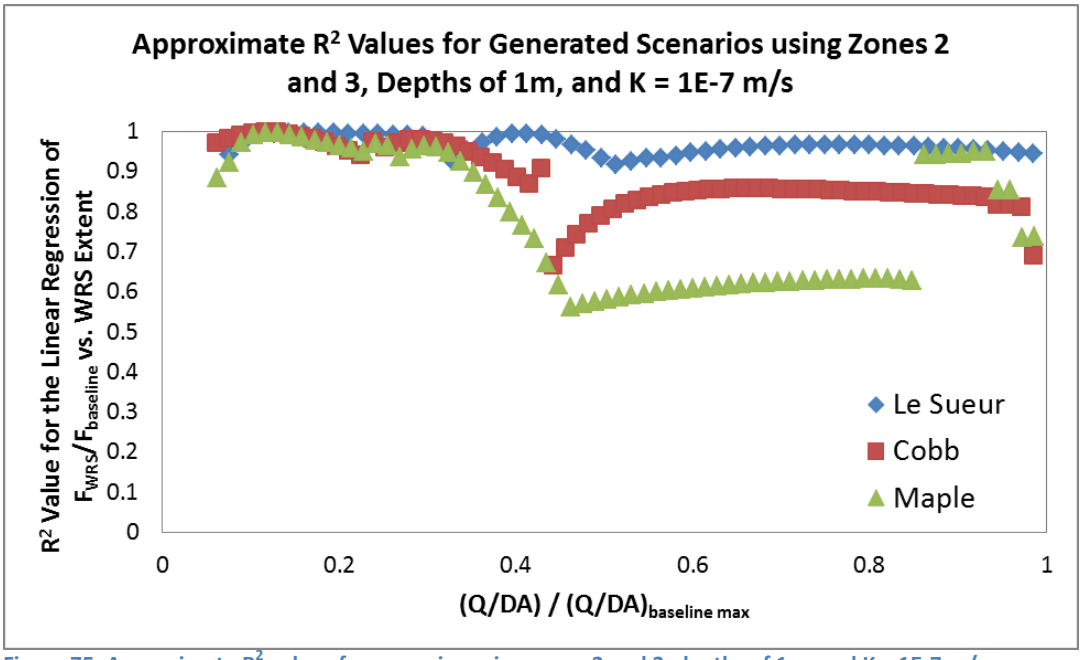

Figure 75. Approximate R^2 values for scenarios using zones 2 and 3, depths of 1m, and K = 1E-7 m/s.

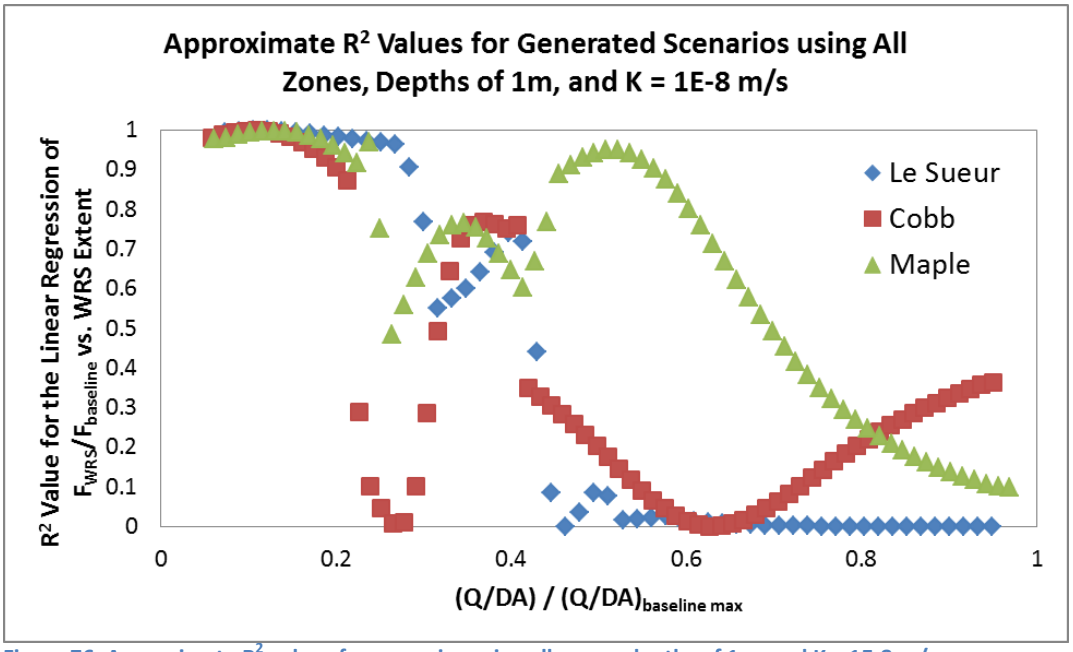

Figure 76. Approximate R^2 values for scenarios using all zones, depths of 1m, and K = 1E-8 m/s.

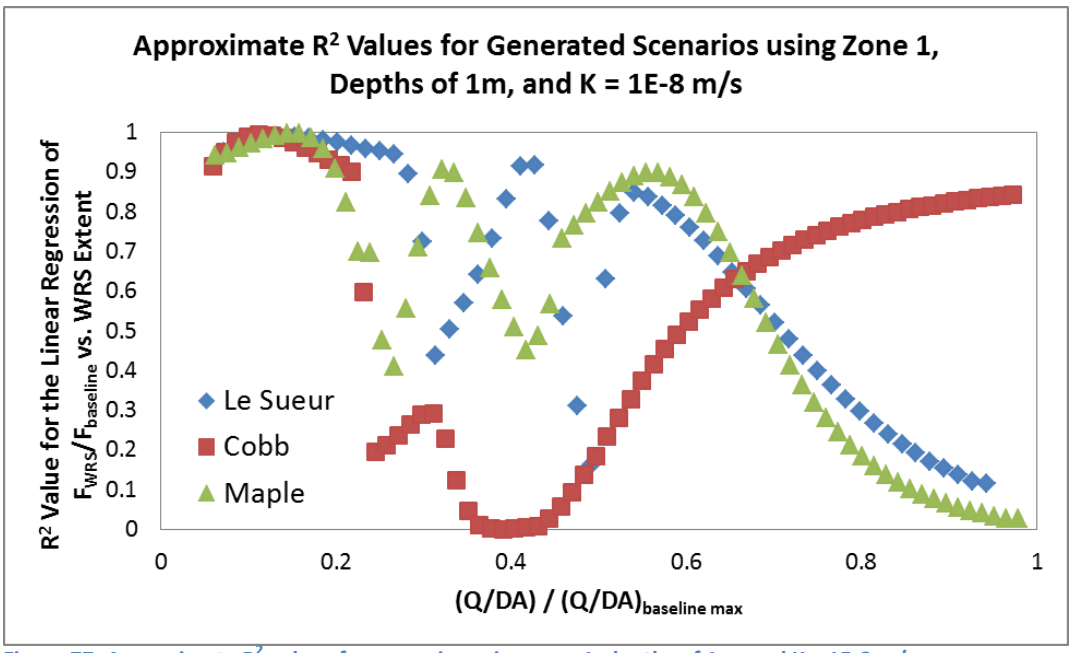

Figure 77. Approximate R^2 values for scenarios using zone 1, depths of 1m, and K = 1E-8 m/s.

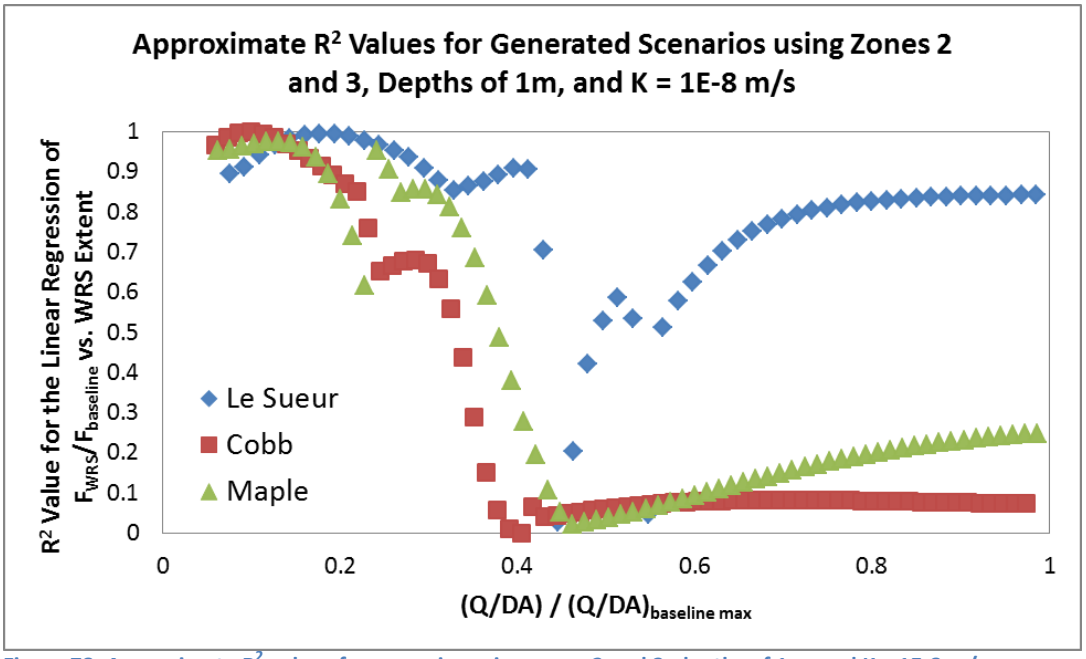

Figure 78. Approximate R^2 values for scenarios using zones 2 and 3, depths of 1m, and K = 1E-8 m/s.

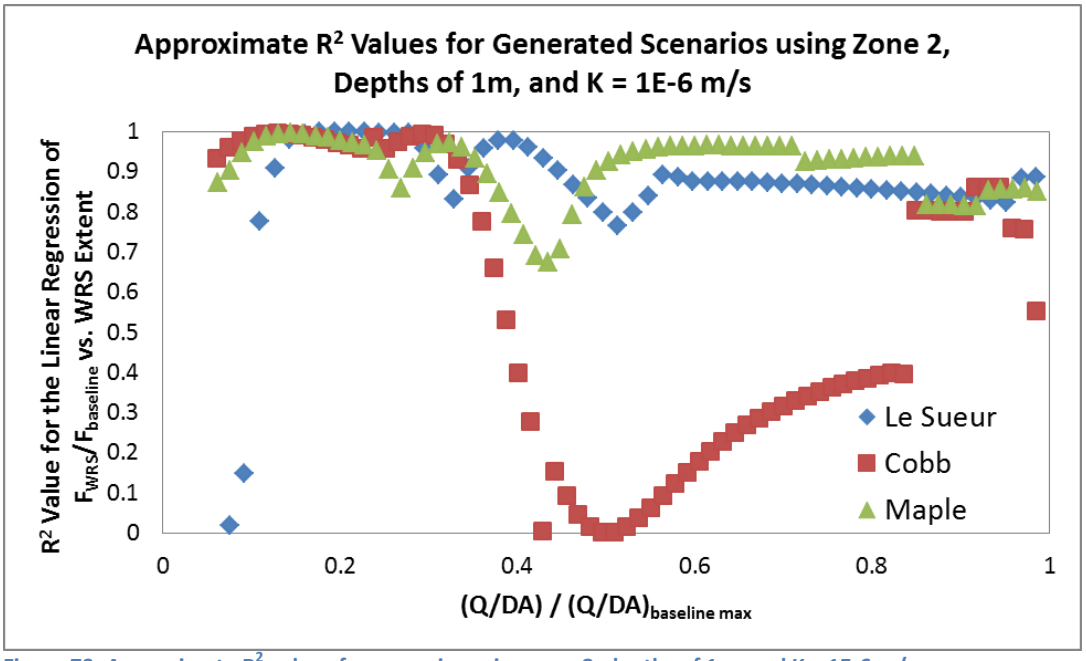

Figure 79. Approximate R^2 values for scenarios using zone 2, depths of 1m, and K = 1E-6 m/s.

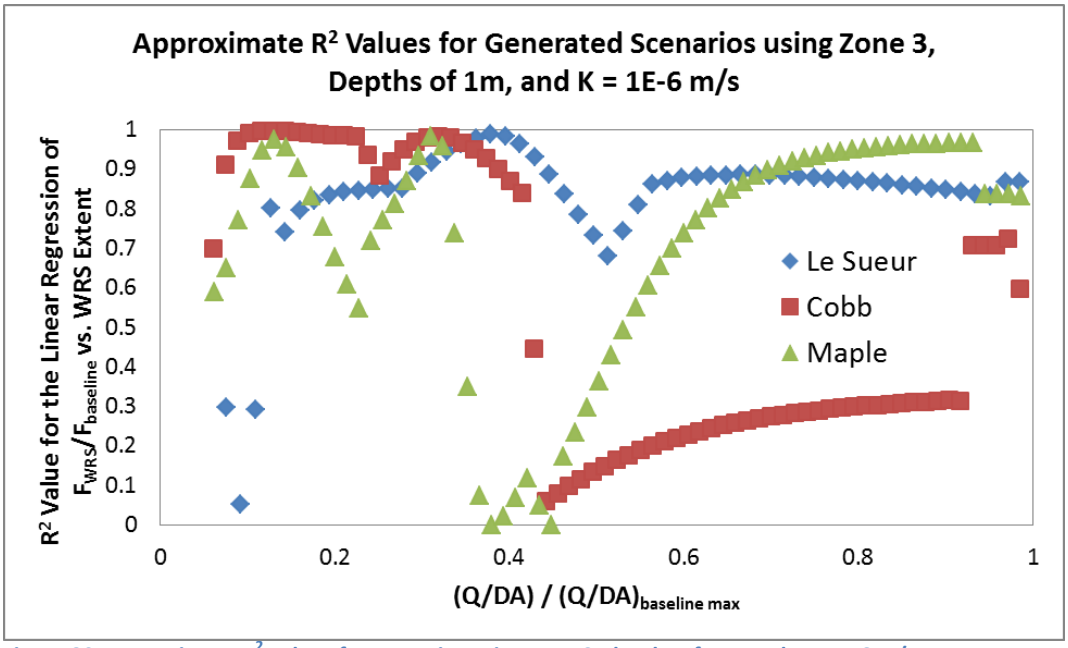

Figure 80. Approximate R^2 values for scenarios using zone 3, depths of 1m, and K = 1E-6 m/s.